2009

LRFD design of double composite box girder bridges

Purvik Patel
University of South Florida

LRFD Design of Double Composite Box Girder Bridges

by

Purvik Patel

A thesis submitted in partial fulfillment
of the requirements for the degree of
Master of Science in Civil Engineering
Department of Civil and Environmental Engineering
College of Engineering
University of South Florida

Major Professor: Rajan Sen, Ph.D.
A.G. Mullins, Ph.D.
William Carpenter, Ph.D.

Date of Approval:
July 2, 2009

Keywords: composite behavior, innovative design, steel bridges, fatigue, concrete

ACKNOWLEDGEMENTS

Firstly, I would like to sincerely thank Dr. Rajan Sen for his support and guidance during my M.S. program at University of South Florida. This project could not be completed without his knowledge and insight. Dr. Rajan Sen was the source of inspiration and motivation throughout the project. I acknowledge Dr. Niranjan Pai for his assistance and support throughout the project. I would like to thank Florida Department of Transportation (FDOT) for supporting for supporting me in this project. This project could not be completed without the help of Marc Ansley, P.E., Will Potter and Steven Eudy of Florida Department of Transportation. I would like to acknowledge the valuable input from Steven Stroh, P.E., and Dennis Golabek, P.E., and of URS Corporations.

This project would not be possible without the help of my colleagues and fellow students at USF. I would like to thank Julio Aguilar, Lori Elkins and Vladimir Simonovsky. I would like to thank Dr. William Carpenter and Dr. Austin Gray Mullins for serving on my committee.

Finally I would like to thank my parents and my family members. They have always supported me in pursuing my education.

TABLE OF CONTENTS

LIST OF TABLES

LIST OF FIGURES

LRFD Design of Double Composite Box Girder Bridges

Purvik Patel

ABSTRACT

Conventional continuous steel bridges only exhibit composite behavior in the positive moment region. Similar composite action may also be achieved in the negative moment region by casting a bottom concrete slab between the points of inflection. Such a section is referred to as "double composite" since it is composite in both the positive and negative moment regions.

Savings in double composite bridges arise because expensive steel is replaced by inexpensive concrete to carry compressive loads. Although double composite bridges have been designed and constructed since at least 1978 there has been limited research. Thus, current designs rely on existing provisions for designing conventional 'single' composite bridges. This fails to fully exploit the advantages or recognize the weaknesses, if any, of double composite action. This thesis presents findings from a cooperative research project involving USF/URS/FDOT in which full-scale tests and theoretical analyses were carried to develop appropriate limit state rules for designing double composite bridges.

A 4 ft. deep, 48 ft. long, 16 ft. wide box girder bridge representing the entire negative moment section at a support of a continuous full-size box girder bridge was fabricated and tested at FDOT's Structural Research Center, Tallahassee under fatigue, service and ultimate loading. Based on the findings from these tests and non-linear finite element analyses conducted by USF, URS proposed new design rules.

This thesis focuses on the applications of these rules to develop a model design example for use by bridge engineers. The example was specifically selected from AISI so that a cost

comparison with conventional design could be made. For completeness, an overview of the experimental results is also included in the thesis.

1. INTRODUCTION

1.1 Overview

Conventional steel bridges are designed to take advantage of composite action between concrete and steel in the positive moment region. This idea can also be extended to "double composite" action by casting a bottom concrete slab in the negative moment region in continuous structures. Since concrete is continuously bonded to the steel, the need for bracing is eliminated thereby bringing about substantial cost savings. Moreover, since the weight of the bottom slab lowers the neutral axis, the depth of the web in compression is reduced and thinner web sections can be designed as compact with attendant benefits since the full plastic moment capacity can be realized.

These advantages have the potential to make double composite girder bridges competitive in the 200-400 ft. span range. Though several double composite bridges have been designed and built in Europe, in particular Spain and Germany, there has been no similar interest in the United States in part due to a lack of design guidelines and uncertainty regarding the behavior of double composite steel bridges.

In 2004, the Florida and US Department of Transportation initiated a 2-year cooperative research program study involving USF/URS/FDOT to develop appropriate design rules for double composite bridges on the basis of full-scale testing and non-linear analysis. This 2-year study became a 5-year study because of delays in fabricating the test specimen, updating Tallahassee's testing facilities to accommodate the enormous loads needed to initiate failure (predicted as 1200 kips), getting forms for the top slab, scheduling the test and providing sufficiently strong sections to serve as an intermediate support.

The design of the test specimen was carried out by URS. The instrumentation and test program was developed by USF with appropriate input from URS and FDOT. Data from the tests was electronically sent to USF for analysis. Following completion of USF's analysis of the test results and Finite Element Analysis (FEA) results, URS proposed design rules for double composite sections. A non-linear Finite Element Analysis (FEA) was conducted to validate the experimental data. The analysis has taken longer because the test data was anomalous; for example the top slab unexpectedly cracked under fairly low loads.

This thesis focuses on the application of the LRFD design rules developed by URS. The model example selected is taken from the AISI manual since it allows designers to immediately recognize the changes in design and the benefits of double composite construction.

1.2 Scope of Study

The primary objectives of the research project was to evaluate the response of a double composite steel box bridge under fatigue, service and ultimate loading, to develop LRFD design rules and a model design example to illustrate their application.

Full-scale testing was intended to evaluate the applicability of existing LRFD provisions for the design of double composite sections and those parameters not addressed by the code. For example, loads on the bottom concrete slab are quite different from those on the top slab since they are not subjected to any localized wheel loads. Moreover, the bottom slab is restrained by steel webs at its ends compared to the top slab where there is no similar restraint. The connection of the bottom slab to the steel plate is through shear connectors over the entire width. This contrasts with the top slab which is attached to the steel flanges over a much narrower width.

Whether the concrete strength and reinforcement in the bottom slab should be the same as that for the top slab is not known. Since cost savings depend on the thickness of the bottom steel plate, construction issues relating to how it can support the weight of the wet concrete become important. Also, since the section is compact, it can reach full plastic capacity; whether

the steel reinforcement provided in the top slab was sufficient to resist the combined effect of shear from localized wheel loads when the top deck was completely cracked at full plastic capacity was a concern.

The test section had to satisfy constraints imposed by the testing facilities. In particular, this dictated the maximum dimensions, the maximum load and the maximum number of parameters that could be instrumented. Based on these considerations, the entire negative section over a continuous support in a double composite box girder was designed. The overall length of the section was 48 feet, its depth of 4 ft. 10⅛ in. and its width 16 feet. The top slab was 8 in. thick and the 6 feet wide bottom slab was 7 in. thick bottom. High performance steel (HPS) was used for the fabrication of the steel box girder. The top steel flange was 1¾ in. thick whereas the bottom flange was only ⅜ in. thick. The webs were each ¾ in thick (Fig. 1.1). The steel box was fabricated by Tampa Steel and shipped to Tallahassee where the top and bottom slabs were cast separately.

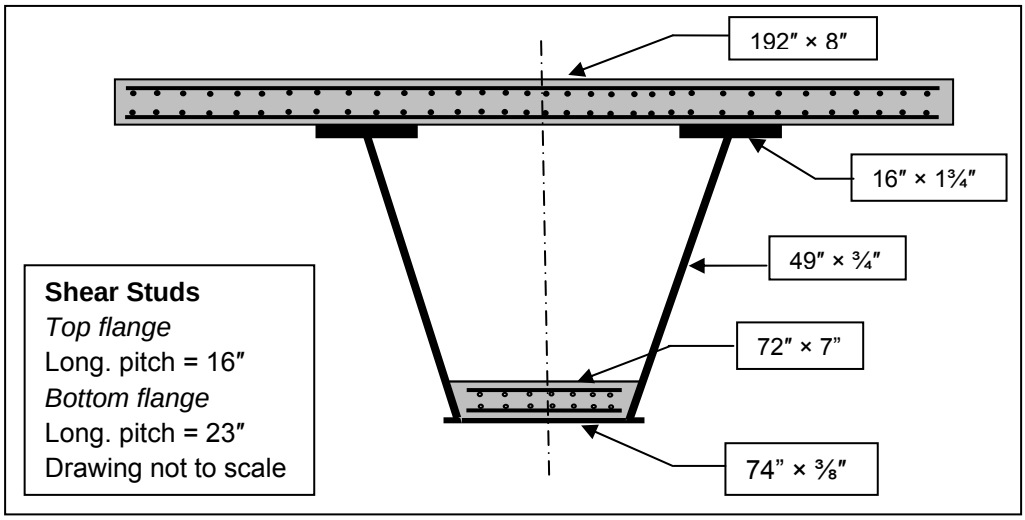

Figure 1.1 Typical Cross-Section of Test Specimen

Load, strain, deflection and slip data were recorded and analyzed to determine the behavior of the double composite box girder test specimen. The analysis of all the results was carried out at USF. Since the test results led to the formulation of the design rules, a brief

overview of the results is presented in this thesis. The focus of this thesis is on the application of the newly developed design rules developed by URS.

1.3 Organization of Thesis

A brief literature review on the state-of-the art on double composite box girder bridges is presented in Chapter 2. An overview of the results from the experimental study is summarized in Chapter 3. The design recommendations and critical issues pertaining to design are discussed in Chapter 4 and their application illustrated in Chapter 5. Conclusions and recommendations for future research are summarized in Chapter 6.

2. LITERATURE REVIEW

2.1 Introduction

Double composite steel bridges were built in Europe using prevailing design codes. However, information regarding their design is fairly limited. This chapter provides details on existing double composite steel bridges and on previous research.

2.2 Applications

The term “double composite” refers to steel sections with concrete slabs in both the positive and negative moment regions as shown in Fig. 2.1. The addition of a concrete slab to the bottom flange raises construction issues and imposes additional load on the foundation. Nonetheless, costs can be lower making steel more competitive.

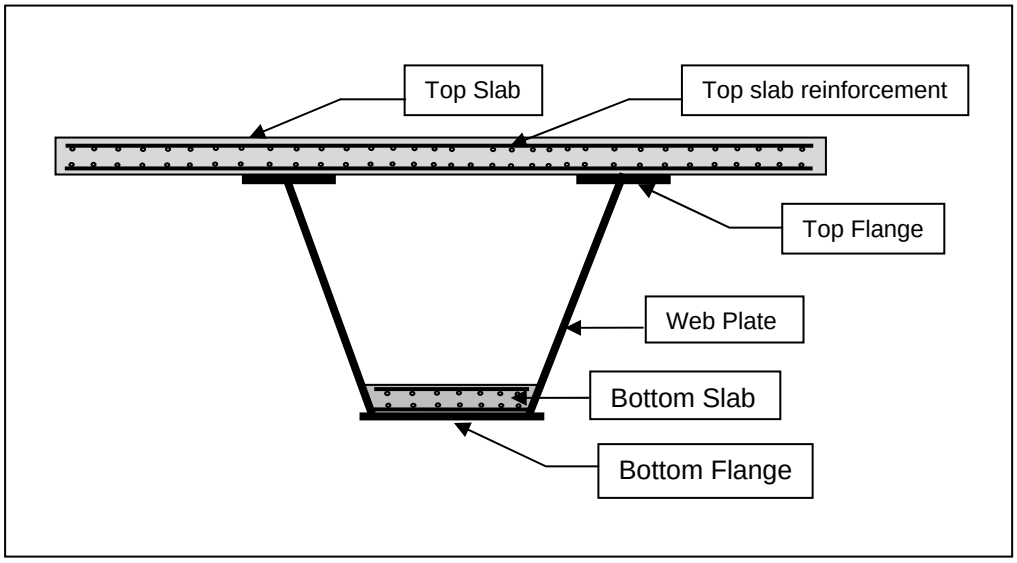

Figure 2.1 Typical Cross-section of Double Composite Bridge

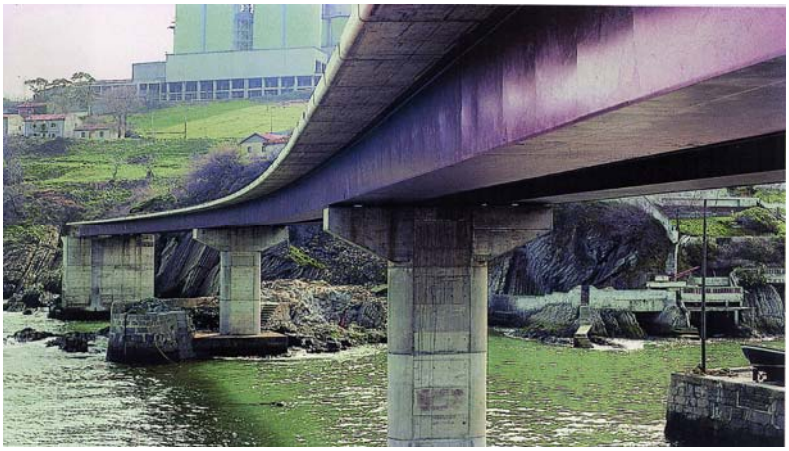

Figure 2.2 First Double Composite Bridge, Ciervana Bridge. (*Courtesy J.M. Calzon*)

The Ciervana Bridge (Fig. 2.2) is the first example of a double composite bridge [1]. The three span continuous bridge with spans of 40-50-40m was built in Spain in 1978. The cross-section consisted of rectangular or trapezoidal box sections fabricated using high strength steel. The concrete bottom slab was reinforced for resisting torsion and its own weight in the transverse direction. It is not clear whether any longitudinal steel was provided to resist negative moments over the supports. Other examples of double composite bridges built in Spain include a bridge over A-7 highway [2], over Tremor river [3] and at Majadahonda [4]. In all these cases the cross section consisted of a single trapezoidal box section.

Examples of the double composite bridges may also be found in Germany and Venezuela [2] and [3]. A five span bridge with a main span of 213.8 m and a total length of 478.8 m was constructed across the Caroni river at Ciudad at the Guyana/Venezuela border. The superstructure of the combined highway-railway bridge consisted of a two cell box girder for the main span and the long spans whereas an I-girder with 3 webs was used for the side spans. The thickness of the bottom slab varied from 85 cm at main pier to 20 cm at the intermediate pier. The thickness of top slab was 24 cm which was heavily reinforced (4.8 %). The design was based on the assumption that the bottom slab over the piers was cast first. Thus, the bottom slab acts compositely to resist the stresses due to weight of the steel structure, the top concrete slab and the applied loads [2].

There are other examples of double composite bridges built in Germany [3-5]. These are largely descriptive and do not contain any details on their design. This is also the case for two double composite box bridges recently completed over St. John and Jemseg Bridges on the Fredericton-Moncton Highway in Canada in 2001 [6, 7]. Fig 2.3 shows the cross section of the Frederiction-Moncton Highway Bridge at mid span and at center support.

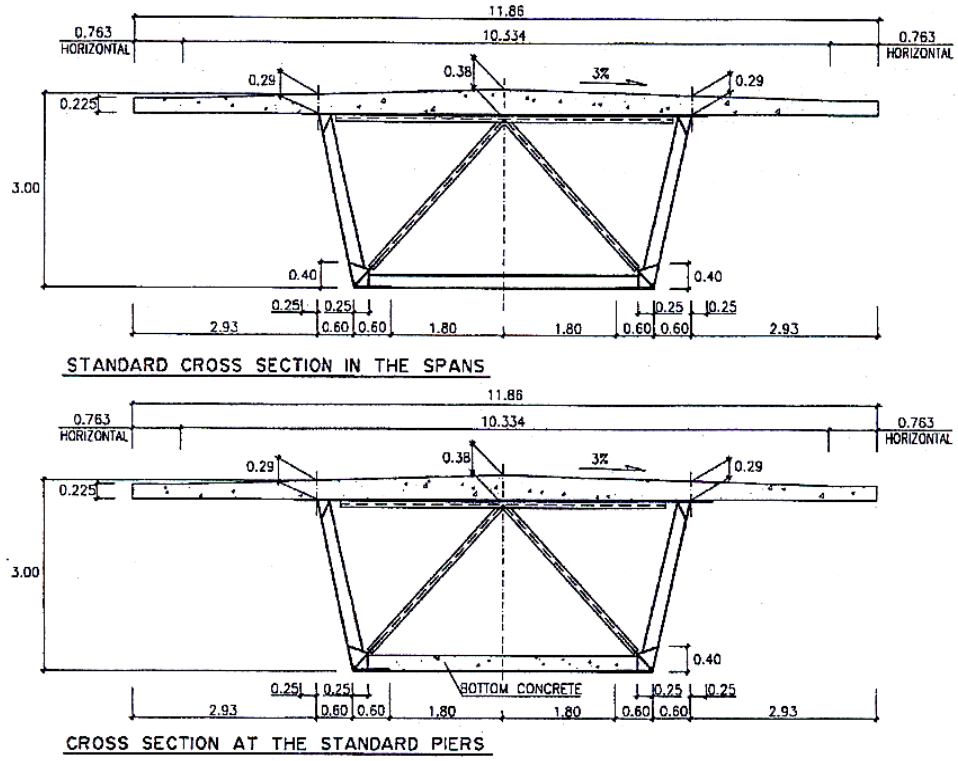

Figure 2.3 Cross-section of St. John River Bridge, New Brunswick, Canada

2.3 Experimental Research

A fatigue test was conducted in Germany to evaluate the fatigue performance of a high speed railway bridge. In the test, two 6.8 m long and 1.1 m deep girders were tested under negative moment. The girders were attached to a 120 cm × 30 cm slab reinforced longitudinally with a reinforcement ratio of 2.5%. The slab cracked after 2.0 million cycles with the cracks evenly distributed at 15 cm. The maximum crack width did not exceed 7.8 mils (0.0078 inch). The tensile stresses in the reinforcement and the girder were smaller than the predicted values.

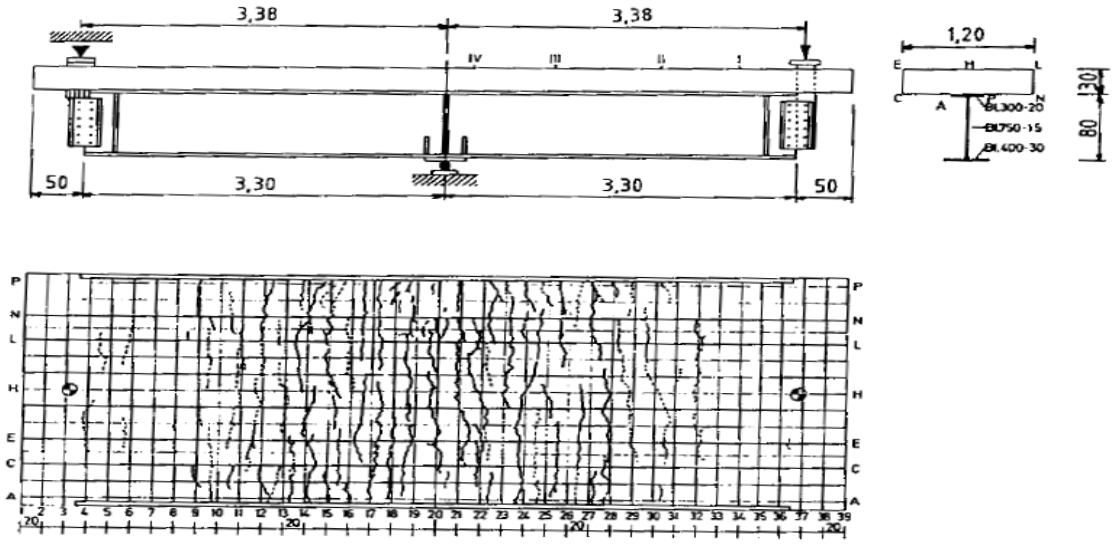

Figure 2.4 Test Set-up and Slab Cracking in Double Composite Girder Test. [3]

An ultimate load test was carried out that showed that the full plastic capacity of the girder was reached. “Perfobond” shear connectors were used to connect the slab to the girders. Fig. 2.4 shows the experimental test set-up used in Germany and the cracking observed in the top slab. This set up was used in our study.

2.4 Code Provisions

The limited information available indicates that there are concerns relating to the reinforcement that is to be provided in the top slab in double composite applications. The bridge built in Venezuela used 4.8% steel whereas the German railway bridge used 2.5%.

The prevailing LRFD provisions in AASHTO require a reinforcement ratio of 1% with two-thirds of the rebars placed in the top layer and the remaining one-third in the bottom layer. The Spanish code [8] incorporate provisions for designing double composite slabs. For the design of reinforced slabs supported on transverse members, this states:

“When the deck slab is supported on steel, concrete or composite transverse members, it is necessary to analyze, in the area of negative bending, the combined effect of shear stress in the slab caused by external loading and tensile stress due to the general bending of the slab. In thin

slab and where there is no shear reinforcement this effect may be decisive; and it will be necessary to guarantee the slab strength by testing, as at present the standards do not include realistic values of resistance to shear stress for high qualities of longitudinal reinforcement.

In order to control cracking, a minimum quantity of 1 % should be allowed, limiting the characteristic width of cracking to 0.2 mm under normal conditions."

3. OVERVIEW OF EXPERIMENTAL STUDY

3.1 Introduction

A brief review of the published literature showed that a number of double composite bridges have been built primarily in Europe using prevailing codes. However, it was not known whether their provisions were valid or whether they took full advantage of the benefits offered by this type of design. In view of this, full-scale tests were conducted to evaluate the response of a double composite box girder section under different loadings and also to validate and develop LRFD provisions of the AASHTO specifications for the design of double composite bridges.

A full-scale box girder test specimen 48 ft. long, 16 ft. wide, 4 ft 10⅛ in. deep representing a section of a bridge between inflection points was tested under fatigue, service and ultimate loads. The specimen was designed to be supported at the middle; however, this was not possible. As a result, it was asymmetrically supported with spans of 23 ft. and 25 ft. The load was applied at the free end of the longer span while a hold down frame prevented movement at the other end. Thus, the entire section was subjected to negative moments, see Fig 3.1 and 3.2. Table 3.1 summarizes the test program.

As noted earlier, the fabricated steel box was shipped to Tallahassee where the top and bottom slabs were cast separately. The 16 feet wide top slab was 8 inches thick while the 6 feet wide bottom slab was 7 inch thick. Composite action was ensured through shear connectors welded to the top and bottom flanges of the box.

Table 3.1 Test Program

Description	Load (kips)	Criteria	Critical
Fatigue	5-105	5.65 million cycles	Slip, changes in stiffness
Service I	421	0.6 F_y stress in rebar	Crack width, stresses in rebar, steel and concrete, and deflections
Service II	638	0.95 F_y in top steel flange based on Grade 50 steel	Crack width, stresses in rebar, steel and concrete, and deflections
Service III	894	0.95F_y in top steel flange based on HPS (F_y= 70 ksi)	Crack width, stresses in rebar steel and concrete and deflections
Ultimate	1200	AASHTO	Failure Mode, Ductility

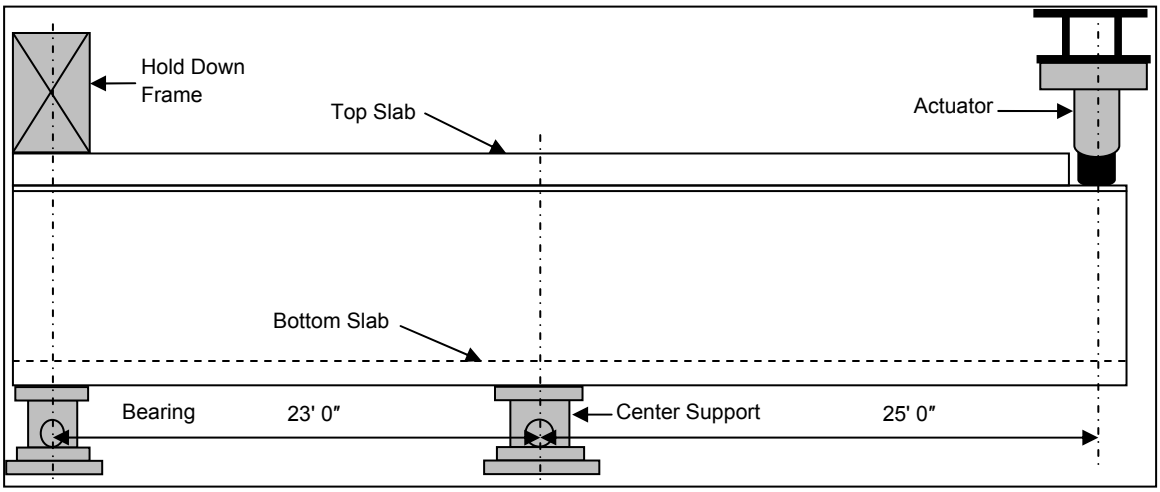

Figure 3.1 Test Set-up

Load cells, LVDTs and strain gages were used to monitor the response of the test specimen. A total of 162 channels were used initially of which 140 were set aside for the fatigue test. In essence, two cross-sections distant h (the full depth of the section including the slab is 4 ft. 10⅛ in.) were fully instrumented to allow determination of the strain variation in the cross-section and the position of the neutral axis. Additionally, 32 rebars in the top slab 1 ft away from the center support on either span were instrumented. Slip was monitored in the top and bottom slabs at both the hold and actuator ends with deflections measured along the entire length of the member at the supports, quarter point and the loaded end.

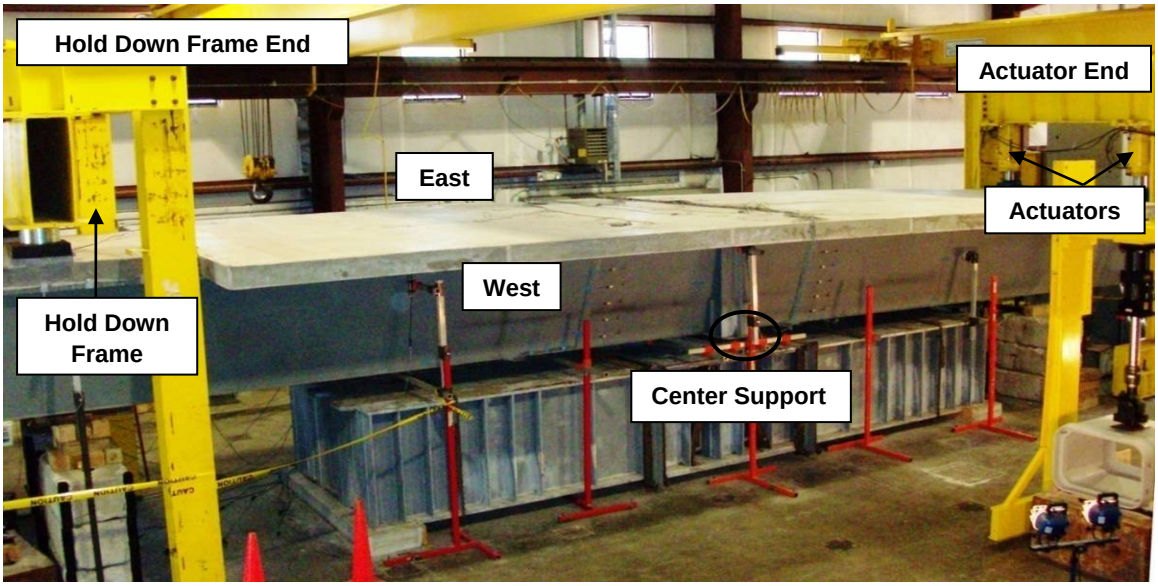

Figure 3.2 Service Test Set-up

However, the first application of the fatigue load that varied from 5 to 105 kips resulted in unexpected cracking of the top slab. This destroyed all 17 strain gages that were bonded to the top concrete surface. As a result, 123 channels were monitored for the fatigue test and 145 channels for the service and ultimate tests.

3.2 Fatigue Test

The fatigue test was conducted as there was no prior experimental data available on the performance of double composite bridges under fatigue loading. This was particularly the case because of the thin (⅜ in.) bottom steel flange used. The welding of shear studs to such a thin bottom plate can induce deformation and localized stresses that may be unfavorable under fatigue loading. The intent of the test was to verify the AASHTO LRFD provisions for the design of shear connectors and to document the performance of stud shear connectors in the negative flexure region.

3.2.1 Test Parameters

The key parameters in the fatigue testing were the load range, the frequency and the number of fatigue cycles. The load range was decided by the capacity of the fatigue testing system (110 kips). For this reason, the load range was limited to 100 kips and varied from 5 kips to 105 kips. The fatigue load was applied at the free end as shown in the test set-up.

The predicted fatigue cycles were calculated based on this load range in accordance with the *Article 6.10.10.2-2* of AASHTO LRFD specifications as 5.65 million cycles. The calculations were adjusted to take into account the asymmetric test set-up and the actual strength of the concrete measured just prior to the testing (Table 3.2).

Table 3.2 Fatigue Test Parameters

Parameter	Fatigue Test
Load Range	5-105 kips
Frequency	1.16 Hz
Number of Cycles	5.65 million
Concrete strength	
Top slab	
Actuator span	9905 psi
Hold down span	7590 psi
Bottom slab	8178 psi

The frequency was selected to be 1.16Hz. This meant that 100,000 fatigue cycles were completed over 24 hours of continuous testing.

3.2.2 Test Procedure

The fatigue test was carried out after completion of two static tests to provide baseline measurements. In these tests, the specimen was loaded to 105 kip at the rate of 1 kip/sec and all measurements recorded.

Following completion of these tests, the instrumentation was zeroed out and the load range set from 5 to 105 kips. The fatigue test was then initiated at a frequency of 1.16 Hz by the

means of the hydraulic load actuator under electronic feedback control operating in a load control mode. The fatigue loading was interrupted periodically and a static cycle applied between the minimum and maximum load to monitor response. Ten measurements were taken at approximate 0.5 million intervals with the last one at the end of the test. Since results overlapped, not all 11 static cycles are plotted; only selected cycles are presented in the results of the fatigue test.

3.3 Service Test

The top concrete slab was designed based on LRFD provision of AASHTO specifications with the longitudinal reinforcement ratio set at 1%. It may be noted from the previous chapter that a very large reinforcement ratio (in one case as high as 4.8 %) was used in the top concrete deck in a previously built double composite railway bridge [3]. It was not known whether a higher limit was necessary although compact double composite sections can support higher loads than conventional composite bridges. Tests were therefore conducted to evaluate three AASHTO specified service loads, referred to as Service I, Service II and Service III (Table 3.1). Critical parameters in these tests were the stresses in the rebar, stresses in the concrete and steel, and the maximum crack width (Table 3.1).

Under Service I, the stresses in the rebar were targeted to $0.6f_y$. Service II loads were targeted to $0.95F_y$ in the top steel flange, with F_y taken as 50 ksi. This was intended to represent performance of normal grade structural steel. The final service load test, Service III targeted the stress in the top steel flange at $0.95F_y$, with F_y taken as 70 ksi to represent the high performance steel (HPS) used for the specimen. The loads corresponding to these three service conditions were respectively 421 kips, 638 kips and 894 kips. In each series, the loads were planned to be applied and released a total of five times.

A final ultimate load test corresponding to a 1200 kip load was planned following the conclusion of the service tests. However the ultimate load test was not conducted because of failure in the bottom steel flange that occurred in the first cycle of the service III load case. For

this reason, this test is referred to as the ultimate load test in this thesis. It was evident from the buckling failure that there was reduction in stiffness of the test-specimen during fatigue test.

3.4 Fatigue Test Results

As stated earlier, the fatigue test was intended to evaluate the performance of shear connectors that ensured composite action for the bottom slab. Loss of composite action could be detected from slip measurements of both the top and bottom slabs.

The results from the test that are significant are (1) deflection at the cantilevered end and (2) slip at the respective actuator and hold down ends. However, since the bottom steel plate failed prematurely in buckling in ultimate test, the strain profile in the concrete and steel close to the center support became important as well.

Of these 11 cycles, the fatigue results are presented only for the 1st static cycle, 0.5 million, 1.5 million, 3.0 million, 4.9 million and 5.65 million cycles. The location of the relevant sensors is indicated in all the plots.

3.4.1 Deflection Under Fatigue Load

The deflection at free end is the most critical deflection since it is the largest and was used for evaluating the effects of the fatigue loading.

Fig. 3.3 and 3.4 shows the deflection at the cantilevered end measured by LVDTs # 7 and # 8. The results for 0.5 million and 3 million cycles in Fig. 3.3 are anomalous since they are not reproduced in Fig. 3.4. This is probably due to instrumentation problems.

The deflection profile in Fig. 3.3 indicates that the maximum deflection was 0.65 in. after the 1st static test (the predicted deflection from simple cracked beam analysis was 0.56 in.) and progressively increased to 0.78 in. after completion of 5.65 million cycles. Thus, there is approximately a 17 % reduction in stiffness of the section. The progressive increase in deflection

suggests an overall stiffness reduction caused by additional cracking of the top and bottom slabs. This is confirmed by the strain data shown later.

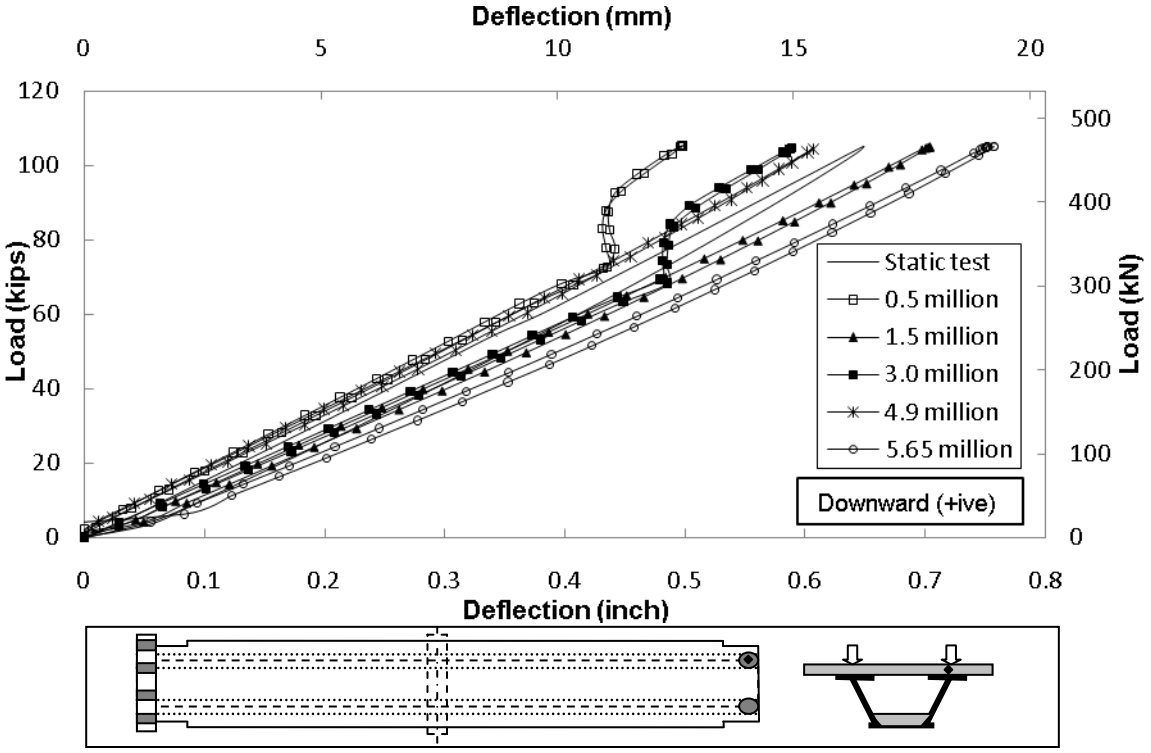

Figure 3.3 Deflection at Actuator End LVDT # 7

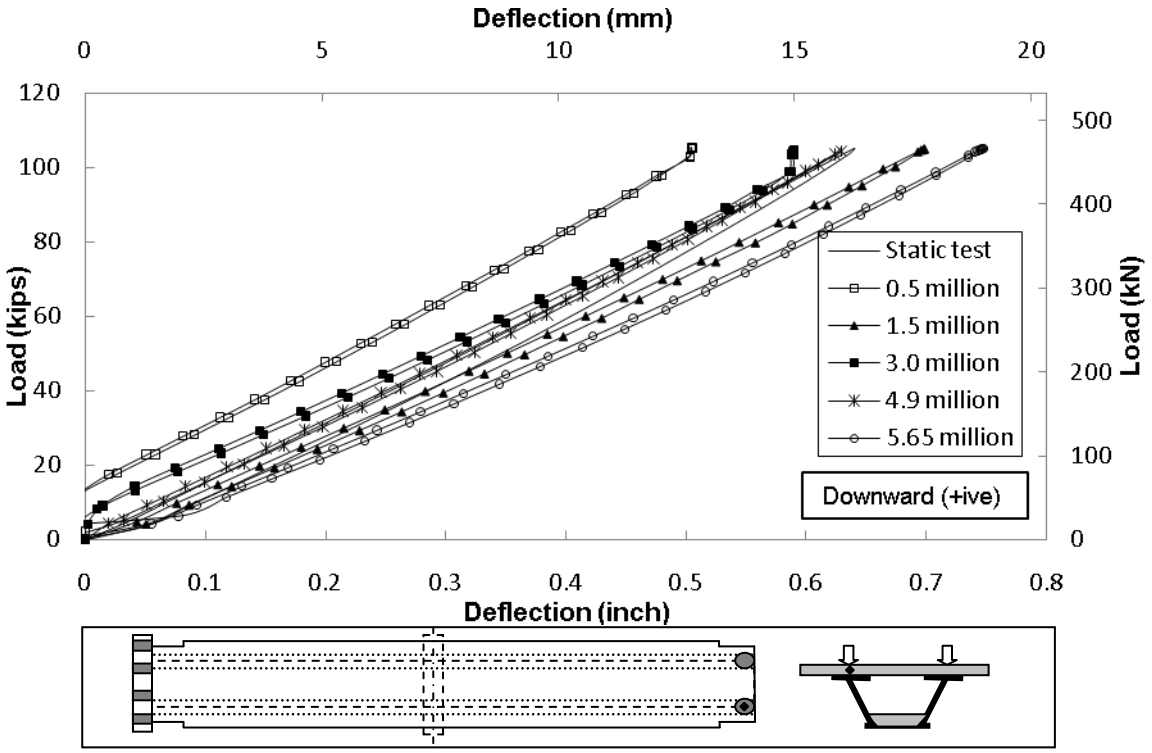

Figure 3.4 Deflection at Actuator End LVDT # 8

3.4.2 Slip

The relative horizontal movement between the concrete and the steel interface at both the loaded and the hold down ends were monitored throughout the testing. No slip was recorded at either ends for both the top and bottom slabs.

3.4.3 Strain in Concrete Under Fatigue Load

The strain in concrete in the bottom slab was monitored at the section located 4 ft. 10⅛ in. from the center support on either side. Although the applied load was well within the elastic limit, the strain variation observed in the concrete was non-linear. The non-linearity in the concrete strain can be caused by secondary effects other than loading e.g. restraint at its ends by the steel webs, differential shrinkage, temperature difference etc.

The concrete strain variation in Fig. 3.5 indicates a change in the response after 1.5 million cycles. There is a marked reduction in the stiffness at low loads (upto 30 kips) followed by increased stiffness in the range from 30-50 kips after which the stiffness remains constant. This kind of behavior of concrete was not expected. The placement of concrete blocks (6 in × 6 in × 6 in.) at 4 ft on centers during the casting of the bottom slab may be the possible reason for such behavior in the concrete (Fig. 3.6). Similar profile of strain was not observed on the corresponding actuator side and corresponding strain gage located on the symmetric flange location (not presented in this thesis).

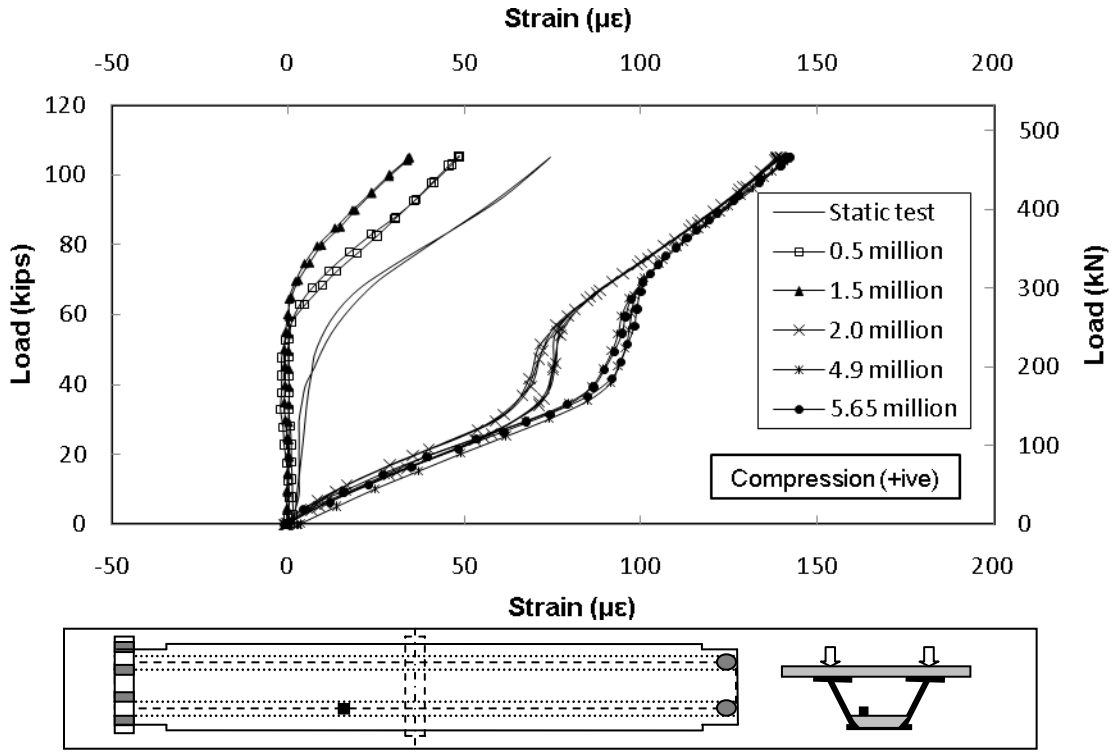

Figure 3.5 Strain in Bottom Concrete Slab on Hold Down Side SG 111

Figure 3.6 Placement of Bottom Concrete Slab

3.4.4 Summary of Fatigue Test Results

1) The fatigue test was conducted over a load range of 100 kips which is significantly lower than the cracking load of 154 kips; still the top slab cracked. This could be possibly due to the weaker concrete mix on the hold down side. The maximum crack width recorded on the top concrete slab was of 7 mils.
2) It can be concluded from the deflection data that there was a 17 % reduction in stiffness of the test-specimen.
3) Strain data in the concrete suggest a reduction in stiffness at low loads. This may be because of possible debonding of the bottom flange and bottom slab and secondary effects like restraint by the webs, shrinkage and presence of concrete blocks (Fig 3.6).
4) The strain in the top slab reinforcement 1 ft away from the center support in either span increased by 25% increase signifying that there was additional cracking in the concrete.
5) The strain variation in the web of the cross-section indicated a lowering of the neutral axis after completion of the fatigue test. This again indicated cracking in the top slab so that a larger area was required to support the same force.

3.5 Service I Test Results

The stress in the top slab rebars was limited to $0.6f_y$ for Service I load test. The maximum load required to develop this stress was 421 kips. The load was applied and removed for 5 times and the loading rate was 1 kip/sec.

The most important results for this test were the deflection and strain developed in the rebars. The analysis of the slip data indicated that there was no slip recorded at the either end of the test specimen.

3.5.1 Deflection Under Service I Load

Deflections were recorded at the cantilevered end, close to center support (2 ft. ¼ in.) on either side and along the length of the beam. The deflections close to the center support on hold down side are critically important because of the buckling failure that occurred in the ultimate load test.

Fig. 3.7 shows the plot of the deflection recorded at the cantilevered end. The average maximum deflection of 3.1 in. was recorded with the load of 421 kips. This is significantly (39%) greater than the prediction of 2.25 in. obtained from a simplified cracked beam analysis. The increase in deflection suggests additional cracking in the concrete.

Fig 3.8 shows the longitudinal deflection profile at 100 kip intervals recorded along the length of the beam. The portion of the profile highlighted with circle indicates the out of plane bending of the bottom flange. The profile indicates temporary out of plane bending of the bottom flange close to center support on hold down side. This was probably due to debonding of the concrete and steel (Fig. 3.6).

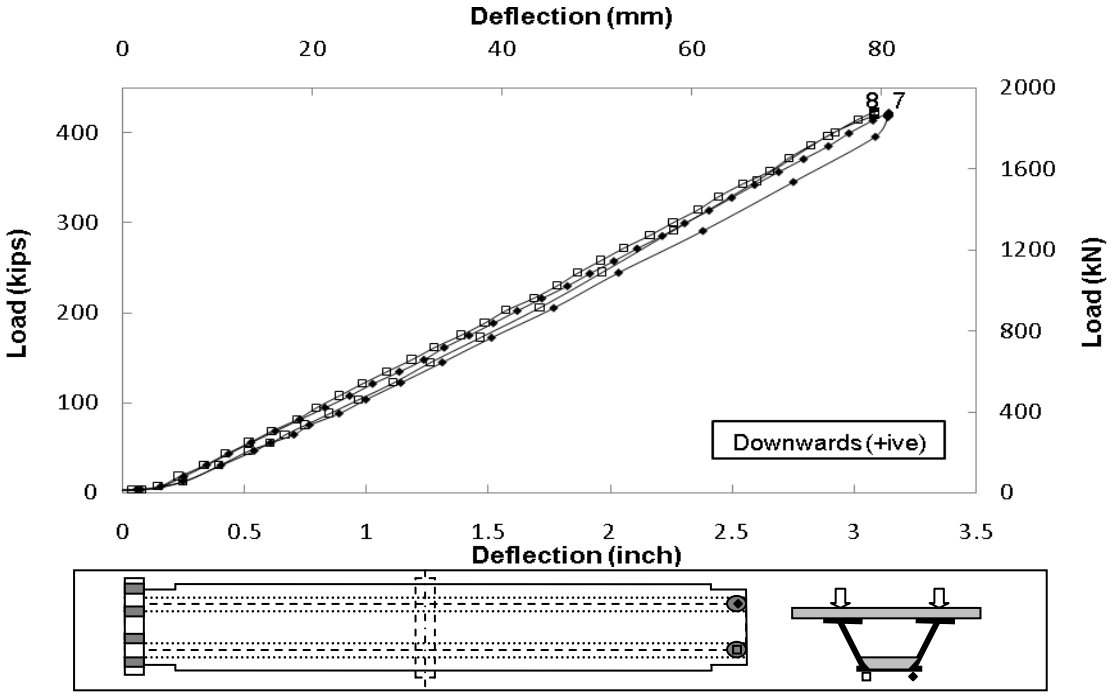

Figure 3.7 Deflection at Cantilevered End

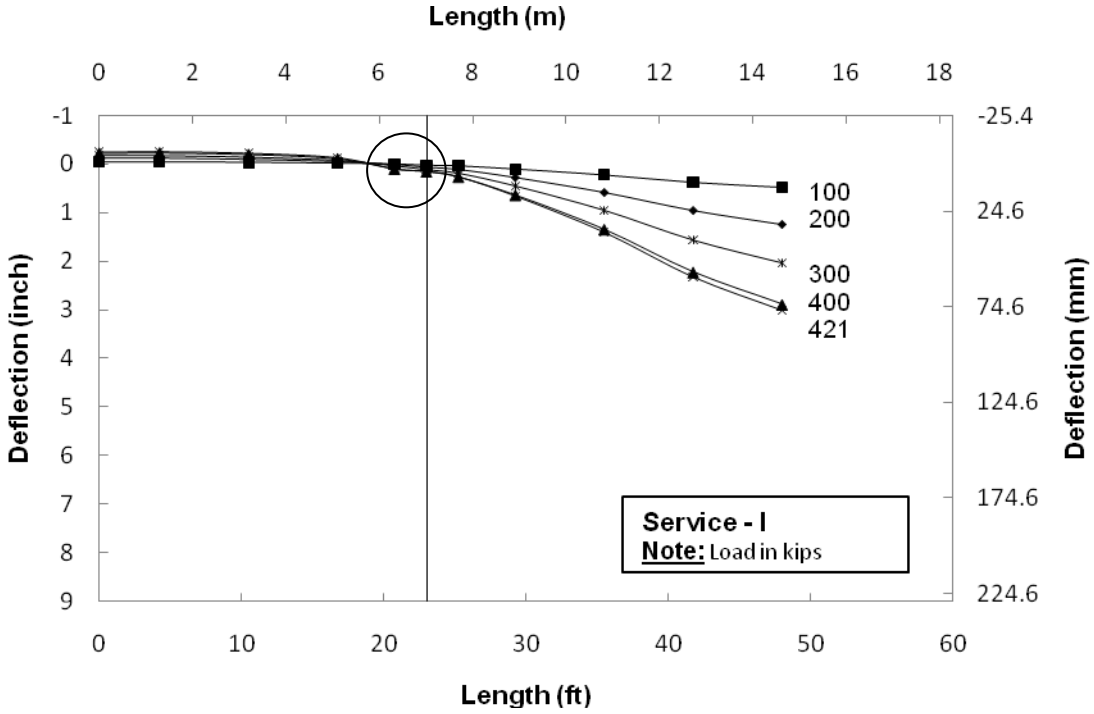

Figure 3.8 Longitudinal Deflection of Double Composite Box Girder

3.5.2 Top Rebar Strain

Strain in the rebars was monitored at 1 ft from center support in either span. The strain was recorded in 16 rebars on either side of the center support. Since all the 16 gages could not be included in single plots, the results for the eight gages are presented in Fig. 3.9 and Fig. 3.10. The applied moment on the actuator side was higher because of the asymmetric test set-up. Static moment on the actuator side was 10,104 kip-ft. and on the hold down side, 10067 kip-ft. Therefore, the results presented are for rebars located in the actuator span.

In this test, the stress in top slab rebars was limited to $0.6f_y$. Fig. 3.9 and Fig. 3.10 show the straight line corresponding to maximum strain of 1241με, which corresponds to the limit of $0.6f_y$ in the rebars. The highest strain was recorded in the rebars placed over the web exceeded the stipulated limit of 1241 με. This was the case because of shear lag effects. However the average stress in rebars in either hold down span and actuator span was found to be 36 ksi and 33 ksi respectively.

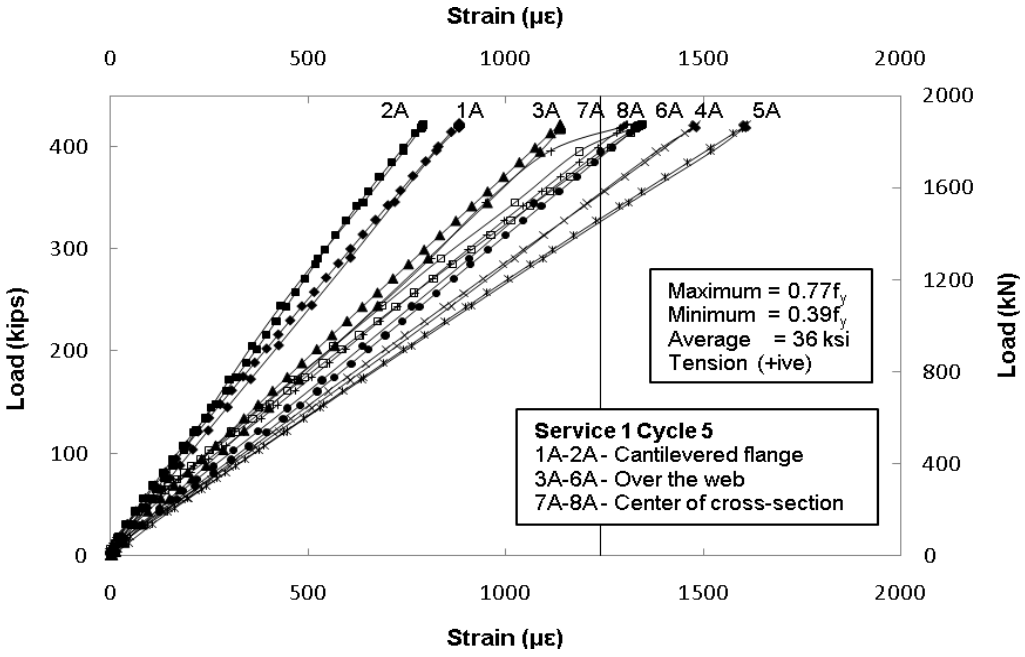

Figure 3.9 Strain in Top Slab Reinforcement on Actuator Side-I

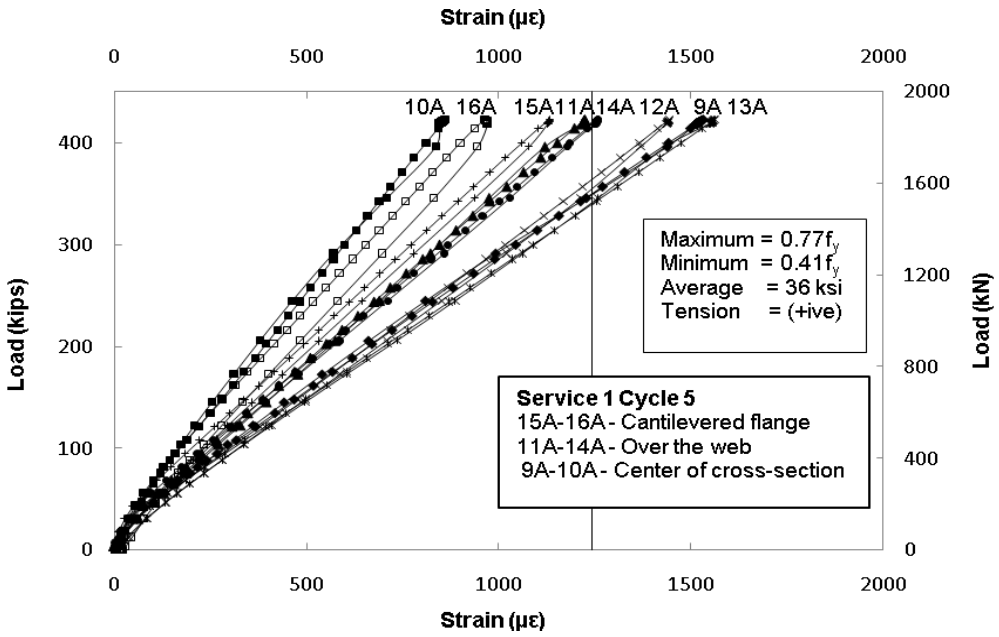

Figure 3.10 Strain in Top Slab Reinforcement on Actuator Side-II

3.5.3 Summary of Service I Test Results

1) The maximum deflection recorded at the cantilevered end was 39 % higher than the theoretically calculated value.
2) The deflection close to center support suggest localized distortion in steel plate(Fig. 3.6).
3) The strain data validates the AASHTO's provision of 1 % steel for top concrete slab. The average stress recorded in the rebars was 36 ksi and 30 ksi in actuator and hold down span respectively.

3.6 Service II Test Results

The only change made in the service II load test was the maximum load was increased from 421 kips to 638 kips, rest all the test parameters and instrumentation were kept same. This load corresponded to the condition where the stress in the flange was limited to $0.95F_y$ with F_y

taken as 50 ksi, that is 47.5 ksi. The results reported for the Service II load case are deflection and strain variation in steel top flange and bottom flange.

3.6.1 Deflection Under Service II Load

The maximum deflection recorded at the cantilevered end was 4.72 inch. Fig 3.11 plots the variation of deflection with load for the sensors located at the free end. The overlapping of deflection profile indicates the absence of any torsion effects. The actual recorded deflection is 38 % higher than the predicted deflection of 3.4 in.

Fig. 3.12 shows the variation in the average deflection of the box specimen along its length for loads ranging 100 to 638 kips. A discontinuity close to the support (2 ft. ¼ in.) is observed in the hold-down span suggesting localized distress.

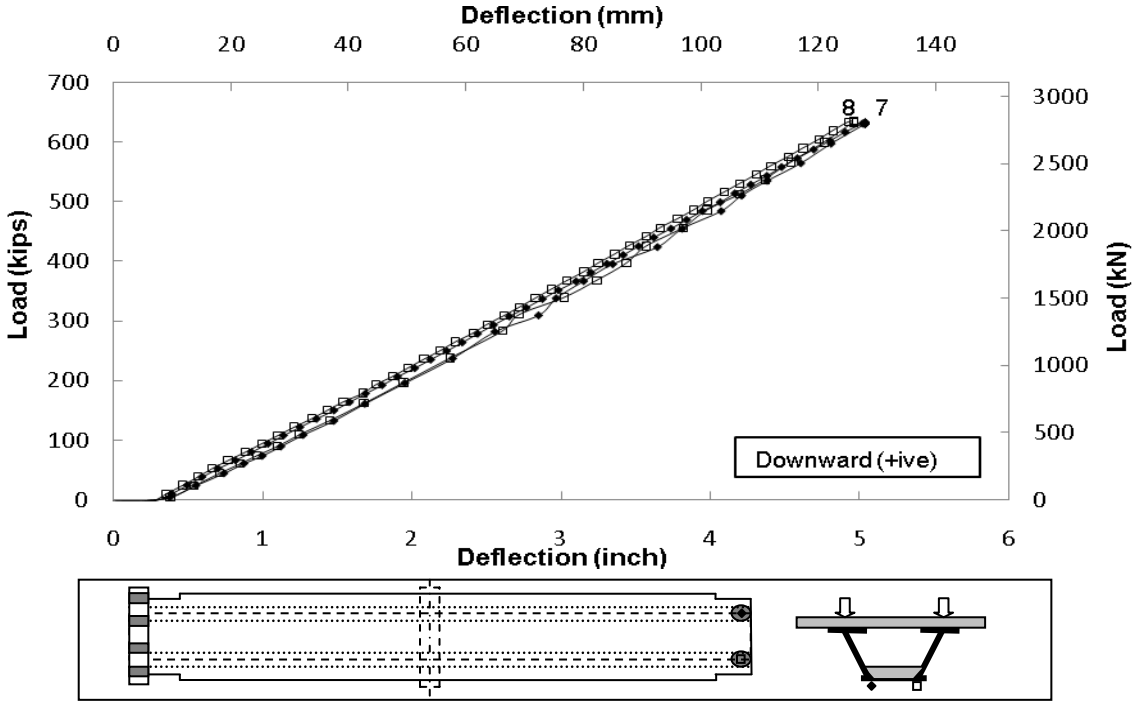

Figure 3.11 Deflection at Cantilevered End for Service II Load Test

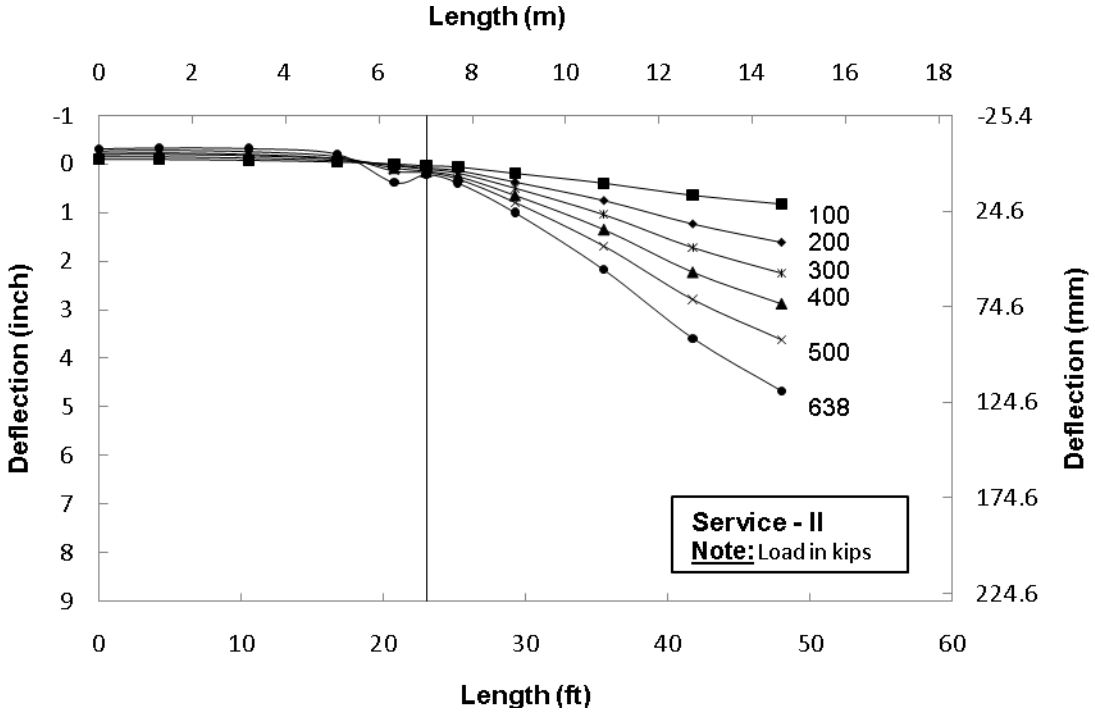

Figure 3.12 Longitudinal Deflection of Double Composite Box Girder for Service II

3.6.2 Strain in Steel Under Service II Load

The stress in steel top flange was limited to $0.95F_y$ in this test. For this reason, the results for the top flange steel strain at the center support are plotted (gages 73, 74) in Fig. 3.13. The strain variation with the applied load is linear. The maximum recorded strain was 1603με which corresponds to a calculated stress of $0.93F_y$ for Grade 50 steel, close to the targeted $0.95F_y$ stress.

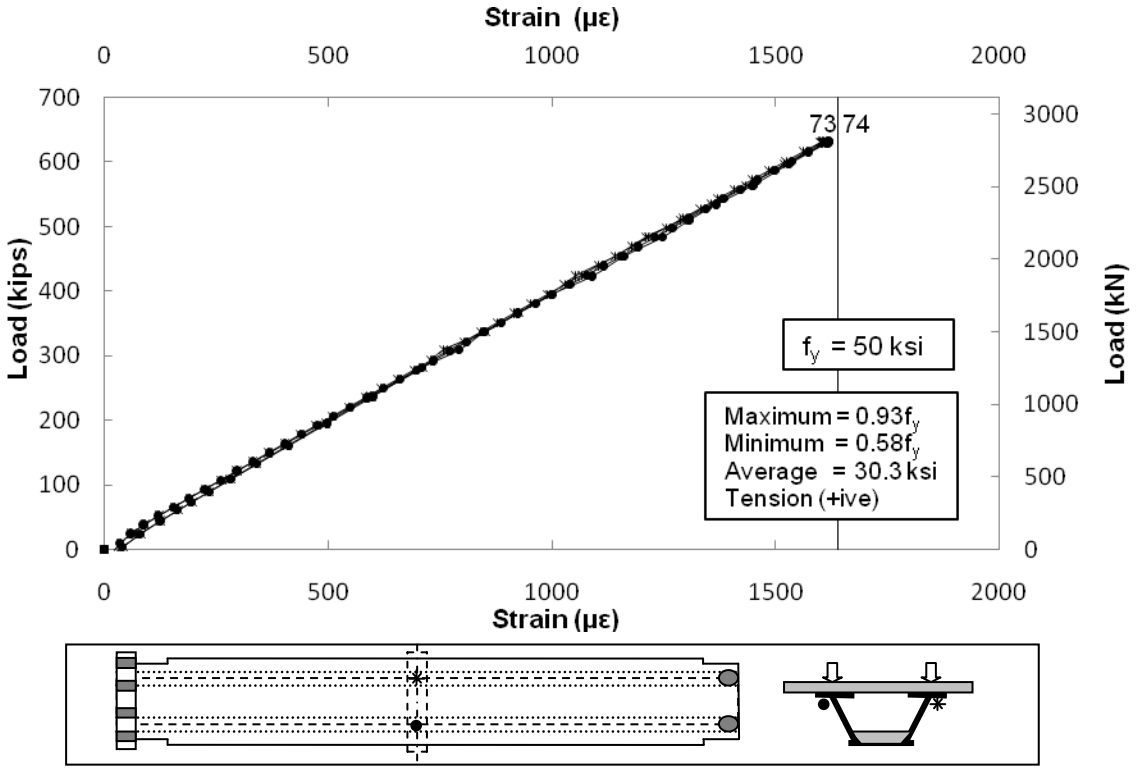

Figure 3.13 Strain in Top Flange at Center Support

The strain was also recorded in the bottom flange on the hold down side and actuator side at 4 ft. 10⅛ in. from the center support. The strain recorded on the hold down side (gage 122 – 125) is presented herein because of the unusual response of the steel bottom flange. Fig. 3.14 shows the variation of strain recorded with the applied load in the bottom flange on hold down side. The gage positioned in the center (gage 124) shows the unusual response compared to the gages located at the same location. The strain reverses from compression to tension after 150 kips of load. This trend is not repeated for the two gages located over the web (123, 125). For these gages, the response is non linear but similar. However the calculated stress on the hold down side exceeded the nominal yield value of 50 ksi as the maximum recorded strain in gage 125 was 1754 με, which exceeds the yield strain of 1638 με.

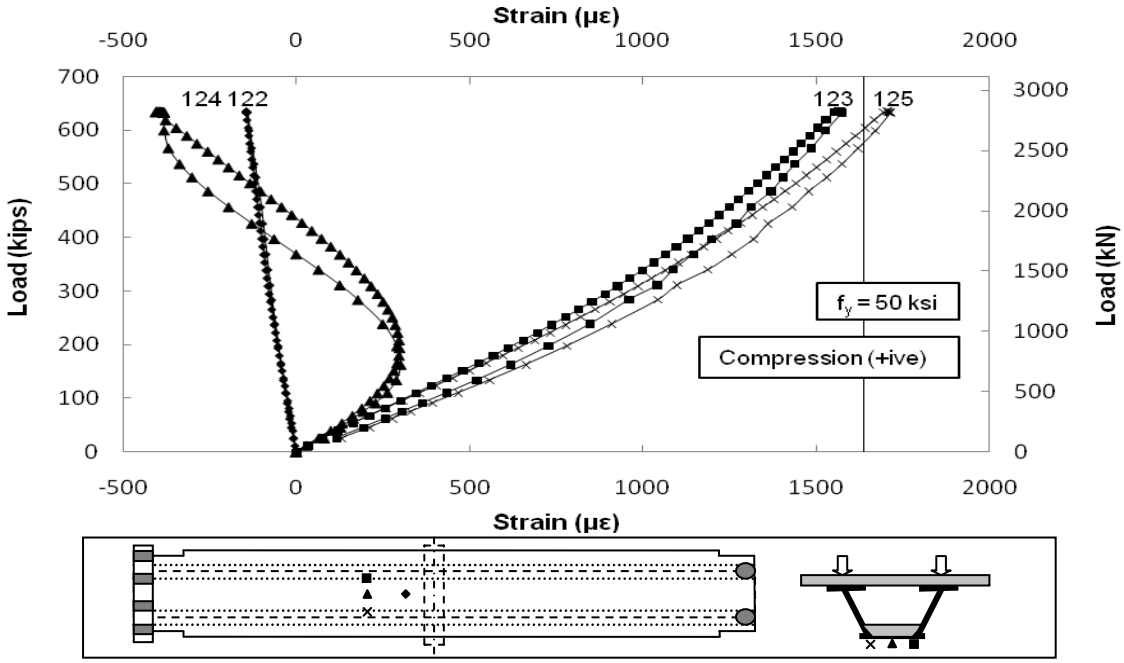

Figure 3.14 Strain in Bottom Flange on Hold Down Side

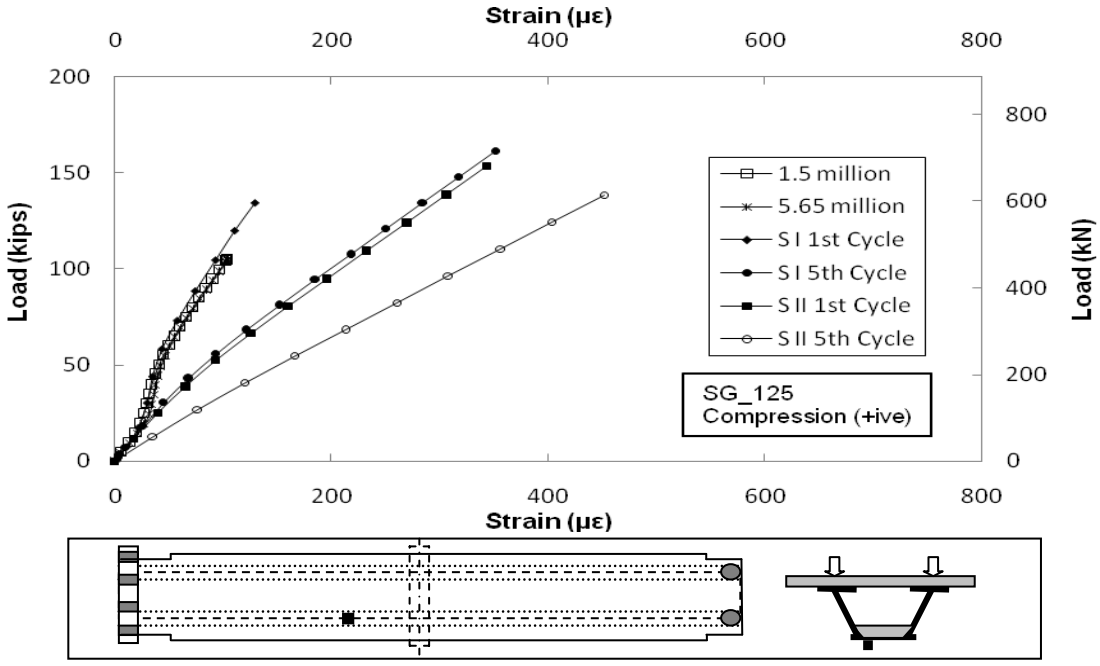

Figure 3.15 Comparison of Steel Strain of Fatigue and Service Test

The strain recorded in the service II load test was compared with the fatigue test, service I and 1st cycle of service II load case. Fig 3.15 compares the strain variation in gage 125 on hold down side for the fatigue and for 1st and 5th cycle of Service I and II. Again, this suggests that there was some degradation of the specimen under service II loading. The repetitive loading of same magnitude is causing damage to the test-specimen.

3.6.3 Summary of Service II Test Results

1) The maximum recorded deflection was 38 % higher than the estimated deflection. The longitudinal deflection profile inidcates the localized distortion in bottom flange close to center support (2 ft. ¼ in.) on hold down side (see Fig 3.12).
2) The strain recorded in the top flange is within the $0.95F_y$ (47.5 ksi) limit (see Fig 3.13). Strain recorded for the bottom flange was non-linear and exceeded the targeted value (see Fig. 3.14).
3) Comparison of strain with fatigue and service I load test reveals that there is reduction in stiffness of specimen due to increased strain in bottom plate on hold down side. Fig. 3.15 also indicated that repetitive loading is responsible for loss in stiffness.

3.7 Ultimate Test Results

The last service test was designed to evaluate the response when the applied load (894 kips) corresponded to the stress of $0.95F_y$ (66.5 ksi) in Grade 70 steel. The test was to be conducted in the same manner as the previous two service test and instrumentation would remain unchanged.

The intent of this test was to determine service response when the stress in the steel flanges reached $0.95F_y$ or 66.5 ksi. Results are presented for deflection, concrete/steel strains at critical locations.

3.7.1 Failure Mode

The specimen failed in compression mode due to buckling of the bottom flange close to center support on hold down side. The specimen failure occurred when the load was sustained at 894 kips for the inspection of cracking on top slab. Immediately following the failure the load dropped to 394 kips. Since buckling is not possible if the flange were continuously bonded to the concrete bottom slab, failure was inevitably initiated due to debonding of the concrete. Also the confining of the bottom concrete slab was responsible for the endured failure.

Fig 3.16 shows the buckled bottom flange close to center support in the hold down span. The buckled flange extended transversely over almost its 6 ft width and between the first and second shear connectors lines (11 in. and 34 in. from the center support) in the longitudinal direction. Fig 3.17 shows more picture of the failed bottom slab.

Figure 3.16 Failed Bottom Flange on Hold Down Side

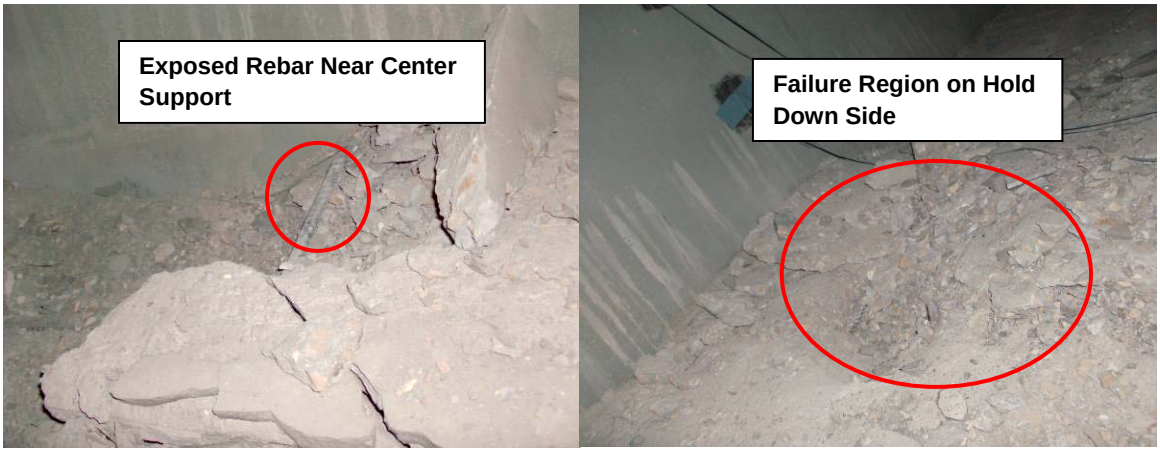

Figure 3.17 Failed Bottom Concrete Slab on Hold Down Side

3.7.2 Deflection Under Ultimate Load

The maximum deflection was measured at the cantilevered end. The maximum recorded deflection at the cantilevered end was 7.75 in. which is 38 % higher than the estimated value of 4.78 in. Fig. 3.18 shows the variation of deflection with load at the cantilevered end. The deflection profile is almost linear.

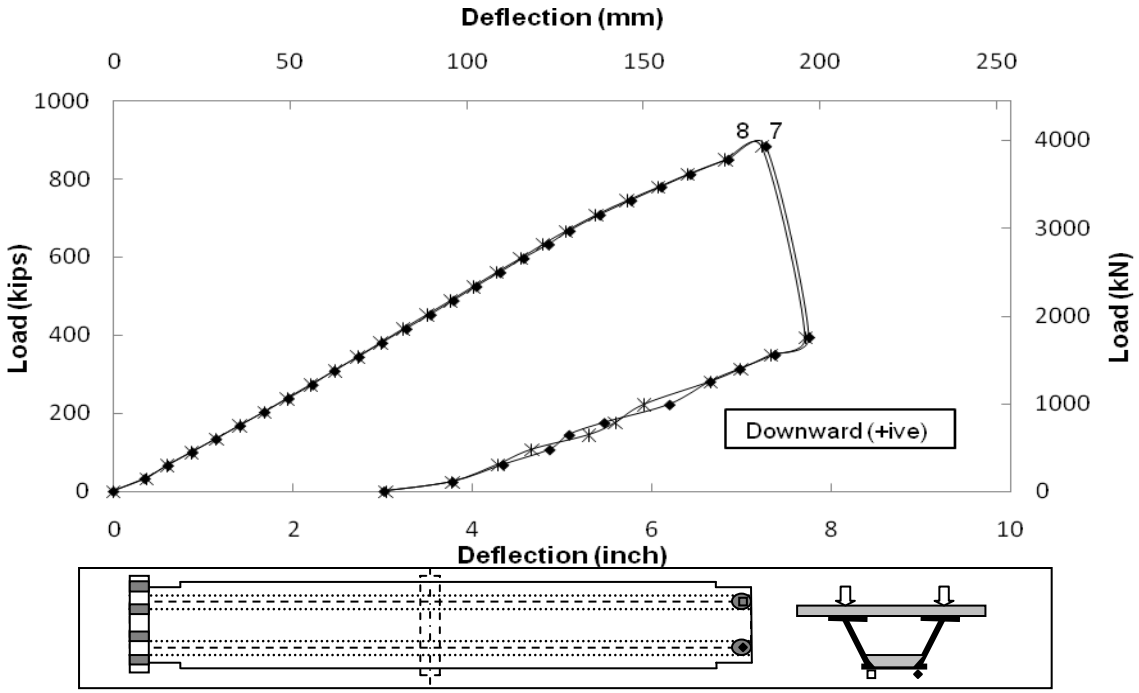

Figure 3.18 Deflection at Cantilevered End for Ultimate Load Test

Fig. 3.19 shows the variation in the deflection along its length with increasing load. The deflection profile indicates the damage to bottom flange close to center support on hold down side. This is partly due to reduction in stiffness because of fatigue loading, shrinkage cracking, localized distortion and other factors.

The failure load of the specimen was 894 kips. Structure response clearly indicates that loads were still transferred despite the serious distress in the thin bottom flange. In this sense, the resistance mechanism in the double composite section follows the well known tension field action in which webs are able to support shear even after they have buckled [8].

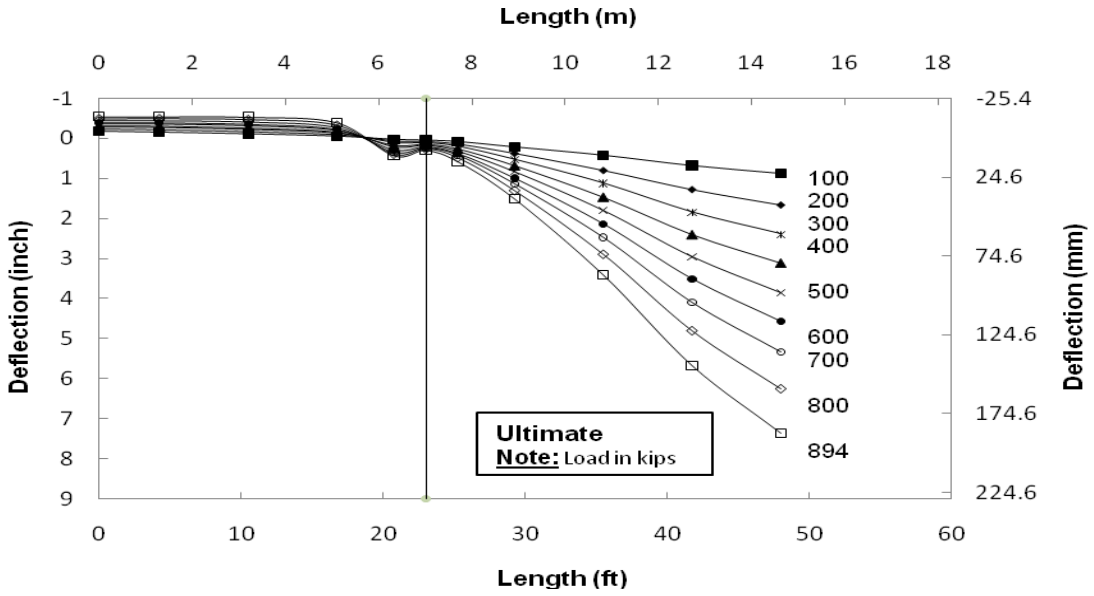

Figure 3.19 Longitudinal Deflection of Double Composite Box Beam for Ultimate

3.7.3 Strain in Concrete Under Ultimate Load

Strain in the bottom concrete slab was monitored on either side of center support (4 ft. 10⅛ in.). Unfortunately there was no strain gage provided in the failure region. Fig. 3.20 shows the variation in strain with load in the two gages (#109, 111) closest to the failure location on the hold down side. The variation is initially non-linear but is largely linear subsequently. The concrete underwent stress reversal from tension to compression at low loads in gage 109. The

maximum stress of $0.6f'_c$ was recorded in gage 111. This clearly indicates that the failure mode was complex.

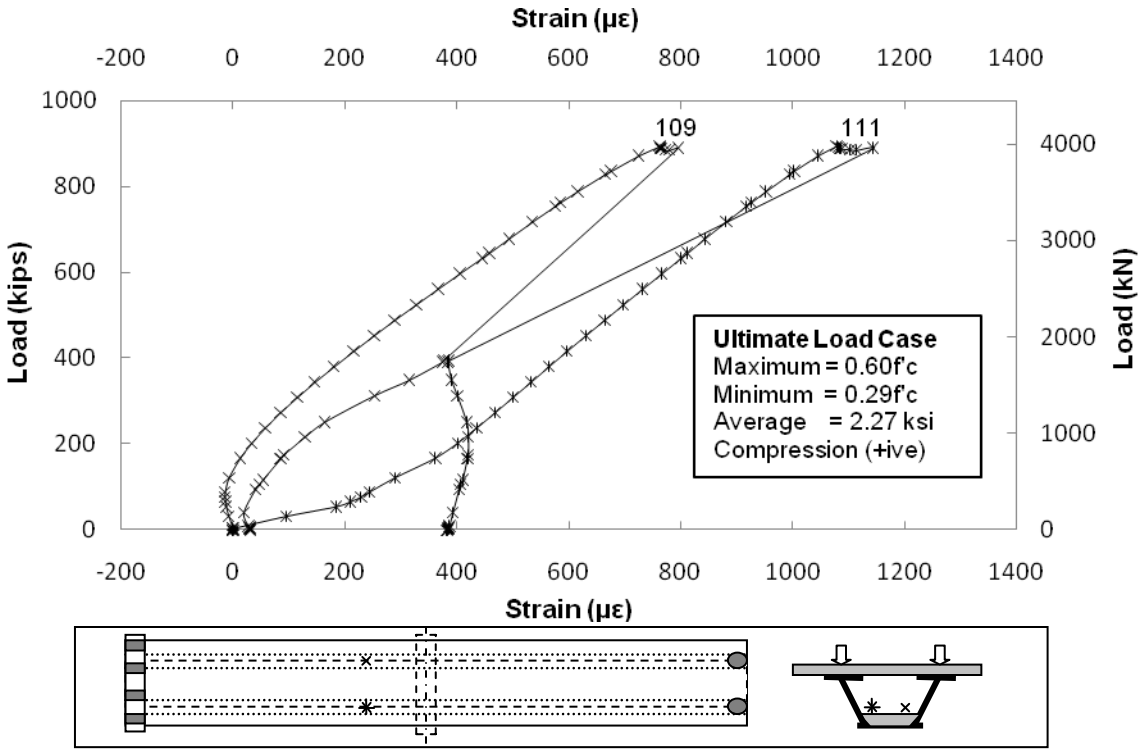

Figure 3.20 Strain in Concrete in Failure Region

3.7.4 Strain in Steel Under Ultimate Load

The most critical section is located 4 ft 10⅛ in. from center support on the hold down side. Unfortunately there was only one transverse strain gage located in the failure region. Fig. 3.21 plots the variation in strain developed in the top flange at the location of the maximum moment at the center support. The top flange began to yield at 680 kips and the maximum recorded strain was 3500 με.

The behavior of the bottom flange is more complex. No transverse strains were recoded by gage 122. The variation of strain with load for the three gages (123-125) located at the exterior surface of the bottom flange 4 ft 10⅛ in. from the center support in the hold down span is shown in Fig. 3.22. The maximum compressive strain occurs at the web/flange intersection measured by

gages 123 (2292 με) and 125 (2414 με). The response of these gages is somewhat non-linear with a discontinuity at a load of 638 kips.

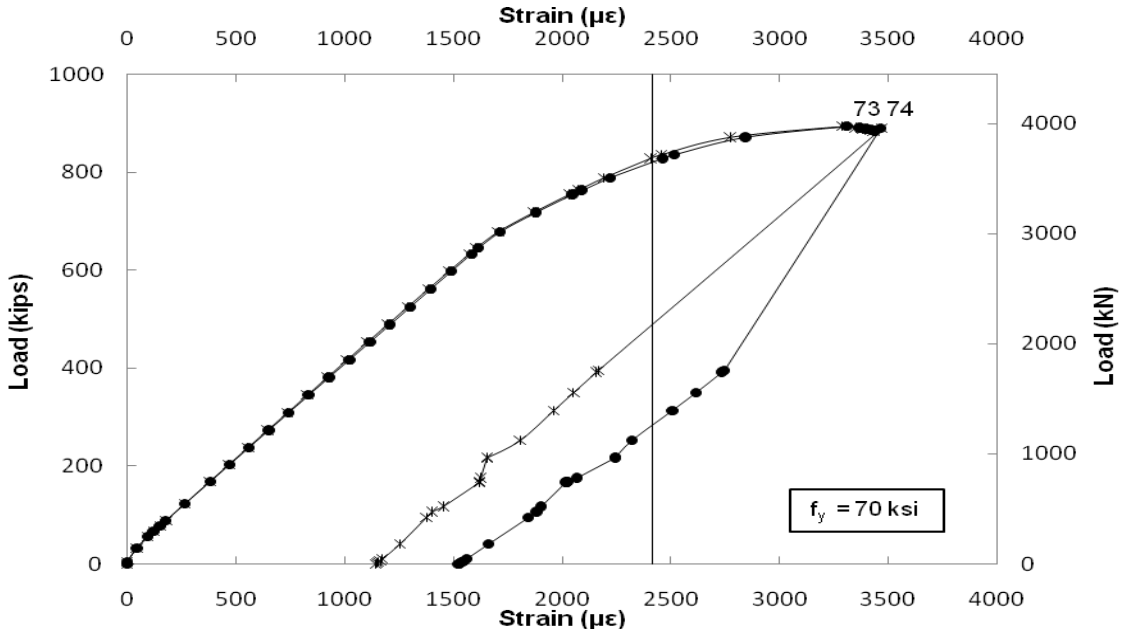

Figure 3.21 Strain in Top Flange at Center Support for Ultimate Load Test

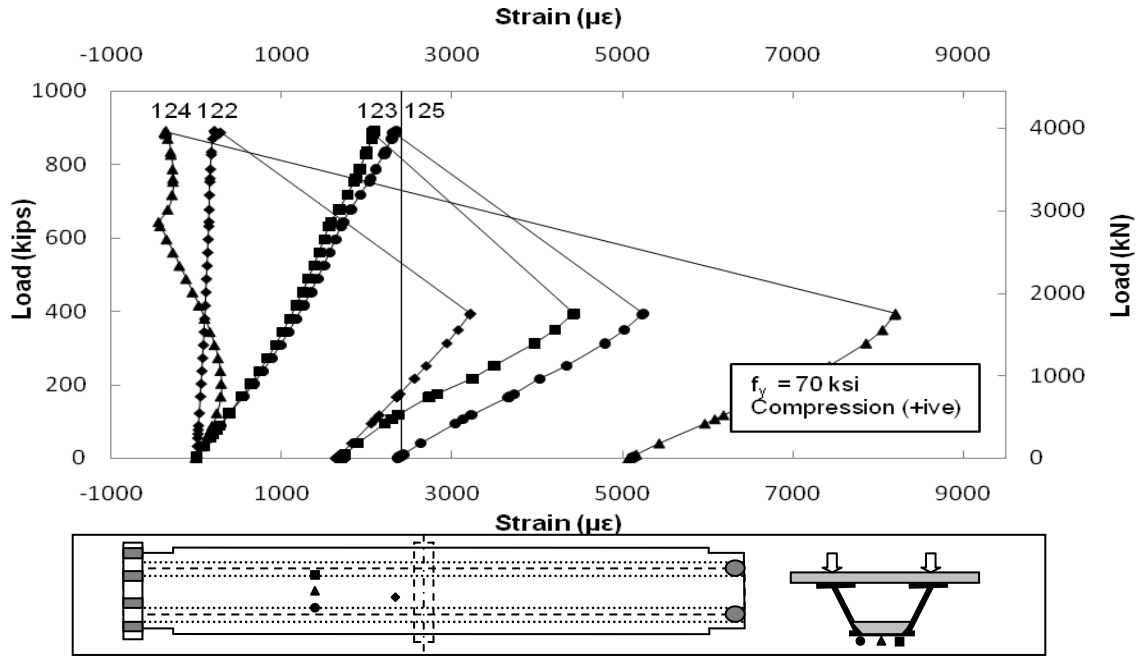

Figure 3.22 Strain in Bottom Flange on Hold Down Side for Ultimate Load Test

A similar discontinuity was recorded by gage 124. The strain in this gage started as compressive but changed to tensile at around 150 kips. Subsequently, it continued as tensile reaching a maximum value of around 600 με. This reversal signifies localized bending stresses caused by separation of the concrete surface from the bottom plate.

3.7.5 Summary of Ultimate Load Test Results

1) The specimen failed in the very first minute under the sustained loading close to center support on hold down side (Fig. 3.16-3.17). The failure was compression failure.
2) The bottom concrete slab crushed in the failure region following buckling of the bottom flange. Deflection data suggested localized distress of bottom flange in the failure zone.
3) The stress in top slab rebars exceeded the yield point in 27 of the 32 rebars.
4) Strain data recorded for concrete and steel was non linear. The top flange yielded at a load of 680 kips.
5) The maximum strain in the bottom flange at maximum load was $0.95F_y$. The strain in the bottom flange exceeded the yield point after the failure of the bottom concrete slab. Since there was only one strain gage (in the transverse direction) in the critical region, there was no strain data available for the failed region. Other gages attached to the bottom flange did not provide conclusive evidence.

4. DESIGN RULES FOR DOUBLE COMPOSITE BRIDGES

4.1 Introduction

Prior to testing, there were concerns about the reinforcement that had to be provided in the top slab. There was also a belief that sections at the support would be compact and reach full plastic moment capacity at ultimate. The test results indicated that the concerns regarding the top slab steel reinforcement ratio were unfounded. On the other hand, the expectation that the composite bottom slab would reach full plastic capacity was proven to be incorrect because the shear connectors designed to current AASHTO specifications were ineffective at higher loading. The evidence from the testing was overwhelming and indicated localized separation of the concrete from the steel at relatively low loads.

In the light of these findings, URS proposed changes to current provisions to allow the design of double composite sections. In their proposed rules, the stresses in the bottom slab are limited to $0.6f_y$ at ultimate. Additionally, there is a ductility requirement in terms of limits on the location of the neutral axis. There is no criterion for selecting the minimum thickness of bottom flange. However the bottom flange should be checked for the buckling failure.

Aside from these provisions, the design of doubly composite sections is very similar to that of conventional single composite sections. This chapter summarizes the design rules for double composite bridges based on the experimental results.

4.2 Single Composite Bridges

A ‘single’ composite bridge refers to steel bridges with concrete slab decks in which composite action is limited to the positive moment region. Composite action is ensured by welding stud shear connectors to the steel flange that minimizes slip between the slab and the steel beam under loads.

Unshored construction is typically used. This means that the steel beam alone supports the dead load of the slab while superimposed dead and live load are supported by composite action. The composite section comprises the steel section and an effective width of the concrete slab. Stress analysis utilizes transformed section based on modular ratios that are adjusted to account for stresses due to sustained loads. Ultimate load analysis, however, is based on the nominal material properties of concrete and steel.

Composite bridges are designed in accordance with *Article 6.10.1.1 and 6.11.7.1* of the LRFD guidelines of the AASHTO specifications. Shear connectors conform to *Article 6.10.10 and 6.11.10* of the LRFD guidelines. Table 4.1 summarizes these rules for designing single composite box girder and I-sections.

Table 4.1 Design Rules for Single Composite Bridges

No.	Design Rules for Single Composite Section	LRFD Articles
1.	General Dimensioning and Detailing of Bridge Section	6.7
	Straight I – Sections	6.7.4.2
	Straight Box Sections	6.7.4.3
2.	Design Load and Load Combination	
	Dead Loads	3.5
	Live Load	3.6
	Fatigue Load	3.6.1.4
	Load Factors and Load Combination	3.4
3.	Structural Analysis and Evaluation of Bridge Superstructures	4.6
	Live Load Lateral Distribution Factors	4.6.2.2
4	Cross-Section proportions for I – Section and Box Section	6.10.2 and 6.11.2
5.	Non-Composite and Composite Section Properties	Article 6.10.1.1
6.	Plastic Moment Capacity	Article D6.1
7.	Limit States	
	Service Limit State	6.10.4 and 6.11.4
	Fatigue Limit State	6.10.5 and 6.11.5
	Strength Limit State	6.10.6 and 6.11.6
8.	Flexure Resistance	
	Composite Section in Positive Flexure	6.10.7 and 6.11.7
	Non-composite and Composite Section in Negative Flexure	6.10.8 and 6.11.8
9.	Shear Resistance	6.10.9 and 6.11.9
10.	Shear Connectors	6.10.10 and 6.11.10

4.3 Double Composite Bridges

In continuous bridges, the concrete deck slab is cracked in the negative moment region over the support and therefore any composite action is limited to the contribution of the reinforcing steel. Since concrete can support compressive loads more efficiently than steel, the structure can be made composite in the negative moment region by casting a bottom concrete slab between the points of contraflexure.

4.3.1 Contraflexure Points

The point of contraflexure refers to the zero moment location in continuous structures. Its location in a structure is not fixed since it depends on many factors such as the type of deck, span geometry, relative stiffness of the spans and loading. The maximum contraflexure length is

relevant in design since this is the length where the steel compression flange needs to be continuously braced so that the cross-section is compact.

Design moments in bridge structures are controlled by loading consisting of a combination of truck and lane loads. The location of the point of contraflexure for such loading can only be accurately determined from appropriate numerical analysis. However, for continuous beams with the same stiffness and the same length, information on the contraflexure location may be readily found, e.g. AISC handbook.

Table 4.2 summarizes information from the AISC handbook for 3-span and 4-span structures of the same span and stiffness under pattern loading [10]. Inspection of this table indicates that the largest distance corresponds to loading of adjacent spans (0.23L, 0.24L) and the smallest where alternate spans are loaded (0.10L, 0.10L). In design, the higher value, that is 0.24L will be used. In general, contraflexure lengths will be greater under distributed load than concentrated loaded.

Because moments are highest at the first support, it is customary for the end spans to be made shorter so that moments are equalized. The optimal ratio between the interior to the end span falls in the range 1.2 to 1.4. Table 4.3 summarizes information on the location of the point of contraflexure for this case. Information summarized in Table 4.3 is from the web resource [11]. Based on Table 4.2 the length of the distance of contraflexure point from interior support can be generalized to 0.30L, considering the optimum span ratio is in the range of 1.2 to 1.4.

Table 4.2 Contraflexure Points for Different Load Cases

Load Pattern	Number of Spans	Contraflexure point from Interior Support
Maximum Negative Moment (adjacent spans loaded)	3	0.23L
Maximum Positive Moment (alternate spans loaded)	3	0.10L
Dead Load (all Span Loaded)	3	0.20L
Maximum Negative Moment (adjacent spans loaded)	4	0.24L
Maximum Positive Moment (alternate spans loaded)	4	0.10L
Uniformly Distributed Load (All span Loaded)	4	0.21L

Note: L denotes the length of the span.

Table 4.3 Contraflexure Points for Different Span Ratios

Number of Spans	End Span	Main Span	Ratio of Main span to End Span	Location of Contraflexure Point from Interior Pier
3	50	50	1.0	0.20L
3	50	55	1.1	0.22L
3	50	60	1.2	0.243L
3	50	65	1.3	0.271L
3	50	70	1.4	0.302L
3	50	75	1.5	0.336L
3	50	80	1.6	0.375L
3	50	85	1.7	0.41L

Note: L denotes the length of the end span.

4.4 Design Provisions for Double Composite Bridges

One of the main attractions for using double composite construction is that it is designed using the same provisions as single composite girders. The double composite sections should also be checked for the same fatigue, service and strength limit state criteria as the single composite bridges. As with the design of the single composite structure, the steel beam supports the dead load of the slab in unshored construction. In this case, however, there are two slabs one at the bottom over the supports and the deck slab; since it is possible to cast either slab first, the design steps will depend on how the bridge is constructed. However, as a practical matter of access, it is more convenient to cast the bottom slab first and after it has cured, the top deck slab can be cast.

4.4.1 Construction Sequence

The construction of double composite bridges is slightly different compared to that of the single composite bridges. Several additional steps are necessary for the construction of steel box girders in the field. The construction sequence for the double composite bridges is listed below.

1) The box section and I–section should be fabricated in the shop as single composite section. The shear connectors on the bottom flange should be installed during the fabrication. Temporary bottom flange bracing should also be bolted during the fabrication of steel section. Temporary bracing is required to support bottom concrete slab. Also install guide rails for screeding the bottom concrete slab using the bolted and/or welded connections.
2) Once the structural steel is received on the field, the erection of structural steel is dependent on the placement of the bottom concrete slab.
3) The reinforcement for the bottom concrete slab should be first. Once the reinforcement is in place, bottom concrete slab can be placed and screeded to the designed thickness.
4) Remove the temporary bracing after the bottom slab cures.
5) Top slab shall be casted after the bottom slab has hardened. The self weight of top slab is supported by the composite bottom flange in the negative flexure region. Continue with the normal bridge construction.

4.4.2 Design Provisions

The design provisions for the double composite box girder section are summarized in this section. These are based on experimental results and non-linear FEM analysis. These rules presented only pertain to the design of negative flexure section; the design of the positive section is same as that for single composite bridges.

As noted already, the same design provisions of the LRFD guidelines for the design of single composite section should be followed for the design of double composite sections. The

detailed rules in the design of double composite sections are listed in Table 4.4. However, some additional rules are necessary because of the addition of the bottom concrete slab in the negative flexure region. These are listed below.

1) Determination of *"point of contraflexure"* for the placement of bottom slab. The points of contraflexure should be determined by using appropriate numerical analysis. In general, based on the ratio of interior span to exterior span, the distance from the interior pier to inflection point can be maximized to 0.3L for optimum span ratio of 1.2–1.4, where L is the length of the end span.
2) The maximum longitudinal compressive stress in the bottom slab at the strength limit state, determined as specified in AASHTO Article 6.10.1.1.1d, should not exceed $0.6f'_c$.
3) Reinforcement ratio of 1% is with two-thirds placed in the top layer as per prevailing LRFD provisions is adequate for the top slab reinforcement. It may be noted from the literature review that in some cases, the reinforcement ratio considered for the top slab was as high as 4.8%. However, from the experimental results it is concluded that the AASHTO specified provision for design of top concrete slab is sufficient.
4) To prevent the premature crushing of concrete in the bottom slab the ductility requirement shall be satisfied as follows:

   $D_p<0.42D_t$

   where: D_p = distance from the bottom of the bottom slab to the neutral axis of the composite section at the plastic moment (in.)

   D_t = depth of the composite section measured from the top layer of reinforcing to the bottom of the concrete bottom slab (in.)
5) Shear connectors installed in the bottom flange shall be designed as per LRFD provisions of Article 6.10.10 and 6.11.10.
6) Lateral bracing requirements of the compression flange is eliminated as the entire section is fully braced with the concrete.

7) Designers must consider temporary bracing of bottom flange to support dead weight of concrete till it hardens. The deflection of the bottom flange at all times shall be less than L/360 and stress should be limited to 20 ksi for through thickness bending.

Table 4.4 Design Rules for Double Composite Bridges

No.	Design Rules for Double Composite Section	LRFD Articles
1.	General Dimensioning and Detailing of Bridge Section Straight I – Sections Straight Box Sections	6.7 6.7.4.2 6.7.4.3
2.	*Points of Contraflexure* Points of contraflexure shall be determined based on the appropriate numerical and structural analysis. Analysis should consider AASHTO provisions for geometry and structural analysis. Example: Live load lateral distribution factors	
3.	Design Load and Load Combination Dead Loads Live Load Fatigue Load Load Factors and Load Combination	 3.5 3.6 3.6.1.4 3.4
4.	Structural Analysis and Evaluation of Bridge Superstructures Live Load Lateral Distribution Factors	4.6 4.6.2.2
5.	Cross-Section proportions for I – Section and Box Section	6.10.2 and 6.11.2
6.	Non-Composite and Composite Section Properties	Article 6.10.1.1
7.	Plastic Neutral Axis	Article D6.1
8.	Limit States Service Limit State Fatigue Limit State Strength Limit State	 6.10.4 and 6.11.4 6.10.5 and 6.11.5 6.10.6 and 6.11.6
9.	Flexure Resistance Composite Section in Positive Flexure Non-composite and Composite Section in Negative Flexure	 6.10.7 and 6.11.7 6.10.8 and 6.11.8
10.	*Bottom Slab* The maximum longitudinal Compressive stress in bottom slab at strength limit state shall be less than 0.6f'c. To prevent the premature crushing of the bottom slab the slab ductility requirement shall be satisfied.	 6.10.1.1.1d
11.	Shear Resistance	6.10.9 and 6.11.9
12.	Shear Connectors	6.10.10 and 6.11.10
13.	*Temporary Bracing of Bottom Flange* Bottom Flange at all time shall satisfy the deflection criteria of L/360 and thru thickness bending limited to less than 20 ksi.	

5. MODEL DESIGN OF A DOUBLE COMPOSITE BRIDGE

5.1 Introduction

A model design of a double composite box girder bridge is presented in this chapter. Normal grade 50 steel is used. The design is based on the *AASHTO LRFD Bridge Design Specifications, 3rd Edition, 2004* [12], the *FDOT Structures Design Guidelines (FSDG), January 2005* [13] and design recommendations presented in the previous chapter based on the results of the testing.

A three span continuous twin box girder bridge consisting of two 190 ft end spans and a 236 ft main span s is designed. This configuration was selected because it is identical to an AISI design example for a composite box girder bridge [14]. The design illustrates the application of the design provisions for flexure and shear at an interior pier section where the moments are negative. In the design it was assumed that the bottom slab was cast first, with the top slab cast after the bottom slab had hardened. As a result, the weight of the top slab is resisted by the composite bottom flange.

Design moments were determined using *QConBridge*, a software program developed by the *Washington State Department of Transportation (WSDOT)*. All detailed calculations were carried out using *MathCAD v14.0* as shown in Appendix A.

5.2 Design Overview

The design of double composite bridges involves designing two composite sections corresponding to both the positive and negative moment regions in the continuous element. The basis of design for both sections is similar; differences arise because the load for which the

section acts compositely is not identical and depends on the sequence in which the slabs are cast. Since efficient design requires the bottom steel flange to be as thin as possible, limits are set on its minimum thickness based on buckling considerations. Additional requirements have been proposed in this thesis that limits the maximum stress in the bottom concrete slab as outlined in the previous chapter.

5.2.1 Design Steps

The steps involved in the design example are summarized in this section. Only a design for the negative moment section is presented here. The steps listed below are consistent with those followed in the design example included in the AISI reference.

1) General information and bridge geometry (Section 5.3).
2) Material properties in accordance with AASHTO and ASTM specifications (Section 5.4).
3) Calculation of loads in accordance with AASHTO LRFD provisions (Section 5.5)
4) Calculation of load factors and load combinations for Strength I and Fatigue limit states in accordance with *Article 3.4* of LRFD guidelines (Section 5.6 and Section 5.8).
5) Structural analysis for the load distribution in accordance with *Article 4.6.2.2* of LRFD provisions (Section 5.7).
6) Calculation of section properties for non-composite, short-term composite and long-term composite sections (Section 5.9)
7) Determination of the plastic neutral axis location in accordance with *Article D6.1.*
8) Checking section for Strength I limit state and flexural requirements. Specifically the section should be checked for web slenderness, nominal flexural capacity and flexural resistance of box flanges, stresses in the concrete bottom slab, and shear (Section 5.11 and 5.13).
9) Check that bottom slab satisfies slab ductility requirement to avoid premature crushing of concrete slab (Section 5.11).

10) Detail shear connectors in bottom flange per prevailing LRFD provisions for fatigue and ultimate limit states (Section 5.14).

11) Consider provisions for temporary bracing of bottom flange to support the bottom concrete slab until it hardens (Section 5.15).

5.3 General Information and Geometry

This section presents general information on the bridge and its geometry. Figure 5.1 shows the entire cross-section of the double composite bridge with two box girders. Figure 5.2 shows the typical cross-section of the box girder section considered for the design of negative flexure section. General information is summarized in Table 5.1. Information on the bridge geometry including its cross sectional dimensions are summarized in Table 5.2.

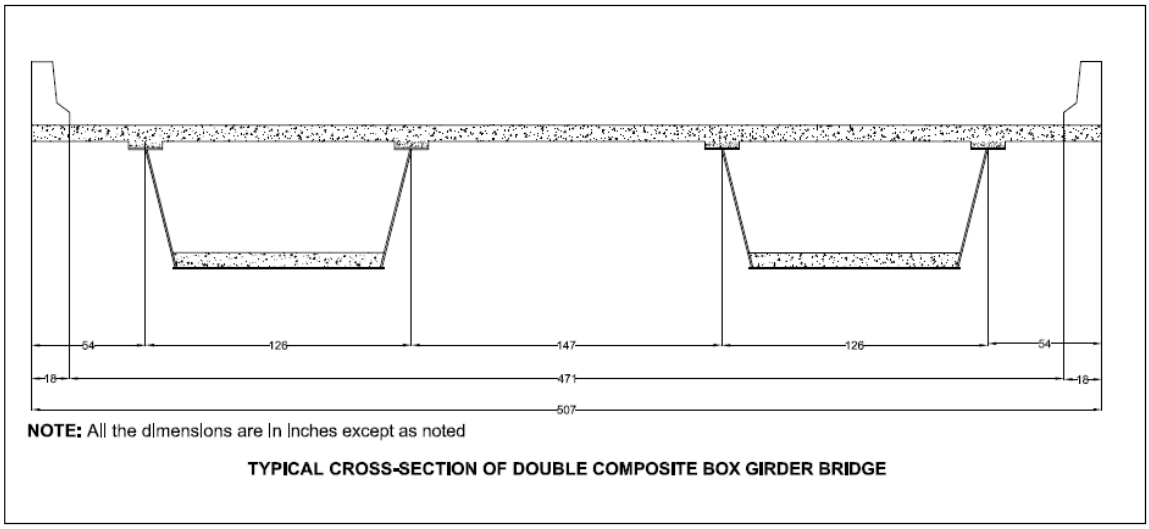

Figure 5.1 Typical Cross-section of Double Composite Bridge

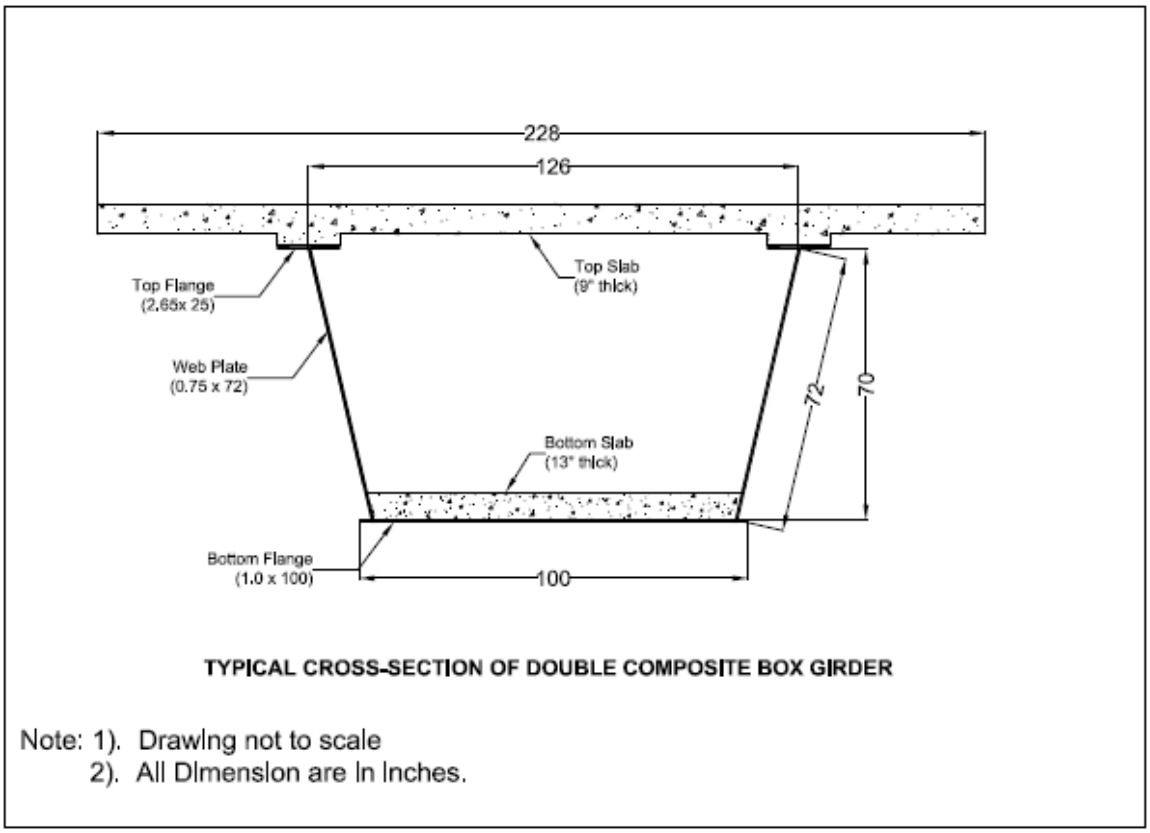

Figure 5.2 Typical Cross-section of Double Composite Box Girder

Table 5.1 General Information

General Information	Notation	Parameter
Number of box girders	N_g	2
Number of spans	N_{sp}	3
Number of design lanes	N_L	3
Length of middle span	L_2	236 ft.
Length of side span (equal length)	L_1	190 ft.
Girder spacing	GS	11.375 ft.
Roadway width	R_w	40 ft.
Concrete deck thickness (structural)	t_{ts}	9 in
Concrete bottom slab thickness	t_{bs}	13 in.
Concrete deck overhang (width)	OH_c	4.5 ft.
Side walks		None
Haunch thickness	t_h	3 in.
Reinforcement ratio	R_r	0.01

Table 5.2 Geometry of Box Girder Section

Girder Dimensions	Notation	Parameter
Web Depth (plumb)	D_w	70 in.
Inclination to vertical is 14.03 deg	θ	14.036°
Web Depth (inclined)	D	72.15 in.
Web plate thickness	t_w	0.75 in.
Top flange thickness	t_{tf}	2.65 in.
Top flange width	b_{tf}	25 in.
Bottom flange thickness	t_{bf}	1.00 in.
Bottom flange width	b_{bf}	100 in.
Height of girder	HG	73.65 in.
Top slab width	b_{ts}	507 in.
Top slab thickness	t_{ts}	9 in.
Bottom slab width	b_{bs}	99.25 in.
Bottom slab thickness	t_{bs}	13 in.
Area of web plate	$A_w = 2Dt_w$	108.23 in.^{2}
Area of top flanges	$A_{tf} = 2b_{tf}t_{tf}$	132.5 in.^{2}
Area of bottom flange	$A_{bf} = b_{bf}tb_f$	100 in.^{2}
Area of Steel Section	$A_s = A_w + A_{tf} + A_{bf}$	340.73 in.^{2}
Area of top slab	$A_{ts} = b_{ts}t_{ts}$	4563 in.^{2}
Area of bottom slab	$A_{bs} = b_{bs}t_{bs}$	1290.25 in.^{2}

5.4 Materials

Table 5.3 summarizes information on the compressive strength of the concrete, the yield strength of the steel and the unit weight of the stay-in-place form and future wearing surface assumed in the design.

Table 5.3 Material Properties

Material	Notation	Unit Weight	Notation	Design Value (ksi)
Concrete	γ_c	145 pcf	f'_c	6.5
Structural steel	γ_s	490 pcf	F_y	50
Reinforcing steel	-	-	f_{yr}	60
Shear connectors	-	-	f_{ys}	60
Stay in place form	γ_{sip}	20 psf	-	-
Future wearing surface	γ_{ws}	21 psf	-	-

5.4.1 Concrete

The compressive strength of the concrete is assumed to be 6500 psi. The concrete used in the bridge must conform to AASHTO Specifications. Normal weight concrete is used with a unit weight of 145 pcf. Table 5.4 summarizes design parameters assumed in the design.

Table 5.4 Design Parameters

Design Parameters	**Notations**	**Design Value (ksi)**
Design concrete strength	f_c	6.5
Modulus of concrete	E_c	4181
Yield strength of steel	F_y	50
Modulus of steel	E_s	29000
Shear modulus of steel	G_s	12000

The modulus of concrete in Table 5.4 was calculated in accordance with FSDG for limestone aggregates as:

$$E_c = 0.9 \times 33000 \times w_c^{1.5} \times \sqrt{f'_c} = 0.9 \times 33000 \times \left(0.145\right)^{1.5} \times \sqrt{6.5} = 4181\text{ksi}$$

5.4.2 Structural Steel

Grade 50 structural steel conforming to ASTM A709 specifications was used for the box girder plates. Nominal yield strength is 50 ksi and unit weight is 490 pcf.

5.4.3 Steel Reinforcement

Grade 60 steel bars conforming to ASTM 615 specifications are used for reinforcing both the top and bottom slabs. Nominal yield strength is 60 ksi.

5.4.4 Shear Connectors

Shear connectors used are in accordance with AASHTO M 169 and ASTM A108 specifications. The ¾ in. diameter shear connectors used in the top and bottom concrete slab have a nominal yield strength of 60 ksi.

5.4.5 Miscellaneous

Stay-in-place forms are used for the placement of the top concrete slab. Unit weight is 20 psf. The unit weight of the future wearing surface is taken as 21 psf. The unit weight of the 1.5 ft wide concrete barrier is taken as 581 plf.

5.5 Design Loads

This section provides information for the design dead, live and fatigue loads which were calculated in accordance with AASHTO LRFD provisions. The loads presented here were calculated for the negative moment section at an interior pier. Since the model bridge is straight and has uniform deck and overhang widths, the design loads are equally shared between the two box girders.

5.5.1 Dead Load

Dead loads used in the design were grouped into four separate load cases to account for the various stages of construction and differing load factors specified in AASHTO LRFD. Permanent loads which generated moments resisted by the steel girder only (i.e., non-composite section) were grouped into load case DC1 as shown in Table 5.5. This included the self-weight of the steel girder, an additional 10% allowance for steel detailing elements (e.g., shear studs, stiffeners, etc.) and the reinforced concrete bottom slab prior to curing.

Table 5.5 Non-composite Dead Loads Per Box Girder

Dead Loads	Load Case	Unit Weight	Cross-sectional Area (in^2)	Load (klf)
Steel Section	DC1	490 pcf	340.73	1.16
Steel Details	DC1	490 pcf	31.82	0.116
Bottom Slab	DC1	150 pcf	1287	1.34
Total				2.62

Permanent loads which resulted in negative moments carried by the composite section, comprised of the structural steel and the bottom slab, were grouped into load case DC2 as shown in Table 5.6. This included the weight of the stay-in-place forms and the reinforced concrete top slab, including haunches.

Table 5.6 Composite Dead Loads Per Box Girder

Dead Loads	Load Case	Unit Weight	Cross-sectional Area (in^2)	Load (klf)
SIPs	DC2	20 psf	n/a	0.27
Haunches	DC2	150 pcf	132	0.156
Top Slab	DC2	150 pcf	2281.5	2.377
Total				2.803

The superimposed loads resulting from the placement of the concrete traffic barriers and future wearing surface were classified as separate load cases (i.e., DC3 and DW) in order to account for the differing load factors specified in AASHTO LRFD. The weight of the barrier and the weight allowance for the wearing surface, as shown in Table 5.7, were selected to match the values used in the AISI example in order to maintain a consistent loading condition.

Moments generated by the superimposed dead loads are resisted by the fully composite box girder, including the structural steel webs and flanges, the bottom slab concrete and the longitudinal reinforcing steel located in the top slab.

Table 5.7 Superimposed Dead Loads Per Box Girder

Dead Loads	Load Case	Unit Weight	Length (ft)	Load (klf)
Concrete barrier	DC3	n/a	n/a	0.581
Wearing Surface	DW	21 psf	20	0.420

5.5.2 Live Load

Vehicular live load considered for the design was based on the AASHTO HL-93 model, whereby live load is a combination of a design truck or a design tandem and design lane loads (see *AASHTO 3.6.1.2*). The design truck used was the HS 20 truck.

Since the calculation of live load moments for multi-span continuous bridges is tedious, *QConBridge*, a free software program from the Washington State Department of Transportation, was used to calculate the design live load moments, as well as the dead load moments. The calculated live load moments are resisted in full by the short-term composite section, D, as defined in section 5.9.

5.5.3 Fatigue Load

The fatigue loading used in the design of the bottom slab shear connectors was calculated in accordance with AASHTO *Article 3.6.1.4*. An HS 20 design truck was used to calculate the maximum fatigue related moments using the *QConBridge* software.

5.6 Load Factors and Load Modification Factors

This section provides information on the load factors for the Strength I and Fatigue limit states and the load modification factors used in the design.

5.6.1 Load Factors

The load factors for dead load, live load and fatigue load for the Strength I and Fatigue limit states are specified in Table 5.8. These factors are in accordance with *Article 3.4* of LRFD guidelines.

Table 5.8 Load Factors for Strength I and Fatigue

Limit State	Dead Load γ_{DC}	Wearing Surface γ_{DW}	Live Load γ_{LL}
Strength I	1.25	1.50	1.75
Fatigue	-	-	0.75

5.6.2 Load Modification Factors

Load modification factors are multipliers associated with ductility, redundancy and operational importance as described in *Articles 1.3.2, 1.3.3 and 1.3.4* of the AASHTO LRFD specifications. Once determined, the individual modification factors are multiplied together to obtain a single number. They can also vary in relation to the limit state under consideration. However, in this design example, the load modifier for each of the limit states considered, Strength I and Fatigue, is simply one. Therefore, the final design moments are unaffected by the load modification factors.

5.7 Distribution Factors

Distribution factors are used to distribute the live load moments and shears in the lateral direction. The distribution factors used in this design were determined using the approximate method for beam-slab bridges in accordance with *Article 4.6.2.2* of the LRFD guidelines. The following conditions must be satisfied to use the approximate method:

1) Width of the deck is constant.
2) Number of beams is not less than four unless otherwise specified.
3) Beams are parallel and have approximately the same stiffness.
4) The roadway portion of the overhang does not exceed 36 inches, unless otherwise specified.
5) The cross-section is consistent with one of the cross-sections shown in *Table 4.6.2.2.1-1* in the LRFD specifications.

Since the conditions specified above are met, live loads may be uniformly distributed among all of the beams. The following equation is used for determining the distribution factors for live load moment and shear. The live load distribution factor, DF_{LL}, for moment and shear works out to be 1.467.

$$DF_{LL} = 0.05 + \left(0.85 \times \frac{N_L}{N_g}\right) + \frac{0.425}{N_L} \qquad \text{(AASHTO Table 4.6.2.2.2b-1)}$$

DF_{LL} = Distribution factor for Live Load, N_L = Number of lane, N_g = Number of girders

$$\therefore DF_{LL} = 0.05 + \left(0.85 \times \frac{3}{2}\right) + \frac{0.425}{3} = 1.467$$

In this example there are 3 design lanes (N_L) and two box girders (N_g), so the ratio N_L/N_g is 1.5. If this ratio exceeds 1.5, a more refined analysis is required to take into consideration torsional effects.

Since fatigue load is placed only on one lane, its distribution factor must accordingly be adjusted using the above equation. This distribution factor turns out to be 0.9 as follows:

$$DF_{FL} = 0.05 + \left(0.85 \times \frac{1}{2}\right) + \frac{0.425}{1} = 0.9$$

In addition to lateral distribution, live load has to account for dynamic effects in accordance with *Article 3.6.2*. The dynamic load allowance factor for the strength and fatigue limit states are 1.33 and 1.15, respectively.

5.8 Load Combinations

The AASHTO LRFD load combinations considered for the model design were Strength I and Fatigue. The box girder section was designed for Strength I, and the shear connectors were designed for strength and fatigue. The maximum negative moment occurs at the interior pier supports. The maximum unfactored and factored moments for the Strength I load combination

are summarized in Table 5.9. Table 5.10 summarizes the maximum unfactored and factored shear forces at the interior pier section.

In these tables, the DC1 load case represents dead load forces resisted by the non-composite steel girder section only, DC2 forces are resisted by the composite steel girder and bottom slab section, the DC3 forces were generated by the placement of the concrete traffic barriers, DW represents loads from a future wearing surface, and LL+IM are live load plus impact forces.

Table 5.9 Maximum Unfactored and Factored Moments at Interior Pier Section

DC1	DC2	DC3	DW	LL+IM	1.25 DC1	1.25 DC2	1.25 DC3	1.5 DW	1.75 LL+IM	Max. Neg. Moment M_u
6536	12410	2670	1930	10580	8170	15513	3338	2895	18515	48430

Note**:** All moments are expressed in ft-kips

Table 5.10 Maximum Unfactored and Factored Shear at Interior Pier Section

DC1	DC2	DC3	DW	LL+IM	1.25 DC1	1.25 DC2	1.25 DC3	1.5 DW	1.75 LL+IM	Max. Shear V_u
206	321	70	49	302	258	401	88	74	529	1348

Note**:** All shear forces are expressed in kips

5.8.1 Location of Inflection Points

The negative moment section extends from the points of inflection in the end span (L_1) and the main span (L_2). The location of these inflection points is affected by several factors such as the type of loading (uniform or concentrated), position of load (placement of truck load for maximum effect), span geometry (interior to exterior span ratio).

In this example, the ratio of the main to the end span is 1.24 (236/190). For this case, the inflection point is $0.27L_1$ [10, 11] from the interior support. This works out to be 0.27 x 190 = 51 ft from the interior support in the end span.

The inflection point in the main span (L_2) for different span ratios ranging from 1.0 to 1.7 was found to vary from $0.2L_2$ to $0.25L_2$. For this case where the ratio is 1.24, the inflection point is at a distance of $0.22L_2$ (52 ft) from interior support in the main span. The total length of the section under negative moment is therefore 51 ft + 52 ft = 103 ft.

On a conservative note, the inflection points can be generalized to be taken as 0.3L, where L is the span length for span ratio varying from 1.2-1.4.

5.9 Section Properties

The section properties of the steel box girder cross-section must be calculated for both non-composite and composite action. Composite action additionally takes into consideration the effects of concrete creep for transient (i.e., short-term) and sustained (i.e., long-term) loading by using different values of the modular ratio, *n*, in accordance with *Article 6.10.1.1*. The modular ratio is given by:

$$n = \frac{E_S}{E_C} = \frac{29000\,ksi}{4181\,ksi} = 6.9 \quad \text{whereby} \quad 3n = 20.7$$

Section properties for five different sections must be calculated. These are non-composite (Section A), short-term composite section with bottom slab (Section B), long-term composite section with bottom slab (Section C), short-term composite section considering top slab rebars, bottom slab and structural steel (Section D), and long-term composite section considering top slab rebars, bottom slab and structural steel (Section E). These properties are summarized in Table 5.11. The section property calculations can be found in Appendix A.

Table 5.11 Section Properties for Non-composite and Composite Sections

Section	Section Properties						
	Cross-sectional Area ($in.^2$)	Moment of Inertia ($in.^4$)	Neutral Axis (in.)		Section Modulus ($in.^3$)		
			Bottom	Top	Bottom Flange	Bottom Slab	Top Flange
A	341	340456	39.707	33.943	8574	-	10030
B	528	449569	28.295	45.355	16551	118390	10325
C	403	395991	34.726	38.924	11403	243044	10173
D	549	525077	30.329	55.321	17312	123529	12120
E	424	439256	37.039	48.611	11859	252302	11997

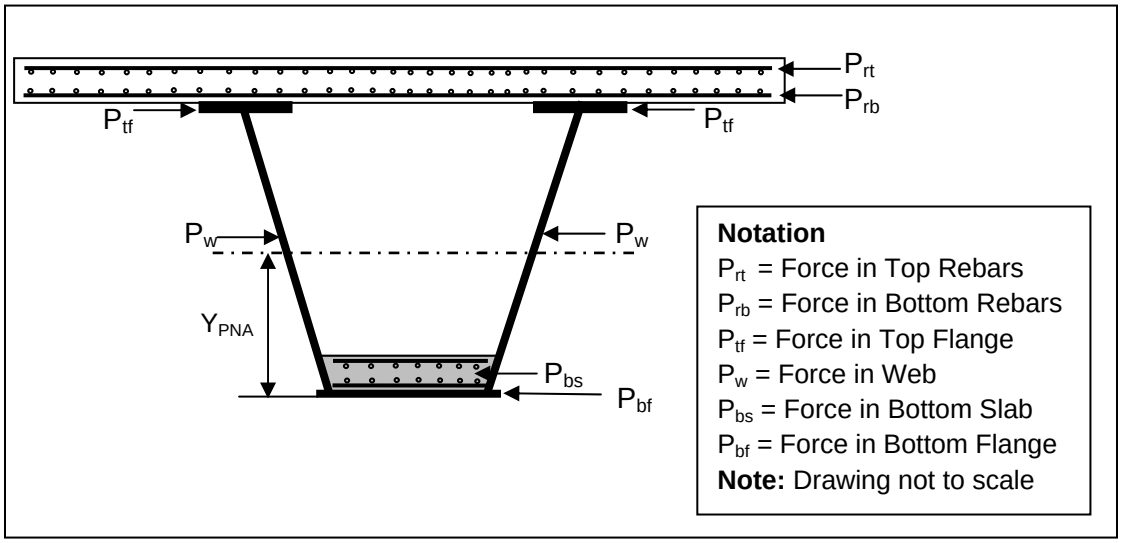

Figure 5.3 Forces in the Cross-section

5.10 Plastic Neutral Axis

The location of the plastic neutral axis must be determined in order to ensure that the section meets the ductility requirement described in *Article 6.10.7.3* of AASHTO LRFD. The location of the plastic neutral axis can be determined using the formulas presented in *Article D6.1* of the LRFD guidelines. The following steps are used to calculate the plastic moment:

1) Determine general location of the plastic neutral axis (P.N.A) by comparing forces in the flanges and webs

Calculate forces due to structural steel, bottom concrete slab and reinforcement in top concrete slab. Table 5.12 shows the calculation of forces in the cross-section.

Table 5.12 Forces in the Cross-section

Force	Expression	Input Values	Force (kips)
Force in top rebars	$P_{rt} = 0.0067 \times b_{eff} \times t_{ts} \times f_{yr}$	$= 0.0067 \times 232\ in. \times 9\ in. \times 60\ ksi$	841.2
Force in bottom rebars	$P_{rb} = 0.0033 \times b_{eff} \times t_{ts} \times f_{yr}$	$= 0.0033 \times 232\ in. \times 9\ in. \times 60\ ksi$	414.3
Force in top flange	$P_{tf} = 2 \times b_{tf} \times t_{tf} \times F_y$	$= 2 \times 25\ in. \times 2.5\ in. \times 50 ksi$	6625
Force in web	$P_w = 2 \times D \times t_w \times F_y$	$= 2 \times 72.15\ in. \times 0.75\ in. \times 50 ksi$	5411.4
Force in bottom flange	$P_{bf} = b_{bf} \times t_{bf} \times F_y$	$= 100\ in. \times 1.0\ in. \times 50\ ksi$	5000
Force in bottom slab	$P_{bs} = 0.85 \times f_c \times b_{bs} \times t_{bs}$	$= 0.85 \times 6.5 ksi \times 99\ in. \times 12\ in.$	7128

The total tension force in the top slab rebar, flanges and webs is greater than the compression force in the bottom flange and bottom concrete slab. Therefore, the plastic neutral axis lies somewhere in the web. Since the magnitude of force in bottom flange and bottom slab is greater the neutral axis lies in bottom concrete slab along with web.

$$P_{re} + P_{tf} + P_w > P_{bf} + P_{bs}$$

2) Calculate the location of the plastic neutral axis from the bottom of the bottom flange.

The plastic neutral axis (Y_{PNA}) is taken from the bottom of the bottom flange. Its location is determined by summing forces as follows:

$$P_{re} + P_{tf} + \left(\frac{P_w}{D}\right) \times \left[\frac{\left(D_w + t_{bf}\right) - Y_{PNA}}{\cos\theta}\right] - P_{bf} - P_{bs} - \left(\frac{P_w}{D}\right) \times \left[\frac{Y_{PNA} - t_{bf}}{\cos\theta}\right] = 0$$

Substituting values obtained in the previous step in the above equation, Y_{PNA} is found.

$$\therefore 1255.5 + 6625 + \left(\frac{5411.43}{72.15 in.}\right) \times \left[\frac{\left(70 in. + 1 in.\right) - Y_{PNA}}{\cos\left(14.036\right)}\right] - 5000 - 7128$$
$$- \left(\frac{5411.43}{72.15 in.}\right) \times \left[\frac{Y_{PNA} - 1 in.}{\cos\left(14.036\right)}\right] = 0$$

$$\therefore Y_{PNA} = \frac{1325\, kip}{154.5\left(kip/in.\right)} = 8.603 in.$$

Thus, Y_{PNA} is located 8.603 in. from the extreme bottom fiber of the box girder section, which places it within the concrete bottom slab.

Note: The equilibrium equation used here does not account for the loss of compressive force for the bottom slab concrete above the plastic neutral axis. However the result is adequate for the design.

5.11 Strength I Limit State

Design checks related to the Strength I limit state are presented in this section. The model design section must satisfy the AASHTO LRFD requirements for composite members and the design recommendations presented in Chapter 4 of this document, including limits for web slenderness, concrete compressive stress, steel top flange stress and concrete slab ductility.

5.11.1 Web Slenderness

Web slenderness criterion is checked as per *Article 6.10.6.2.3* of the AASHTO specifications. The following equation defines the slenderness limit of the web in composite and non-composite sections in the negative flexure region.

$$2\ \frac{D_c}{t_w} \le 5.7\ \sqrt{\frac{E_s}{F_y}}$$

Where D_c = depth of the web in compression in the elastic range determined as specified in *Article D6.3.1.*

$$D_c = \left(\frac{-f_c}{|f_c| + f_t}\right) d - t_{tf} = \left(\frac{-(-46.90)}{|-46.90| + 52.64}\right) - 2.5 \ge 0$$

$$\therefore D_c = 30.32 in.$$

Substituting the value of D_c in the above equation.

$$L.H.S = 2 \times \frac{30.32 in.}{0.75 in.} = 80.89 \qquad R.H.S = 5.7 \times \sqrt{\frac{29000 ksi}{50 ksi}} = 137.27$$

$$\therefore L.H.S \le R.H.S$$

Therefore, the section satisfies the AASHTO web slenderness criteria.

5.11.2 Slab Ductility Requirement for Bottom Slab

In order to prevent premature crushing of the concrete in the bottom slab, the ductility requirement for the bottom concrete slab must be satisfied. The following equation gives the ductility criteria to avoid premature crushing of concrete.

$D_p < 0.42 D_t$

where:

D_p = distance from the bottom of the concrete bottom slab to the neutral axis of the composite section at the plastic moment (in.)

D_t = depth of the composite section measured from the top layer of reinforcing to the bottom of the concrete bottom slab (in.)

$$D_p = Y_{PNA} - t_{bf} = 8.603\, in - 1.0 in = 7.603\, in$$

$$D_t = D_w + t_{tf} + t_h + t_{ts} - 2in = 70in + 2.65in + 3in + 9in - 2in = 82.65in$$

$$\frac{D_p}{D_t} = \frac{7.603\,in.}{82.5in.} = 0.092$$

Therefore, the bottom slab satisfies the slab ductility requirement to avoid the premature crushing of concrete.

5.11.3 Compressive Stress in Concrete Slab

As explained in Chapter 4 of this document, stress in the composite concrete bottom slab shall be limited to 0.6f'c.

The maximum stress developed in the bottom slab due to factored loads is given by:

$$f_{bsu} = \frac{M_{DC2}}{S_{bsB}} + \frac{M_{D3} + M_{DW}}{S_{bsD}} + \frac{M_{LL}}{S_{bsD}} \geq \frac{M_{DC2}}{S_{bsC}} + \frac{M_{D3} + M_{DW}}{S_{bsE}} + \frac{M_{LL}}{S_{bD}}$$

$$\therefore f_{bsu} = \frac{15513\ \ ft - kip}{118391\ \ in^3} + \frac{3338\ + 2895\ \ ft - kip}{123529\ \ in^3} + \frac{18515\ \ ft - kip}{123529\ \ in^3} = 3.97\ ksi$$

$$\therefore f_{bsu} \geq 0.6 \times 6.5ksi = 3.9ksi$$

Eventhough, the stress in bottom concrete slab exceeds 0.6f'c by 2 %, for the purpose of this example the bottom slab is acceptable.

$\therefore f_{bsu} \leq 0.6 f'_c$ is satisfied for the bottom slab

5.11.4 Flexural Resistance of Steel Flanges

The flexural resistance of the bottom steel flange in compression and the top steel flanges in tension to resist negative moments are checked in this section. The flexural resistance of the box flanges in negative flexure shall be determined in accordance with *Article 6.11.8* of the LRFD guidelines.

Assuming that torsional shear stresses in the flange are negligible, the nominal flexural resistance of the compression flange is determined in accordance with *Article 6.11.8.2*.

$$F_{nc} = R_b \times R_h \times F_y \times \Delta$$

Where, R_b = 1.0, web load-shedding factor determined as specified in *Article 6.10.1.10.2.*

R_h =1.0, hybrid factor determined as specified in *Article 6.10.1.10.1.*

Δ = 1.0 (assumed)

$$\therefore F_{nc} = 1.0 \times 1.0 \times 1.0 \times 50ksi = 50ksi$$

Similarly the flexural resistance of the tension flange is $F_{nt} = F_y$

$$\therefore F_y = 50ksi$$

Flexural Resistance limit state of Compression Flanges

$$f_{bu} \le \phi_f \times F_y$$

The maximum stress developed in the compression flange due to factored loads is given by:

$$f_{bu} = \frac{M_{DC1}}{S_{bA}} + \frac{M_{DC2}}{S_{bB}} + \frac{M_{D3} + M_{DW}}{S_{bD}} + \frac{M_{LL}}{S_{bD}} \quad \ge \quad \frac{M_{DC1}}{S_{bA}} + \frac{M_{DC2}}{S_{bC}} + \frac{M_{D3} + M_{DW}}{S_{bE}} + \frac{M_{LL}}{S_{bD}}$$

$$\therefore f_{bu} = \frac{8170\ ft - kip}{8574\ in.^3} + \frac{15513\ ft - kip}{16551\ in.^3} + \frac{(3338 + 2895)\ ft - kip}{11859\ in.^3} + \frac{18515\ ft - kip}{17312\ in.^3} = 46.90\,ksi$$

$$\therefore f_{bu} \le 1.0 \times 50ksi = 50ksi$$

$\therefore f_{bu} \le \phi_f \times F_y$ is satisfied for the compression flange. Similarly, the tension flange can be checked using the same criteria. Calculations for the tension flange are shown in Appendix A.

5.12 Shear Design

The section must be checked for the maximum shear force. Since the maximum shear is at the interior support section, this section will be checked. Shear design of the web is in accordance with *Article 6.10.9 and 6.11.9*.

Table 5.10 indicates that the maximum factored shear is 1348 kips for Strength I limit state. This shear is not accounted for the impact at ultimate limit state. The total shear for ultimate limit state is 1348 kips. However, this shear is equally distributed to both webs of the box girder section.

Maximum shear for the single web $V_{us} = 674\ kips$

The inclination of the web should also be taken into consideration.

$$V_u = \frac{V_{us}}{\cos\theta} = \frac{674\,kips}{\cos 14.036} = 695\,kips$$

Therefore the maximum shear considered for design is 695 kips.

5.12.1 Nominal Shear Resistance of Unstiffened Webs

The nominal shear resistance for the unstiffened webs is calculated as per *Article 6.10.9* in this section. The resistance factor (Φ_v) for shear design is 1.0 as per *Article 6.5.4.2*. The following steps show the shear design of the web.

1) Determine plastic shear force in accordance with *Article 6.10.9.2.*

$V_P = 0.58 \times F_y \times D \times t_w$ $\quad\quad$ $\therefore V_P = 0.58 \times 50ksi \times 72.15in \times 0.75in$

$\therefore V_P = 1569\ kips$

2) Determine the nominal shear resistance of the web.

$V_n = C \times V_p$, Where C is the ratio of shear buckling stress to the yield strength

C should be determined in accordance with *Article 6.10.9.3.2-6.*

If $\frac{D}{t_w} > 1.40\sqrt{\frac{E_s \times k}{F_y}}$ then $C = \frac{1.57}{\left(\frac{D}{t_w}\right)^2}\left(\frac{E_s \times k}{F_y}\right)$

Where, k = 5.0, shear buckling co-efficient.

In this case, $\frac{D}{t_w} = \frac{72.15\,in}{0.75\,in} = 96.2$ and $1.40\sqrt{\frac{E_s \times k}{F_y}} = 1.40 \times \sqrt{\frac{29000ksi \times 5}{50ksi}} = 75.392$

Since, $\frac{D}{t_w} > 1.40\sqrt{\frac{E_s \times k}{F_y}}$ hold true, the above equation for calculating C can be used.

$$\therefore C = \frac{1.57}{\left(\frac{72.15\,in.}{0.75\,in.}\right)^2}\left(\frac{29000\ ksi \times 5}{50\ ksi}\right) = 0.492$$

$\therefore V_n = 0.492 \times 1569 = 772\ kips$ $\therefore \phi_v \times V_n = 1.0 \times 772 = 772\ kips$

Therefore, the nominal shear capacity of single web is 772 kips. Since, Vu = 695 kips is less than $\phi_v \times V_n = 772\ kips$, the section satisfies the nominal shear criteria.

5.13 Shear Connectors

There is no change in the design procedure of the shear connectors for the top flange in the negative flexure region. The shear connectors on the bottom flange are designed for the same provisions as the top flange in *Article 6.10.10* and *6.11.10.*

The fatigue life and nominal fatigue resistance of shear connecters are designed as per *Article 3.6.1.4* and *Article 6.6.1.2.5.* The detailed calculations for the design of shear connectors are presented in the Appendix A. However, the steps in the design of shear connectors are summarized below.

1) Ultimate resistance of shear connectors shall be calculated in accordance with *Article 6.10.10.4.*
2) Number of shear connectors shall be determined based on the ultimate resistance of the shear connectors.
3) Determine the fatigue life of the bridge in accordance with the *Article 3.6.1.4* and *Article 6.6.1.2.5.*

4) Determine the nominal fatigue resistance of shear connectors as per *Article 6.6.1.2.5* and *Article 6.10.10.2*.
5) Lateral spacing and longitudinal pitch of shear connector should be determined as per existing LRFD guidelines.

In this case, the total number of shear connectors required to connect the bottom slab to the bottom flange is 1940 with a longitudinal pitch of 18 in.

However the bottom flange should be checked for buckling between the shear stud lines. The spacing between two shear stud lines on bottom flange is 18 in. Classical theory on stability of plates is used to determine plate buckling. From the analysis it was found that the longitudinal spacing of 20 in. was adequate to prevent buckling failure. Refer Appendix G for the detailed calculations.

5.14 Temporary Bracing of Bottom Flange

Temporary bracing of the bottom flange should be considered by the designer to support the dead weight of the bottom concrete slab until it cures. The bottom flange deformation should follow the L/360 criteria for deflection and the through thickness bending stress in the bottom flange during construction should not exceed more than 20 ksi. The bottom flange should always be in accordance with the *Article 6.10.3* and *6.11.3* which describes the construction related guidelines. Lateral bracing of the bottom flange should be removed once the bottom slab hardens.

In this case, the bottom flange was braced with WT 8 × 13 members. The maximum spacing between the braced sections was 2 ft. and maximum stress was limited to 7.8 ksi. The maximum deflection of 0.287 in. was observed with bracing at 2 ft. Detailed calculations of the composite section properties, load, deflection and stress are included in the Appendix A.

5.15 Material Cost Comparison

The material (concrete and steel) cost of the double composite bridge was compared with the referenced AISI example having the overall dimensions, span configuration under the same loading. The difference in cost is due to the difference in the amount steel required by the negative moment region for the two designs. Several alternates with different concrete strength and different thickness of bottom flange and bottom slab were compared to select optimum section.

Table 5.13 Cost Analysis of Materials used in Negative Flexure Region for Single Composite Section

Qty	Single Composite Section	Dimensions				Total		Cost ($)
		Length (ft)	Width (in)	Thickness (in)	X-Sect Area (in^2)	Volume (ft^3)	Weight (lbs)	
4	Bottom Flange	100.0	100.0	1.375	-	381.94	187153	$402,378
4	Stiffener (WT 12x34)	100.0	-	-	10.0	27.78	13611	$71,458
Total								$473,837

Table 5.14 Cost Analysis of Materials Used in Negative Flexure Region for Double Composite Section

Qty	Single Composite Section	Dimensions				Total		Cost ($)
		Length (ft.)	Width (in.)	Thickness (in.)	X-Sect Area ($in.^2$)	Volume ($ft.^3$)	Weight (lbs)	
4	Bottom Flange	100.0	100.0	1.0	100	278	136111	$292,639
4	Bottom Slab	100.0	99	13	1290	3575	518375	$105,926
-	Reinforcing Steel	-	-	-	-	-	17875	$19,663
1940	Shear Connectors	0.5	-	0.75 (diameter)	-	3.31	1620	$2,430
204	Temporary Bracing	8.33	-	-	3.84	33.17	22213	$19,437
Total								$440,094

In the comparison, costs are based on the latest cost data; these are $ 800 per cubic yard for structural concrete and $ 2.15 per pound of steel. The corresponding costs per cubic feet are $35 for structural concrete and $1053 for structural steel.

Table 5.14 and 5.15 shows the cost analysis of the materials used in negative flexure region for both ‘single’ and ‘double’ composite sections. The inspection of Table 5.14 and 5.15 shows that there is approximate saving of $ 33,743 in terms of materials used in negative flexure region for double composite section. This approximates to net savings of 7 %.

Table 5.15 Cost Comparison of Double Composite Sections

Double Composite Sections					
Alternate	Concrete Strength (psi)	Bottom Slab Thickness	Bottom Flange Thickness	Cost Savings ($)	Cost Savings (%)
1	6500	13	1.0	33,743	7
2	7500	10	1.0	62,215	13
3	8500	9	0.875	107,375	23
4	10,000	7	0.875	126,860	27

5.16 Summary

The thickness of the bottom flange in the referenced AISI example was 1.375 in. and the bottom flange was stiffened by WT sections with an approximate cross-sectional area of 10 sq. in. In contrast, in the double composite section, the bottom flange thickness reduced to 1.0 in. and no stiffeners were needed. The thickness of bottom concrete slab between the contraflexure points was maintained constant at 12 in. in the proposed design.

Several other alternate with high strength concrete were considered. Table 5.16 summarizes cost savings for all the different alternates for double composite section. In all the cases, stress in the bottom concrete slab was limited to 0.6f'c. Table 5.16 shows that by using high strength concrete, the thickness of bottom slab and steel bottom flange can be reduced. This increases the cost savings significantly for double composite sections in the negative flexure region.

The double composite design required the bottom slab to be checked for the new slab ductility requirement to avoid premature crushing of the concrete slab. Also, the section was designed as non-compact in the negative flexure region. The concrete slab continuously braces the compression flange and therefore eliminates the need for lateral bracing.

The bottom flange was temporarily braced every 2 ft to limit deflection and through thickness bending while it supported the weight of the weight concrete during construction.

6. CONCLUSIONS AND RECOMMENDATIONS

6.1 Introduction

The work reported in this thesis is from a cooperative research project between USF/FDOT/URS. In the project, a full-scale 'double composite' box girder section designed to the AASHTO specifications were tested under fatigue, service and ultimate loads. Following completion of the testing and analysis of the data by USF, design rules were proposed by URS Corporation. This thesis focuses on the application of these newly developed design rules for the LRFD design of double composite box girder bridges. For completeness, it also provides an overview of the experimental testing conducted by FDOT and URS' interim design provisions. These rules will be finalized following completion of the non-linear finite element analysis.

6.2 Conclusions

Based on the information presented in the thesis and the experience of the author, the following conclusions may be drawn:

1) The proposed rules incorporate minor changes to current AASHTO LRFD provisions. As such they do not add undue complexity and the design of double composite box girder bridges is simple and straight forward.
2) The envelope of the points of contraflexure was used in this study to identify the negative moment section that is made composite. In practice, it may be simpler to use a single value, e.g. 0.3L.

3) The illustrative example showed that compared to “single” composite design, the double composite design with the use of high strength concrete provided cost savings up to27% and cost savings of $ 126,860 in the negative flexure region.

6.3 Future Work

This study did not address all issues relating to the design of double composite box girders. The following issues need further investigation:

Since negative moments drop off rapidly, the thickness of the bottom slab may be varied. Guidelines are needed based on the specified locations of the contraflexure point.

1) The type of reinforcement provided in the bottom slab needs to be evaluated. The bottom slab is restrained by the steel webs and is not subjected to localized wheel loads. There may be a need for additional shrinkage and temperature steel above current requirements to prevent the type of cracking that occurred in the test specimen.
2) Guidelines should be prepared to provide information on the (1) minimum thickness of the bottom flange, (2) optimal shear connector configuration for the bottom flange and (3) grade of concrete to be used in the bottom slab.
3) Hybrid sections in which different grades of steel are used for the top and bottom flanges and the web may be the most economical. Guidelines should be developed based on appropriate numerical analysis.
4) Creep effects in the bottom slab need to be explored since it sustains larger permanent loads than the top slab.

REFERENCES

1. Martinez-Calzon, Julio (1995). *Strict Box Composite Bridges A New Design of the Optimum Use of Composite Topology*, Proceedings of the 12th Annual International Bridge Conference and Exhibition, June 19-21, Pittsburgh, PA, pub. Engineers' Society of Western Pennsylvania, pp. 258-264.

2. Saul, Reiner (1996). *Bridges with Double Composite Action*, Structural Engineering International, International Association for Bridge and Structural Engineering, Vol. 6, No 1, pp. 32-36.

3. Saul, Reiner (1997). *Design and Construction of Long Span Steel Composite Bridges in Composite Construction in Steel and Concrete III*: Proceedings of an Engineering Foundation Conference, Irsee, Germany, pp. 700-712.

4. Stroh, Steven (1994). *Design of a Double Deck Cable Stayed Bridge for Combined Highway and Railway Traffic*, Proceedings of the 10th Joint US-Japan Workshop on Performance on Strengthening of Bridge Structures and Research Needs, Lake Tahoe, Nevada, May.

5. Stroh, Steven, and Lovett, Thomas (1995). *Kap Shui Mun Cable Stayed Bridge*, Proceedings of the Fourth International Bridge Engineering Conference Volume I, Transportation Research Board, San Francisco, August, pp. 259-265.

6. Calzon, J.M. (1998). Strict Box Composite Bridges: A Proposal for the Optimization of Materials, in Developments in Short and Medium Span Bridges '98, Calgary, Canada, 1-16.

7. Saul, Reiner (1992). *Longspan Bridges with Double Composite Action*, *Composite Construction in Steel and Concrete II* - Proceedings of an Engineering Foundation Conference, June 14-19, Potosi, MO, Pub. ASCE New York, pp. 608-622.

8. RPX – 95 (1995). *Recommendations for the Design of Composite Road Bridges*. Madrid, Spain.

9. Salmon, C.G. and Johnson, J.E. (1996). *Steel Structures: Design and Behavior*. Harper Collins, NY, NY. Fourth Edition. p.639.

10. AISC Manual of Steel Construction (2007), 13th Edition, Chicago, IL, pp 3-224–3-225.

11. Retrieved on June 26, 2009, from http://www.bridgesite.com.

12. AASHTO LRFD Bridge Design Specifications (2004), 3rd Edition, Washington, DC.

13. Florida Structures Design Guidelines (2005), Tallahassee, FL.

14. AISI (1995). *Four LRFD Design Examples of Steel Highway Bridges.* Vol. II Ch 1A, Highway Structures Design Handbook, Prepared by HDR Engineering Inc, Chicago, IL.

APPENDICES

Appendix A: Design of a Double Composite Box Girder Bridge

This appendix presents all the design calculations for the negative flexure region of three span continuous box girder test specimen. All the design calculations are performed in MathCAD v.14 Software.

A.1 Given Requirements

Number of girders	$N_g := 2$
Number of spans	$N_{sp} := 3$
Number of design lanes	$N_L := 3$
Length of middle span	$L_2 := 236\ ft$
Length of side span (equal length)	$L_1 := 190\ ft$
Girder spacing	$GS := 11.375\ ft$
Roadway width	$RW := 40\ ft$
Concrete deck thickness (structural)	$T_{ts} := 9\ in$
Concrete deck overhang	$OH_c := 4.5\ ft$
Haunch thickness	$t_h := 3\ in$
Reinforcement Ratio	$R_r := 0.01$

Appendix A (Continued)

A.2 Materials

This section provides the information about the materials used in the design of box girder bridge

Concrete

Compressive strength of concrete, f_c	$f_c := 6500\ psi$
Unit weight of reinforced concrete, γ_{rc}	$\gamma_{rc} := 150\ pcf$
Unit weight of concrete, γ_c	$\gamma_c := 145$

Note: Unit weight of concrete is for calculation of Elastic modulus only

Reinforcing steel

ASTM 615, Grade 60 (ksi)	$f_{yrebar} := 60\ ksi$

Structural steel

ASTM A709, Grade 50 (ksi)	$f_y := 50\ ksi$
Unit weight of steel, γ_s	$\gamma_s := 490\ pcf$

Stay in place forms

Surface area density,γ_{sip}	$\gamma_{sip} := 20\ psf$

Future wearing surface

Surface area density, γ_{ws}	$\gamma_{ws} := 21\ psf$

Barrier

Weight per unit length	$m_{barr} := 0.581\ klf$
Width of the barrier	$w_{barr} := 1.50\ ft$
Number of barriers	$n_b := 2$

Appendix A (Continued)

A.3 Geometry of the Box Girder Section

This section provides information on geometry of the cross-section and design parameters.

A.3.1 Girder Geometry

Web depth (plumb), D_w	$D_w := 70\ in$	
(inclination to vertical is 14.03 deg)	$\theta := 14.03\ deg$	$D := \frac{D_w}{\cos(\theta)}$
Web depth (inclined), D	$D = 72.152\ in$	
Web plate thickness, t_w	$t_w := 0.75\ in$	
Area of web plate, A_w	$A_w := 2D\ t_w$	$A_w = 108.229\ in^2$
Top flange thickness, t_{tf}	$t_{tf} := 2.65\ in$	
Top flange width, b_{tf}	$b_{tf} := 25\ in$	
Area of top flanges, A_{tf}	$A_{tf} := 2\ b_{tf}\ t_{tf}$	$A_{tf} = 132.5\ in^2$
Bottom flange thickness, t_{bf}	$t_{bf} := 1.00in$	
Bottom flange width, b_{bf}	$b_{bf} := 100\ in$	
Area of bottom flange, A_{bf}	$A_{bf} := b_{bf}\ t_{bf}$	$A_{bf} = 100\ in^2$
Height of girder, H_G	$H_G := t_{tf} + D_w + t_{bf}$	$H_G = 73.65\ in$
Top slab width, b_{ts}	$b_{ts} := 507\ in$	
Top slab thickness, t_{ts}	$t_{ts} := 9\ in$	
Bottom slab thickness, t_{bs}	$t_{bs} := 13\ in$	
Bottom slab width, b_{bs}	$b_{bs} := \left(96\ in + \frac{t_{bs}}{4}\right)$	$b_{bs} = 99.25\ in$
Area of steel section, A_{sec}	$A_{sec} := A_{tf} + A_w + A_{bf}$	$A_{sec} = 340.729\ in^2$

A.3.2 Design Parameters

Design concrete strength	$f_c = 6.5\,ksi$
Modulus of Elasticity of concrete	$E_c := 0.9\ 33\ (\gamma_c)^{1.5}\ \sqrt{f_c\ psi}$
(0.9 is a factor for florida's limerocks)	$E_c = 4180.855\,ksi$
Yield strength of steel	$f_y = 50\,ksi$
Modulus of Elasticity of steel	$E_s := 29000\ ksi$

Appendix A (Continued)

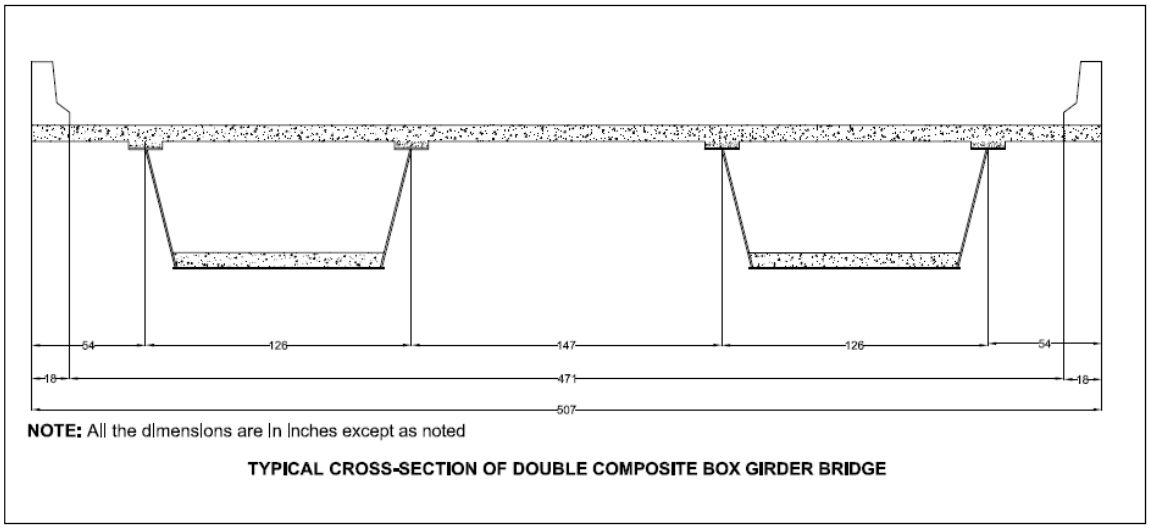

Figure A.1 Typical Cross-section of Bridge

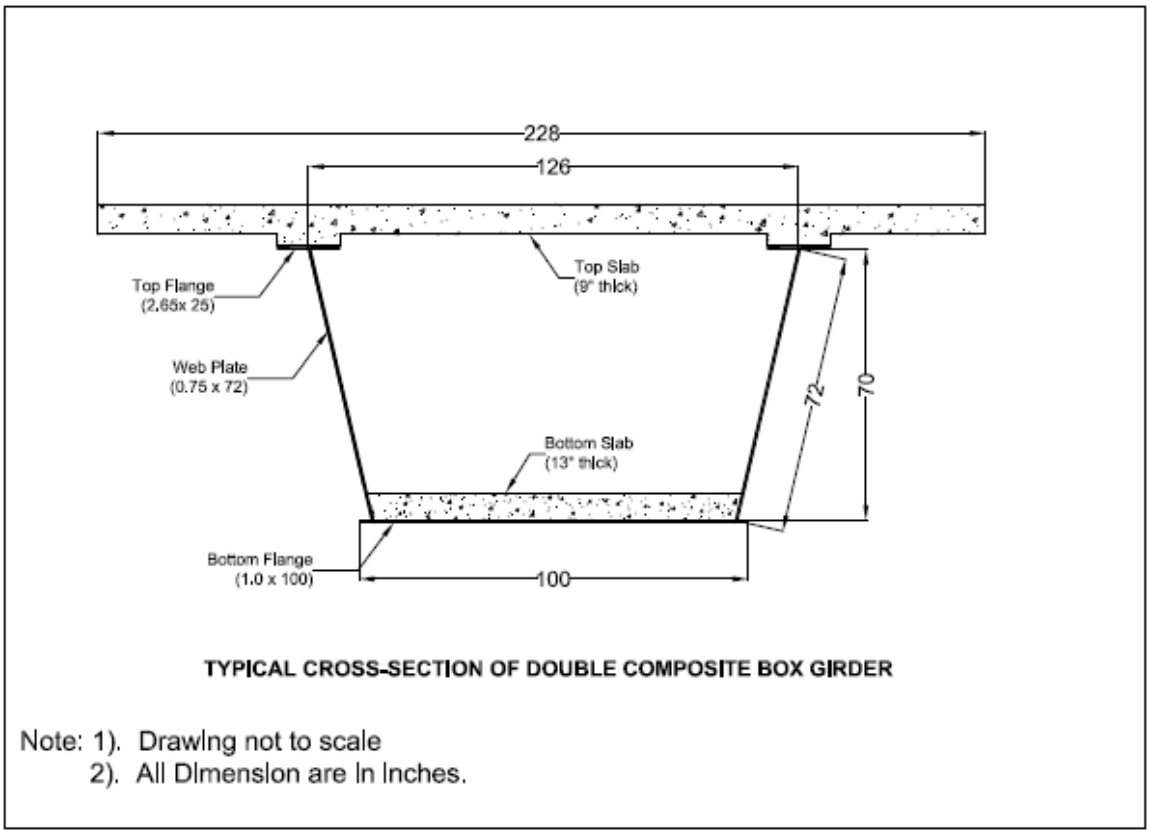

Figure A.2 Typical Cross-section of Box Girder

Appendix A (Continued)

A.4 Load Calculation Per Girder

Non Composite Dead Load

Dead load due to top slab, w_{ts} (klf) $\quad w_{ts} := t_{ts} \frac{b_{ts}}{2} \gamma_{rc}$ $\quad w_{ts} = 2.377\,klf$

Dead load due to haunch, w_h (klf) $\quad w_h := 2b_{tf}\, t_h\, \gamma_{rc}$ $\quad w_h = 0.156\,klf$

Dead Load due to bottom slab, w_{bs} (klf) $\quad w_{bs} := b_{bs}\, t_{bs}\, \gamma_{rc}$ $\quad w_{bs} = 1.344\,klf$

Stay in Place forms, w_{sip} (klf) $\quad w_{sip} := \left[(126in - b_{tf}) + \left(\frac{147\,in - b_{tf}}{2} \right) \right] \gamma_{sip}$ $\quad w_{sip} = 0.27\,klf$

Note: 126 inch is the c/c distance between top flanges of box girder

Dead load of steel section, w_s (klf) $\quad w_s := A_{sec}\, \gamma_s$ $\quad w_s = 1.159\,klf$

Dead load of steel details, w_{sd} (klf) $\quad w_{sd} := 0.1\, w_s$ $\quad w_{sd} = 0.116\,klf$

(Assumed 10 % of the steel weight)

Total non composite dead load, DC_1 $\quad DC_1 := w_s + w_{sd} + w_{bs}$

$DC_1 = 2.619\,klf$

Total composite dead load, DC_2 $\quad DC_2 := w_{ts} + w_h + w_{sip}$ $\quad DC_2 = 2.803\,klf$

Long Term Composite Dead Load

Dead load due to barrier, w_b (klf) $\quad w_b := \frac{m_{barr}\, n_b}{N_g}$ $\quad w_b = 0.581\,klf$

Dead load of wearing surface, w_{dw} (klf) $\quad w_{dw} := \frac{\gamma_{ws}\, RW}{N_g}$ $\quad w_{dw} = 0.42\,klf$

Total long term dead load, DC_3 (klf) $\quad DC_3 := w_b$ $\quad DC_3 = 0.581\,klf$

Total dead Load, DC (klf) $\quad DC := DC_1 + DC_2 + DC_3 + w_{dw}$

$DC = 6.423\,klf$

Live Load

Design vehicular live load and fatigue load are based on HS20 truck model of AASHTO LRFD 2004 Bridge Design Specifications, 3rd Edition.

Design vehicular live load is HL93 model.

Live load are assumed to be carried in full by the short term composite section.

Appendix A (Continued)

A.5 Load Factors

Load Modification Factors for Strength Limit States

Ductility factor, $\eta 1_D$ $\eta 1_D := 1.0$

Redundancy factor, $\eta 1_R$ $\eta 1_R := 1.0$

Operational importance factor, $\eta 1_I$ $\eta 1_I := 1.0$

Load modification factor, $\eta 1$ $\eta 1 := \eta 1_D \, \eta 1_R \, \eta 1_I$

$\eta 1 = 1$

Load Modification Factors for All Other Limit States Except Extreme Event Limit States

Ductility factor, $\eta 2_D$ $\eta 2_D := 1.0$

Redundancy factor, $\eta 2_R$ $\eta 2_R := 1.0$

Operational importance factor, $\eta 2_I$ $\eta 2_I := 1.0$

Load modification factor, $\eta 2$ $\eta 2 := \eta 1_D \, \eta 1_R \, \eta 1_I$

$\eta 2 = 1$

Load Factors

Strength I $\gamma 1_{DC} := 1.25$ $\gamma 1_{DW} := 1.50$ $\gamma 1_{LL} := 1.75$

Fatigue $\gamma 3_{LL} := 0.75$

Appendix A (Continued)

A.6 Distribution Factors

This section provides information on distribution factors used for moments and shear.

Live Load Lateral Distribution Factors

In this example, live load distributed to individual girders according to the approximate methods specified in **AASHTO 4.6.2.2**

For concrete deck on multiple box girders following condition shall be satisfied for the use of approximate method.

Conditions for application of approximate methods.

a.) Width of the deck is constant.

b.) Number of beams is not less than four unless otherwise specified.

c.) Beams are parallel and have approximately the same stiffness.

d.) The roadway part of the overhang (d_e) does not exceed 36 inch, unless otherwise specified.

e.) The cross-section is consistent with one of the cross-section shown in Table 4.6.2.2.1-1.

Conditions specified above are met, thus permanent loads of and on the deck may be uniformly distributed among the beams.

$$DF_{LL} := 0.05 + 0.85\frac{N_L}{N_g} + \frac{0.425}{N_L} \qquad DF_{LL} = 1.467 \text{ (AASHTO 4.6.2.2.2b-1)}$$

where,
N_L = number of design lanes
N_g = number of girders in the cross section

$$CHECK\_1 := \text{if}\left(0.5 \le \frac{N_L}{N_g} \le 1.5, \text{"OK"}, \text{"NG"}\right) \qquad CHECK\_1 = \text{"OK"}$$

As the ratio of N_L/N_g increases beyond the upper limit of 1.5 and lesser girders per lane are used, the effects of torsion will increase and a more refined analysis is required. Where there are no depth or deflection limitations, the most effective designs are those having the largest ratios of N_L/N_g.

It should be noted that as per AASHTO 6.11.2.2.2 shear connectors should be provided throughout the negative flexure region of the box girder bridges.

Appendix A (Continued)

Distribution Factor for Fatigue Load

When checking fatigue, fatigue load is placed in single lane. Therefore, the distribution factor for one lane loaded when computing stress and shear ranges due to the fatigue load.

$$DF_{FL} := 0.05 + 0.85\left(\frac{1}{N_g}\right) + \frac{0.425}{1} \qquad DF_{FL} = 0.9$$

Dynamic Load Allowance Factor (AASHTO 3.6.2)

For strength limit state checks:

$IM_{strength} := 33\%$ (AASHTO 3.6.2.1-1)

$$IM_{st} := 1 + \frac{33}{100} \qquad IM_{st} = 1.33$$

For fatigue limit state checks:

$IM_{fatigue} := 15\%$ (AASHTO 3.6.2.1-1)

$$IM_f := 1 + \frac{15}{100} \qquad IM_f = 1.15$$

Appendix A (Continued)

A.7 Load Combinations

Maximum negative moment exists at 1st pier from the exterior support. This is the maximum negative moment in all the three spans. Thus the negative section will be designed and checked for this moment.

Table A.1 Unfactored and Distributed Moments for Single Box Girder

Span	x/L	DC1	DC2	DC3	Total DC	DW	Distributed LL + IM	
							M+	M-
1	0	0	0	0	0	0	0	0
1	0.1	1525	3145	677	5347	489.24	4288	-682
1	0.2	2603	5315	1144	9062	826.87	7389	-1363
1	0.3	3233	6511	1401	11145	1012	9345	-2044
1	0.4	3416	6732	1449	11597	1047	10266	-2725
1	0.5	3151	5978	1286	10415	930.00	10194	-3407
1	0.6	2439	4250	914	7603	661.16	9214	-4090
1	0.7	1279	1547	333	3159	240.67	7345	-4771
1	0.8	-448	-2130	-459	-3037	-331	4699	-6724
1	0.9	-3048	-6782	-1460	-11290	-1055	2069	-8130
1	1	-6536	-12410	-2670	-21616	-1930	1491	-10580
2	0	-6536	-12410	-2670	-21616	-1930	1491	-10580
2	0.1	-2792	-5643	-1214	-9649	-877	2213	-6536
2	0.2	-312	-379	-81	-772	-59.00	5084	-4885
2	0.3	1410	3379	727	5516	525.73	8100	-3577
2	0.4	2443	5635	1212	9290	876.72	9999	-3198
2	0.5	2785	6387	1374	10546	993.00	10610	-2820

Note: Moments are in unit of ft-kip.

Appendix A (Continued)

Table A.2 Factored Moments for Single Box Girder

		1.25	1.5	1.75(LL+IM)		Total Factored and Distributed STRENGTH I Moments	
Span	x/L	DC	DW	M+	M-	M+	M-
1	0	0	0	0	0	0	0
1	0.1	6684	734	7504	-1193	14922	6225
1	0.2	11328	1240	12931	-2386	25499	10182
1	0.3	13931	1518	16354	-3577	31804	11872
1	0.4	14496	1571	17965	-4769	34031	11297
1	0.5	13019	1395	17839	-5962	32253	8452
1	0.6	9504	992	16124	-7157	26620	3338
1	0.7	3949	361	12854	-8349	17164	-4040
1	0.8	-3796	-497	8223	-11767	3931	-16059
1	0.9	-14113	-1583	3620	-14228	-12075	-29923
1	1	-27020	-2895	2610	-18515	-27305	-48430
2	0	-27020	-2895	2610	-18515	-27305	-48430
2	0.1	-12061	-1316	3872	-11438	-9505	-24814
2	0.2	-965	-89	8896	-8549	7843	-9603
2	0.3	6895	789	14176	-6260	21859	1424
2	0.4	11613	1315	17498	-5596	30425	7332
2	0.5	13183	1490	18567	-4935	33239	9737

Note: Moments are in unit of ft-kip.

Appendix A (Continued)

Unfactored Maximum Negative Moments

Total DC maximum negative moment (at pier)	$MDCn := 21616\ kip\ ft$
DC1 maximum negative moment (at pier)	$MDC1n := 6536\ kip\ ft$
DC2 maximum negative moment (at pier)	$MDC2n := 12410\ kip\ ft$
DC3 maximum negative moment (at pier)	$MDC3n := 2670\ kip\ ft$
WDW maximum negative moment (at pier)	$MDWn := 1930\ kip\ ft$
LL maximum negative moment (at pier)	$MLLn := 10580\ kip\ ft$

Strength I

$\Sigma MSTn_{max} := \gamma 1_{DC}\ MDCn + \gamma 1_{DW}\ MDWn + \gamma 1_{LL}\ MLLn$ $\Sigma MSTn_{max} = 48430\ ft{\cdot}kip$

Fatigue

LL range for negative moment span $MLL_{nf} := 2075\ ft\ kip$

$\Sigma MFn_{max} := \gamma 3_{LL}\ DF_{FL}\ IM_f\ MLL_{nf}$ $\Sigma MFn_{max} = 1610.719\ ft{\cdot}kip$

Note : Calculated design moments compare favourably with the design moments used in the AISI example (< 2 % difference)

Appendix A (Continued)

A.8 Section Properties

This section provides calculation of section properties for negative section.

A.8.1 Non-Composite Section Properties (n=infinity) A

a.) Top Flange

$t_{tf} = 2.65\,in$

$b_{tf} = 25\,in$

$A_{tf} = 132.5\,in^2$

b.) Bottom Flange

$t_{bf} = 1\,in$

$b_{bf} = 100\,in$

$A_{bf} = 100\,in^2$

c.) Web

$t_w = 0.75\,in$

$D = 72.152\,in$

$A_w = 108.229\,in^2$

Total area of steel box girder, A_s

$A_s := A_{tf} + A_{bf} + A_w$

$A_s = 340.729\,in^2$

The distance from the extreme bottom fiber to the centroid of item center of gravity, h (inch)

a) Top Flange

$h_{tf} := t_{bf} + D_w + \frac{t_{tf}}{2}$

$h_{tf} = 72.325\,in$

$A_{tf}\,h_{tf} = 9583.063\,in^3$

b) Bottom Flange

$h_{bf} := \frac{t_{bf}}{2}$

$h_{bf} = 0.5\,in$

$A_{bf}\,h_{bf} = 50\,in^3$

c) Web

$h_w := t_{bf} + \frac{D_w}{2}$

$h_w = 36\,in$

$A_w\,h_w = 3896.229\,in^3$

$\Sigma Ah := A_{tf}\,h_{tf} + A_{bf}\,h_{bf} + A_w\,h_w$

$\Sigma Ah = 13529.291\,in^3$

Distance from bottom of section to the Neutral Axis (N.A.) of whole section, Y_b (inch)

$Y_b := \frac{\Sigma Ah}{A_s}$

$Y_b = 39.707\,in$

Distance from top of section to the Neutral Axis (N.A.) of whole section, Y_t (inch)

$Y_t := H_G - Y_b$

$Y_t = 33.943\,in$

Distance between Neutral Axis (N.A.) and Item center of gravity, d (inch)

a) Top Flange

$d_{tf} := h_{tf} - Y_b$

$d_{tf} = 32.618\,in$

b) Bottom Flange

$d_{bf} := h_{bf} - Y_b$

$d_{bf} = -39.207\,in$

c) Web

$d_w := h_w - Y_b$

$d_w = -3.707\,in$

Moment of Inertia, I_0 (in^4)

$I_{0tf} := 2\,\frac{b_{tf}\,t_{tf}^3}{12}$

$I_{0tf} = 77.54\,in^4$

$I_{0bf} := \frac{b_{bf}\,t_{bf}^3}{12}$

$I_{0bf} = 8.333\,in^4$

$I_{0w} := 2\,\frac{t_w\,D^3\,\cos(\theta)^2}{12}$

$I_{0w} = 44193.335\,in^4$

$I_{0s} := I_{0tf} + I_{0bf} + I_{0w}$

$I_{0s} = 44279.208\,in^4$

Appendix A (Continued)

$A_{tf}\ d_{tf}^{2} = 140971.71\ in^{4}$ $A_{bf}\ d_{bf}^{2} = 153718.463\ in^{4}$ $A_{w}\ d_{w}^{2} = 1487.218\ in^{4}$

$\Sigma Ad := A_{tf}\ d_{tf}^{2} + A_{bf}\ d_{bf}^{2} + A_{w}\ d_{w}^{2}$ $\Sigma Ad = 296177.391\ in^{4}$

Moment of Inertia of whole section with respect to Neutral Axis (N.A.) of whole section, I_{st} (in^4)

$I_{st} := I_{0s} + \Sigma Ad$ $I_{st} = 340456.599\ in^{4}$

Section Modulus of Entire Section, S (in^3)

$S_{t\_st} := \frac{I_{st}}{Y_t}$ $S_{t\_st} = 10030.229\ in^{3}$

$S_{b\_st} := \frac{I_{st}}{Y_b}$ $S_{b\_st} = 8574.233\ in^{3}$

Note: St_st and Sb_st defines the section modulus of top fiber and bottom fiber of section respectively.

Appendix A (Continued)

A.8.2 Short-term Composite Section Properties (n=6.9) B

(With Bottom Slab only)

Modular Ratio, n

$n := \text{round}\left(\frac{E_s}{E_c}, 1\right)$ $\quad n = 6.9$

a) Bottom Slab

b) Steel

$A_{bsB} := \frac{b_{bs}\, t_{bs}}{n}$

$A_{bsB} = 186.993\ \text{in}^2$ $\quad A_s = 340.729\ \text{in}^2$

$A_B := A_{bsB} + A_s$ $\quad A_B = 527.721\ \text{in}^2$

The distance from the extreme bottom fiber to the centroid of item center of gravity, h (inch)

a) Bottom Slab

b) Steel

$h_{bsB} := t_{bf} + \frac{t_{bs}}{2}$

$h_{bsB} = 7.5\ \text{in}$

$A_{bsB}\, h_{bsB} = 1402.446\ \text{in}^3$ $\quad A_s\, Y_b = 13529.291\ \text{in}^3$

$\Sigma Ah_B := A_{bsB}\, h_{bsB} + A_s\, Y_b$ $\quad \Sigma Ah_B = 14931.737\ \text{in}^3$

Distance from bottom of section to the Neutral Axis (N.A.) of the whole section, Y_b (inch).

$Y_{bB} := \frac{\Sigma Ah_B}{A_B}$ $\quad Y_{bB} = 28.295\ \text{in}$

Distance from top of section to the Neutral Axis (N.A.) of the whole section, Y_t (inch).

$Y_{tB} := H_G - Y_{bB}$ $\quad Y_{tB} = 45.355\ \text{in}$

Distance between Neutral Axis and Item center of gravity, d (inch)

a) bottom Slab

b) Steel

$d_{bsB} := h_{bsB} - Y_{bB}$

$d_{sB} := Y_b - Y_{bB}$

$d_{bsB} = -20.795\ \text{in}$

$d_{sB} = 11.412\ \text{in}$

Appendix A (Continued)

Moment of Inertia, I_0 (in^4)

$$I_{0bsB} := \frac{b_{bs}\, t_{bs}^{3}}{12\ n}$$

$I_{0bsB} = 2633.481\ in^4$ $\qquad$ $I_{st} = 340456.599\ in^4$

$\Sigma I_{0B} := I_{0bsB} + I_{st}$ $\qquad$ $\Sigma I_{0B} = 343090.08\ in^4$

$A_{bsB}\, d_{bsB}^{2} = 80859.619\ in^4$ $\qquad$ $A_s\, d_{sB}^{2} = 44375.975\ in^4$

$\Sigma Ad_B := A_{bsB}\, d_{bsB}^{2} + A_s\, d_{sB}^{2}$ $\qquad$ $\Sigma Ad_B = 125235.595\ in^4$

Moment of Inertia of whole section with respect to Neutral Axis (N.A.) of whole section, I_{stB} (in^4).

$I_{stB} := \Sigma I_{0B} + \Sigma Ad_B$ $\qquad$ $I_{stB} = 468325.675\ in^4$

Section Modulus required for the weld, Q (in^3).

$$Q_{tfB} := \left(H_G - Y_{bB} - \frac{t_{tf}}{2}\right) A_{tf}$$ $\qquad$ $Q_{tfB} = 5834.01\ in^3$

Section Modulus of entire section, S (in^3)

$$S_{bslabB} := \frac{I_{stB}\ n}{Y_{bB} - t_{bf}}$$ $\qquad$ $S_{bslabB} = 118390.846\ in^3$

$$S_{tbeamB} := \frac{I_{stB}}{Y_{tB}}$$ $\qquad$ $S_{tbeamB} = 10325.719\ in^3$

$$S_{bbeamB} := \frac{I_{stB}}{Y_{bB}}$$ $\qquad$ $S_{bbeamB} = 16551.688\ in^3$

Appendix A (Continued)

A.8.3 Long-term Composite Section Properties (n_c=20.7) C

(With bottom slab only)

Modular Ratio, n_c

$n = 6.9$ $\quad n_c := 3n \quad$ $n_c = 20.7$

a) Bottom Slab

b) Steel

$$A_{bsC} := \frac{b_{bs}\, t_{bs}}{n_c}$$

$A_{bsC} = 62.331\ in^2$ $\quad A_s = 340.729\ in^2$

$A_C := A_{bsC} + A_s$ $\quad A_C = 403.059\ in^2$

The distance from the extreme bottom fiber to the centroid of item center of gravity, h (inch)

a) Bottom Slab

b) Steel

$$h_{bsC} := t_{bf} + \frac{t_{bs}}{2}$$

$h_{bsC} = 7.5\ in$

$A_{bsC}\, h_{bsC} = 467.482\ in^3$ $\quad A_s\, Y_b = 13529.291\ in^3$

$\Sigma Ah_C := A_{bsC}\, h_{bsC} + A_s\, Y_b$ $\quad \Sigma Ah_C = 13996.773\ in^3$

Distance from bottom of section to the Neutral Axis (N.A.) of the whole section, Y_b (inch).

$$Y_{bC} := \frac{\Sigma Ah_C}{A_C} \qquad Y_{bC} = 34.726\ in$$

Distance from top of section to the Neutral Axis (N.A.) of the whole section, Y_t (inch).

$Y_{tC} := H_G - Y_{bC}$ $\quad Y_{tC} = 38.924\ in$

Distance between Neutral Axis and Item center of gravity, d (inch)

a) Bottom Slab

b) Steel

$d_{bsC} := h_{bsC} - Y_{bC}$ $\quad d_{sC} := Y_b - Y_{bC}$

$d_{bsC} = -27.226\ in$ $\quad d_{sC} = 4.981\ in$

Moment of Inertia, I_0 (in^4)

$$I_{0bsC} := \frac{b_{bs}\, t_{bs}^3}{12\, n_c}$$

Appendix A (Continued)

$I_{0bsC} = 877.827\ in^4$ $I_{st} = 340456.599\ in^4$

$\Sigma I_{0C} := I_{0bsC} + I_{st}$ $\Sigma I_{0C} = 341334.426\ in^4$

$A_{bsC}\ d_{bsC}^{\ 2} = 46204.197\ in^4$ $A_s\ d_{sC}^{\ 2} = 8452.329\ in^4$

$\Sigma Ad_C := A_{bsC}\ d_{bsC}^{\ 2} + A_s\ d_{sC}^{\ 2}$ $\Sigma Ad_C = 54656.526\ in^4$

Moment of Inertia of whole section with respect to Neutral Axis (N.A.) of whole section, I_{ltC} (in^4).

$I_{ltC} := \Sigma I_{0C} + \Sigma Ad_C$ $I_{ltC} = 395990.951\ in^4$

Section Modulus of entire section, S (in^3)

$S_{tbeamC} := \frac{I_{ltC}}{Y_{tC}}$ $S_{tbeamC} = 10173.523\ in^3$

$S_{bbeamC} := \frac{I_{ltC}}{Y_{bC}}$ $S_{bbeamC} = 11403.194\ in^3$

$S_{bbslabC} := \frac{I_{ltC}}{Y_{bC} - t_{bf}}\ n_c$ $S_{bbslabC} = 243044.975\ in^3$

Appendix A (Continued)

A.8.4 Short-term Composite Section Properties (n=6.9) D

(Negative Live Load)

Modular Ratio, n

$n = 6.9$

Effective flange width (AASHTO 4.6.2.6)

For an interior web, b_{eff} is lesser of:

$L_{eff} := 136.4\ ft$ $\quad \frac{L_{eff}}{4} = 409.2\ in$ $\quad 12\ t_{ts} + \frac{b_{tf}}{2} = 120.5\ in$

Here L_{eff} is taken as the distance between the inflection points of permanent load.

$b_{eff\_int} := if\left[\frac{L_{eff}}{4} < \left(12\ t_{ts} + \frac{b_{tf}}{2}\right), \frac{L_{eff}}{4}, 12\ t_{ts} + \frac{b_{tf}}{2}\right]$ $\quad b_{eff\_int} = 120.5\ in$

For an exterior web, beff is lesser of:

$\frac{L_{eff}}{8} = 204.6\ in$ $\quad 6\ t_{ts} + \frac{b_{tf}}{4} = 60.25\ in$ $\quad OH_c = 54\ in$ (Governs)

By inspection overhang governs the effective width of the top slab.

$b_{eff\_ext} := OH_c + \frac{b_{eff\_int}}{2}$ $\quad b_{eff\_ext} = 114.25\ in$

Thus total beff of the entire box girder

$b_{eff} := b_{eff\_int} + b_{eff\_ext}$ $\quad b_{eff} = 234.75\ in$

a) Top Rebar

$A_{rebarD} := R_r\ b_{eff}\ t_{ts}$

$A_{rebarD} = 21.127\ in^2$

b) Bottom Slab

$A_{bsD} := \frac{b_{bs}\ t_{bs}}{n}$

$A_{bsD} = 186.993\ in^2$

c) Steel

$A_s = 340.729\ in^2$

$A_D := A_{rebarD} + A_{bsD} + A_s$ $\quad A_D = 548.849\ in^2$

The distance from the extreme bottom fiber to the centroid of item center of gravity, h (inch)

a) Top Rebar

$h_{rebarD} := t_{bf} + D_w + t_{tf} + t_h + \frac{t_{ts}}{2}$

$h_{rebarD} = 81.15\ in$

b) Bottom Slab

$h_{bsD} := t_{bf} + \frac{t_{bs}}{2}$

$h_{bsD} = 7.5\ in$

c) Steel

$Y_b = 39.707\ in$

Appendix A (Continued)

$A_{rebarD}\ h_{rebarD} = 1714.497\ in^3$ $A_{bsD}\ h_{bsD} = 1402.446\ in^3$ $A_s\ Y_b = 13529.291\ in^3$

$\Sigma Ah_D := A_{rebarD}\ h_{rebarD} + A_{bsD}\ h_{bsD} + A_s\ Y_b$ $\Sigma Ah_D = 16646.233\ in^3$

Distance from bottom of section to the Neutral Axis (N.A.) of the whole section, Y_b (inch).

$$Y_{bD} := \frac{\Sigma Ah_D}{A_D} \qquad Y_{bD} = 30.329\ in$$

Distance from top of section to the Neutral Axis (N.A.) of the whole section, Y_t (inch).

$Y_{tD} := H_G + t_{ts} + t_h - Y_{bD}$ $Y_{tD} = 55.321\ in$

Distance between Neutral Axis and Item center of gravity, d (inch)

a.) Top Rebar b.) Bottom Slab c.) Steel

$d_{rebarD} := h_{rebarD} - Y_{bD}$ $d_{bsD} := h_{bsD} - Y_{bD}$ $d_{sD} := Y_b - Y_{bD}$

$d_{rebarD} = 50.821\ in$ $d_{bsD} = -22.829\ in$ $d_{sD} = 9.378\ in$

Moment of Inertia, I_0 (in^4)

$I_{rebarD} := 0.0\ in^4$ $$I_{0bsD} := \frac{b_{bs}\ t_{bs}^3}{12\ n}$$

$I_{rebarD} = 0$ $I_{0bsD} = 2633.481\ in^4$ $I_{st} = 340456.599\ in^4$

$\Sigma I_{0D} := I_{rebarD} + I_{0bsD} + I_{st}$ $\Sigma I_{0D} = 343090.08\ in^4$

$A_{rebarD}\ d_{rebarD}^2 = 54566.786\ in^4$ $A_{bsD}\ d_{bsD}^2 = 97456.82\ in^4$ $A_s\ d_{sD}^2 = 29963.375\ in^4$

$\Sigma Ad_D := A_{rebarD}\ d_{rebarD}^2 + A_{bsD}\ d_{bsD}^2 + A_s\ d_{sD}^2$ $\Sigma Ad_D = 181986.981\ in^4$

Moment of Inertia of whole section with respect to Neutral Axis (N.A.) of whole section, I_{stD} (in^4).

$I_{stD} := \Sigma I_{0D} + \Sigma Ad_D$ $I_{stD} = 525077.061\ in^4$

First Moment of Area for Transformed Bottom Slab, Q (in^3).

$$Q_{BslabD} := A_{bsD}\left(Y_{bD} - t_{bf} - \frac{t_{bs}}{2}\right) \qquad Q_{BslabD} = 4268.925\ in^3$$

Appendix A (Continued)

Section Modulus of entire section, S (in^3)

$$S_{trebarD} := \frac{I_{stD}}{Y_{tD} - \frac{t_{ts}}{2}} \qquad S_{trebarD} = 10331.965\ in^3$$

$$S_{tbeamD} := \frac{I_{stD}}{Y_{tD} - t_{ts} - t_h} \qquad S_{tbeamD} = 12120.713\ in^3$$

$$S_{bbeamD} := \frac{I_{stD}}{Y_{bD}} \qquad S_{bbeamD} = 17312.501\ in^3$$

$$S_{bslabD} := \frac{I_{stD}\ n}{Y_{bD} - t_{bf}} \qquad S_{bslabD} = 123529.179\ in^3$$

Appendix A (Continued)

A.8.5 Long-term Composite Section Properties (n_e=20.7) E

(Negative Service Dead Load Moment)

Modular Ratio, n_e

$n = 6.9$ $\quad n_e := 3n \quad$ $n_e = 20.7$

a) Top rebar $\quad$ b) Bottom Slab $\quad$ c) Steel

$A_{rebarE} := R_r\, b_{eff}\, t_{ts} \quad A_{bsE} := \dfrac{b_{bs}\, t_{bs}}{n_e}$

$A_{rebarE} = 21.127\,in^2 \quad A_{bsE} = 62.331\,in^2 \quad A_s = 340.729\,in^2$

$A_E := A_{rebarE} + A_{bsE} + A_s \quad A_E = 424.187\,in^2$

The distance from the extreme bottom fiber to the centroid of item center of gravity, h (inch)

a) Top Rebar $\quad$ b) Bottom Slab $\quad$ c) Steel

$h_{rebarE} := t_{bf} + D_w + t_{tf} + t_h + \dfrac{t_{ts}}{2} \quad h_{bsE} := t_{bf} + \dfrac{t_{bs}}{2}$

$h_{rebarE} = 81.15\,in \quad h_{bsE} = 7.5\,in$

$A_{rebarE}\, h_{rebarE} = 1714.497\,in^3 \quad A_{bsE}\, h_{bsE} = 467.482\,in^3 \quad A_s\, Y_b = 13529.291\,in^3$

$\Sigma Ah_E := A_{rebarE}\, h_{rebarE} + A_{bsE}\, h_{bsE} + A_s\, Y_b \quad \Sigma Ah_E = 15711.27\,in^3$

Distance from bottom of section to the Neutral Axis (N.A.) of the whole section, Y_b (inch).

$Y_{bE} := \dfrac{\Sigma Ah_E}{A_E} \quad Y_{bE} = 37.039\,in$

Distance from top of section to the Neutral Axis (N.A.) of the whole section, Y_t (inch).

$Y_{tE} := H_G + t_{ts} + t_h - Y_{bE} \quad Y_{tE} = 48.611\,in$

Distance between Neutral Axis and Item center of gravity, d (inch)

a) Top Slab $\quad$ b) Bottom Slab $\quad$ c) Steel

$d_{rebarE} := h_{rebarE} - Y_{bE} \quad d_{bsE} := h_{bsE} - Y_{bE} \quad d_{sE} := Y_b - Y_{bE}$

$d_{rebarE} = 44.111\,in \quad d_{bsE} = -29.539\,in \quad d_{sE} = 2.668\,in$

Appendix A (Continued)

Moment of Inertia, I_0 (in^4)

$I_{rebarE} := 0.0\ in^4$ $\quad I_{0bsE} := \frac{b_{bs}\ t_{bs}^3}{12\ n_e}$

$I_{rebarE} = 0$ $\quad I_{0bsE} = 877.827\ in^4$ $\quad I_{st} = 340456.599\ in^4$

$\Sigma I_{0E} := I_{rebarE} + I_{0bsE} + I_{st}$ $\quad \Sigma I_{0E} = 341334.426\ in^4$

$A_{rebarE}\ d_{rebarE}^2 = 41110.319\ in^4$ $\quad A_{bsE}\ d_{bsE}^2 = 54385.33\ in^4$ $\quad A_s\ d_{sE}^2 = 2426.109\ in^4$

$\Sigma Ad_E := A_{rebarE}\ d_{rebarE}^2 + A_{bsE}\ d_{bsE}^2 + A_s\ d_{sE}^2$ $\quad \Sigma Ad_E = 97921.758\ in^4$

Moment of Inertia of whole section with respect to Neutral Axis (N.A.) of whole section, I_{ltE} (in^4).

$I_{stE} := \Sigma I_{0E} + \Sigma Ad_E$ $\quad I_{stE} = 439256.184\ in^4$

Section Modulus required for the weld, Q (in^3).

$Q_{tfE} := \left(H_G - Y_{bE} - \frac{t_{tf}}{2}\right) A_{tf} + \left(H_G + \frac{t_{ts}}{2} - Y_{bE}\right) A_{rebarE}$ $\quad Q_{tfE} = 5544.037\ in^3$

$Q_{bfE} := A_{bf}\left(Y_{bE} - \frac{t_{bf}}{2}\right) + A_{bsE}\left(Y_{bE} - t_{bf} - \frac{t_{bs}}{2}\right)$ $\quad Q_{bfE} = 5495.019\ in^3$

$Q_{BslabE} := A_{bsE}\left(Y_{bE} - t_{bf} - \frac{t_{bs}}{2}\right)$ $\quad Q_{BslabE} = 1841.165\ in^3$

Section Modulus of entire section, S (in^3)

$S_{trebarE} := \frac{I_{stE}}{Y_{tE} - \frac{t_{ts}}{2}}$ $\quad S_{trebarE} = 9957.871\ in^3$

$S_{tbeamE} := \frac{I_{stE}}{Y_{tE} - t_{ts} - t_h}$ $\quad S_{tbeamE} = 11997.781\ in^3$

$S_{bbeamE} := \frac{I_{stE}}{Y_{bE}}$ $\quad S_{bbeamE} = 11859.434\ in^3$

$S_{bslabE} := \frac{I_{stE}\ n_e}{Y_{bE} - t_{bf}}$ $\quad S_{bslabE} = 252302.156\ in^3$

Appendix A (Continued)

A.9 Calculation of Plastic Neutral Axis

This section shows detailed calculation of Plastic Neutral Axis, Y_{PNA}.

Calculation of Forces

Force in top rebars of top slab, P_{rt}	$P_{rt} := 0.0067\ b_{eff}\ t_{ts}\ f_{yrebar}$	$P_{rt} = 849.326\ kip$
Force in bottom rebars of top slab, P_{rb}	$P_{rb} := 0.0033\ b_{eff}\ t_{ts}\ f_{yrebar}$	$P_{rb} = 418.325\ kip$
Total force in rebars of top slab, P_{re}	$P_{re} := P_{rt} + P_{rb}$	$P_{re} = 1267.65\ kip$
Force in Top flange, P_{tf}	$P_{tf} := 2\ b_{tf}\ t_{tf}\ f_y$	$P_{tf} = 6625\ kip$
Force in Web, P_w	$P_w := 2\ D\ t_w\ f_y$	$P_w = 5411.429\ kip$
Force in Bottom flange, P_{bf}	$P_{bf} := b_{bf}\ t_{bf}\ f_y$	$P_{bf} = 5000\ kip$
Force in Bottom slab, P_{bs}	$P_{bs} := 0.85\ f_c\ b_{bs}\ t_{bs}$	$P_{bs} = 7128.631\ kip$

$P_{bf} + P_{bs} = 12128.631\ kip$

Therefore, plastic neutral axis is located in the steel section.

Clear cover to the top rebars of top slab, CL_{rt}	$CL_{rt} := 2in$
Clear cover to the bottom rebars of top slab, CL_{rb}	$CL_{rb} := 2in$
Diameter of top rebar of top slab, DIA_{rt}	$DIA_{rt} := 0.625in$
Diameter of bottom rebar of top slab, DIA_{rb}	$DIA_{rb} := 0.625in$

Assuming Plastic Neutral Axis to be in the web of box girder section.

Location of Plastic Neutral Axis for the Critical Negative Section

Assuming Plastic Neutral Axis to be in the web of box girder section.

$$Y_{pm} := \left(t_{bf} + \frac{D_w}{2}\right) \qquad Y_{pm} = 36\ in$$

$$\text{root}\left[P_{re} + P_{tf} + \left(\frac{P_w}{D}\right)\frac{(D_w + t_{bf}) - Y_{pm}}{\cos(\theta)} - P_{bf} - P_{bs} - \left(\frac{P_w}{D}\right)\frac{Y_{pm} - t_{bf}}{\cos(\theta)}, Y_{pm}\right] = 8.603\ in$$

Appendix A (Continued)

$$Y_{PNA} := 8.603\ in$$

Thus, Plastic Neutral axis is located inside bottom slab from the bottom of the bottom, flange. Since bottom slab is located in the web, the equation will not change.

$Y_{PNA} = 8.603\ in$

Y_{PNA} is the actual position of Plastic Neutral Axis (P.N.A) from the bottom of the section.

Tension force in the cross section, T_c

$$T_c := P_{re} + P_{tf} + \left(\frac{P_w}{D}\right)\left(\frac{D_w + t_{bf} - Y_{PNA}}{\cos(\theta)}\right) \qquad T_c = 12716.32\ kip$$

Compression force in the cross section, C_c

$$C_c := P_{bf} + P_{bs} + \left(\frac{P_w}{D}\right)\left(\frac{Y_{PNA} - t_{bf}}{\cos(\theta)}\right) \qquad C_c = 12716.39\ kip$$

The equilibrium equation used here does not account for the loss of compressive force for the bottom slab concrete above the plastic neutral axis. However the result is adequate for design.

Appendix A (Continued)

A.10 Design and Stress Checks

This section provides information on design and stress checks.

Web Slenderness (AASHTO 6.10.6.2.3)

The section satisfies the web slenderness limit if:

$$\text{if } 2\frac{D_c}{t_w} \le 5.7\sqrt{\frac{E_s}{F_y}} \qquad \textbf{(AASHTO 6.10.6.2.3-1)}$$

D_c = Depth of web in compression in the elastic range determined as specified in Article D6.3.1 (in)

t_w = Web thickness of the box girder

E_s = Elastic Modulus of the Steel

F_y = Yield strength of the girder (flange and web)

f_{cf_s} = Stress in compression flange at strength limit state for DC1, DC2, DC3, DW, LL.

f_{tf_s} = Stress in tension flange at strength limit state for DC1, DC2, DC3, DW, LL.

$$f_{cf\_s} := -\left(\frac{\gamma 1_{DC}\,MDC1n}{S_{b\_st}} + \frac{\gamma 1_{DC}\,MDC2n}{S_{bbeamC}} + \frac{\gamma 1_{DC}\,MDC3n + \gamma 1_{DW}\,MDWn}{S_{bbeamE}} + \frac{\gamma 1_{LL}\,MLLn}{S_{bbeamD}}\right)$$

$$f_{cf\_s} = -46.899\,\text{ksi}$$

$$f_{tf\_s} := \frac{\gamma 1_{DC}\,MDC1n}{S_{t\_st}} + \frac{\gamma 1_{DC}\,MDC2n}{S_{tbeamC}} + \frac{\gamma 1_{DC}\,MDC3n + \gamma 1_{DW}\,MDWn}{S_{tbeamE}} + \frac{\left(\gamma 1_{LL}\,MLLn\right)}{S_{tbeamD}}$$

$$f_{tf\_s} = 52.636\,\text{ksi}$$

$$D_c := \frac{-f_{cf\_s}}{\left|f_{cf\_s}\right| + f_{tf\_s}} D_w - t_{tf} \qquad D_c = 30.332\,\text{in}$$

$$2\frac{D_c}{t_w} = 80.886 \qquad 5.7\sqrt{\frac{E_s}{f_y}} = 137.274$$

$$CHECK\_4 := \text{if}\left(2\frac{D_c}{t_w} \le 5.7\sqrt{\frac{E_s}{f_y}}, \text{"OK"}, \text{"NG"}\right) \qquad CHECK\_4 = \text{"OK"}$$

Therefore, section satisfies web slenderness criteria.

Appendix A (Continued)

Slab Ductility Requirement (AASHTO 6.11.6.2.2)

$$\frac{D_p}{D_t} \le 0.42$$

D_p = Distance from bottom of the bottom concrete slab to the neutral axis of the composite section.

D_t = Total depth of composite section

$D_p := Y_{PNA} - t_{bf}$ $\quad D_p = 7.603\ in$

$D_t := t_{ts} - CL_{rt} + t_h + t_{tf} + D_w$ $\quad D_t = 82.65\ in$ $\quad \frac{D_p}{D_t} = 0.092$

$CHECK\_5 := if\left(\frac{D_p}{D_t} \le 0.42, "OK", "NG"\right)$ $\quad CHECK\_5 = "OK"$

Therefore, section does satisfies Slab Ductility requirement by AASHTO 6.10.7.3. Section is a compact section.

Nominal Flexural Resistance of Box Flanges in Compression (AASHTO 6.11.8)

Assume that there exist negligible torsional shear stresses in the flange due to the factored loads.Therefore, St. Venant torsional stresses can be taken as zero.

Flange stress reduction factor for homogeneous section (AASHTO 6.10.1.10.1) $\quad R_h := 1.0$ $\quad R_b := 1.0$

The resistance factor for flexure $\quad \phi_f := 1.0$

St. Venant torsional shear stresses in the flange $\quad f_v := 0\ ksi$

Nominal yield strength of the compression flange $\quad F_{yc} := f_y$ $\quad F_{yc} = 50\ ksi$

Plate buckling co-efficient for uniform normal stress $\quad k := 4.0$

Plate buckling co-efficient for shear stress $\quad k_s := 5.34$

$\Delta := \sqrt{1 - 3\left(\frac{f_v}{F_{yc}}\right)^2}$ $\quad \Delta = 1$

Nominal flexure resistance of the compression flange $\quad F_{nc} := R_b R_h F_{yc} \Delta$ $\quad F_{nc} = 50\ ksi$

Appendix A (Continued)

The stress developed in the compression flange due to Factored loads.

$$f_{bu} := \frac{MDC1n\ \gamma 1_{DC}}{S_{b\_st}} + \frac{MDC2n\ \gamma 1_{DC}}{S_{bbeamC}} + \frac{MDC3n\ \gamma 1_{DC} + MDWn\ \gamma 1_{DW}}{S_{bbeamE}} + \frac{MLLn\ \gamma 1_{LL}}{S_{bbeamD}}$$

$f_{bu} = 46.899\,ksi$

$CHECK\_6 := if(f_{bu} \le \phi_f F_{nc}, "OK", "NG")$ $CHECK\_6 = "OK"$

Nominal Flexural Resistance of Box Flanges in Tension (AASHTO 6.11.7.2)

Nominal flexure resistance of the tension flange $F_{nt} := f_y$ $F_{nt} = 50\,ksi$

$$f_{bt} := \frac{MDC1n\ \gamma 1_{DC}}{S_{t\_st}} + \frac{MDC2n\ \gamma 1_{DC}}{S_{tbeamC}} + \frac{MDWn\ \gamma 1_{DW} + MDC3n\ \gamma 1_{DC}}{S_{tbeamE}} + \frac{MLLn\ \gamma 1_{LL}}{S_{tbeamD}}$$

$f_{bt} = 52.636\,ksi$

$$\frac{F_{nt} - f_{bt}}{F_{nt}} 100 = -5.272$$

Since the stress in top flange exceeds the yield stress, the top flange would need to be resized. however, for the purpose of this example size is acceptable.

Stress in Bottom Concrete Slab

Stress in bottom concrete slab at Strength I limit state should not exceed 0.6f'c.

$$f_{DC2bs} := \frac{\gamma 1_{DC}\ MDC2n}{S_{bslabB}} \qquad f_{DC2bs} = 1.572\,ksi$$

$$f_{DC3bs} := \frac{MDC3n\ \gamma 1_{DC}}{S_{bslabD}} \qquad f_{DC3bs} = 0.324\,ksi$$

$$f_{DWbs} := \frac{MDWn\ \gamma 1_{DW}}{S_{bslabD}} \qquad f_{DWbs} = 0.281\,ksi$$

$$f_{LLbs} := \frac{MLLn\ \gamma 1_{LL}}{S_{bslabD}} \qquad f_{LLbs} = 1.799\,ksi$$

Appendix A (Continued)

$f_{cbs} := f_{DC2bs} + f_{DC3bs} + f_{DWbs} + f_{LLbs}$

$f_{cbs} = 3.976\,ksi$

$CHECK\_7 := if\left(f_{cbs} \le 0.60\,f_c, "OK", "NG"\right)$ $CHECK\_7 = "NG"$

$f_{clim} := 0.60 f_c$ $f_{clim} = 3.9\,ksi$

$\frac{f_{cbs} - f_{clim}}{f_{clim}} 100 = 1.959$

Eventhough the stress exceeds the 0.6f'c limit by 2 %, for the purpose of this example bottom slab is acceptable.

Appendix A (Continued)

A.11 Shear

Section will be checked for the maximum shear force at the end bearings. Since maximum shear force is observed at interior support, section will be checked at interior support.

Table A.3 Unfactored Shear for Negative Section in Kips

Span	x/L	DC1	DC2	DC3	Total DC	DW	Distributed LL + IM	
							V-	V+
1	0	92	191	41	324	29	-35	258
1	0.1	68	140	30	238	21	-37	216
1	0.2	44	89	19	152	13	-54	179
1	0.3	21	37	8	66	6	-83	144
1	0.4	-2	-14	-3	-19	-2	-111	112
1	0.5	-25	-65	-15	-105	-10	-140	84
1	0.6	-49	-116	-26	-191	-18	-172	60
1	0.7	-72	-167	-37	-276	-26	-205	39
1	0.8	-113	-219	-47	-379	-33	-239	23
1	0.9	-160	-270	-58	-488	-41	-270	11
1	1	-206	-321	-70	-597	-49	-302	7
2	0	187	319	69	575	48	-30	306
2	0.1	129	255	55	439	39	-30	272
2	0.2	87	191	41	319	29	-39	232
2	0.3	58	127	27	212	19	-61	193
2	0.4	29	63	15	107	9	-88	155
2	0.5	0	0	0	0	0	-119	121

Appendix A (Continued)

Table A.4 Factored and Distributed Shear for Negative Section in Kips

		Max	Max			Total Factored and Distributed STRENGTH I Shears	
		1.25	1.5	1.75(LL+IM)			
Span	x/L	DC	DW	V-	V+	V-	V+
1	0	405	44	-61	452	387	900
1	0.1	298	32	-65	378	264	707
1	0.2	190	20	-95	313	114	523
1	0.3	83	9	-144	252	-53	343
1	0.4	-24	-3	-194	197	-220	170
1	0.5	-131	-15	-246	148	-392	1
1	0.6	-239	-27	-301	104	-567	-161
1	0.7	-345	-39	-360	68	-744	-316
1	0.8	-474	-50	-418	40	-941	-483
1	0.9	-610	-62	-473	18	-1145	-653
1	1	-746	-74	-529	12	-1348	-807
2	0	719	72	-52	535	739	1325
2	0.1	549	59	-52	476	555	1084
2	0.2	399	44	-68	406	375	848
2	0.3	265	29	-108	338	186	632
2	0.4	134	14	-154	270	-6	418

Appendix A (Continued)

Maximum shear force due to unfactored loads

Maximum shear force due to total DC $V_{DCn} := 597\ kip$

Maximum Shear force due to DC1 $V_{DC1n} := 206\ kip$

Maximum shear force due to DC2 $V_{DC2n} := 321\ kip$

Maximum shear force due to DC3 $V_{DC3n} := 70$

Maximum shear force due to DW $V_{DWn} := 49\ kip$

Maximum shear force due to LL $V_{LLn} := 302\ kip$

Maximum shear force for fatigue $V_{fn} := 80\ kip$

Strength I Limit State

$\Sigma VSTn_{max} := \gamma 1_{DC}\ V_{DCn} + \gamma 1_{DW}\ V_{DWn} + \gamma 1_{LL}\ V_{LLn}$ $\Sigma VSTn_{max} = 1348.25\ kip$

Fatigue Limit State

$V_{nf} := IM_f\ DF_{FL}\ \gamma 3_{LL}\ V_{fn}$ $V_{nf} = 62.1\ kip$

Maximum shear per web

$\Sigma VSTn_{maxw} := \frac{\Sigma VSTn_{max}}{2}$ $\Sigma VSTn_{maxw} = 674.125\ kip$

Inclination of webs needs to be taken into consideration.

$V_u := \frac{\Sigma VSTn_{maxw}}{\cos(\theta)}$ $V_u = 694.853\ kip$

Nominal Resistance of Unstiffened Webs (AASHTO 6.10.9.2)

$V_u \le \phi_v\ V_n$

Resistance factor for shear $\phi_v := 1.0$

Nominal shear resistance, V_n

$V_n = C\ V_p$ (AASHTO 6.10.9.2-1)

Plastic shear force, V_p

$V_p := 0.58\ f_y\ D\ t_w$ $V_p = 1569.314\ kip$ (AASHTO 6.10.9.2-2)

Shear buckling co-efficient, k_{sh} $k_{sh} := 5$

$\frac{D}{t_w} = 96.203$ $1.40\sqrt{\frac{E_s\ k_{sh}}{f_y}} = 75.392$

Appendix A (Continued)

$$C_w := \begin{cases} \dfrac{1.57}{\left(\dfrac{D}{t_w}\right)^2}\left(\dfrac{E_s\, k_{sh}}{f_y}\right) & \text{if } \dfrac{D}{t_w} > 1.40\sqrt{\dfrac{E_s\, k_{sh}}{f_y}} \\ \text{"NG"} & \text{otherwise} \end{cases} \qquad \text{(AASHTO 6.10.9.3.2-6)}$$

$C_w = 0.492$

$V_n := C_w\, V_p$ $\qquad V_n = 772.02\,\text{kip}$

$\phi_v\, V_n = 772.02\,\text{kip}$ $\qquad V_u = 694.853\,\text{kip}$

$\text{CHECK\_8} := \text{if}\left(V_u < \phi_v\, V_n, \text{"OK"}, \text{"NG"}\right)$ $\qquad \text{CHECK\_8} = \text{"OK"}$

Thus, section satisfies nominal shear criteria.

Appendix A (Continued)

A.12 Shear Connectors

This section provides information on design of shear connectors and fatigue limit state.

Assume diameter of shear connectors $d_{sc} := 0.75\text{in}$

Area of shear connectors $A_{sc} := \pi \frac{d_{sc}^2}{4}$ $A_{sc} = 0.442\ \text{in}^2$

A.12.1 Ultimate Resistance of Shear Connectors (AASHTO 6.10.10.4.3)

Minimum tensile strength of shear connectors $F_u := 60\text{ksi}$

Nominal resistance of one stud shear connectors in concrete deck, Q_n

$0.5\ A_{sc} \sqrt{f_c\ E_c} = 36.414\,\text{kip}$ $A_{sc}\ F_u = 26.507\,\text{kip}$

$Q_n := \text{if}\left(0.5\ A_{sc} \sqrt{f_c\ E_c} \le A_{sc}\ F_u, 0.5 A_{sc} \sqrt{f_c\ E_c}, A_{sc}\ F_u\right)$ $Q_n = 26.507\,\text{kip}$

Resistance factor of shear connectors From (AASHTO 6.5.4.2) $\phi_{sc} := 0.85$

Factored resistance of one stud shear connector, Q_r $Q_r := \phi_{sc}\ Q_n$

$Q_r = 22.531\,\text{kip}$

Maximum shear force in the concrete deck for negative section as per AASHTO 6.10.10.4.2

$P_{1p} := 0.60\ f_c\ b_{bs}\ t_{bs}$ $P_{1p} = 5031.975\,\text{kip}$ (AASHTO 6.10.10.4.2-2)

$P_{2p} := 2f_y\ D\ t_w + 2f_y\ b_{tf}\ t_{tf} + f_y\ b_{bf}\ t_{bf}$ $P_{2p} = 17036.429\,\text{kip}$ (AASHTO 6.10.10.4.2-3)

Maximum shear force is lesser of the two values.

$P_p := \text{if}\left(P_{1p} < P_{2p}, P_{1p}, P_{2p}\right)$ $P_p = 5031.975\,\text{kip}$

Number of shear connector in the bottom flange, n_{sc}

$n_{sc} := \text{round}\left(\frac{P_p}{Q_r}, 0\right)$ $n_{sc} = 223$

Transverse Spacing of Shear Connectors (AASHTO 6.11.10)

$R_1 := 0.57$ $k = 4$ $E_s = 29000\,\text{ksi}$

Appendix A (Continued)

$$S_t \le \frac{R_1\, t_{bf}}{\sqrt{\frac{f_y}{k\, E_s}}}$$ Where

$f_y = 50\,\text{ksi}$ $t_{bf} = 1\,\text{in}$

$$S_t := \frac{R_1\, t_{bf}}{\sqrt{\frac{f_y}{k\, E_s}}}$$

$S_t = 27.455\,\text{in}$

$n_{sh} := 7$

The maximum allowable transverse spacing is 27 in. Try 7 shear connectors at the spacing of 14 in.

A.12.2 Fatigue Resistance of Shear Connectors

$ADTT_{SL} = p\, ADTT$ (AASHTO 3.6.1.4.2-1)

Where:

ADTT = number of trucks per day in one direction averaged over the design life.

$ADTT_{SL}$ = the number of trucks per day in a single-lane averaged over the design life.

p = fraction of truck traffic in single lane (Table 3.6.1.4.2-1)

For 3 or more lanes $p := 0.8$

Assuming one-way traffic $ADTT := 4000$

The number of trucks per day in a single-lane averaged over the design life.

$ADTT_{SL} := p\, ADTT$

$ADTT_{SL} = 3200$

Therefore, the number of trucks per day in a single lane averaged is 3200.

Considering Category C type of detail.

Number of stress range cycles per truck passage $n_s := 1.5$

(From Table 6.6.1.2.5-2)

Number of stress cycle in entire life span of bridge $N_s := 365\ 75\ n_s\ ADTT_{SL}$ (AASHTO 6.6.1.2.5-2)

$N_s = 131400000$

Nominal Fatigue Resistance

Nominal fatigue resistance shall be as per AASHTO 6.6.1.2.5

Appendix A (Continued)

$$\Delta F_n = \left(\frac{A_f}{N_s}\right)^{\frac{1}{3}} \geq \frac{1}{2}\,\Delta F_{TH} \qquad \text{(AASHTO 6.6.1.2.5-1)}$$

where,

ΔF_n = Nominal fatigue resistance

A_f = Constant from Table 6.6.1.2.5-1

N_s = Number of stress cycles in entire life span of bridge

ΔF_{TH} = Constant amplitude fatigue threshold from Table-6.6.1.2.5-3

$A_f := 44 \times 10^8$

$N_s = 131400000$

$\Delta F_{TH} := 10.0$

$$\Delta F_n := \text{if}\left[\left(\frac{A_f}{N_s}\right)^{\frac{1}{3}} \geq \frac{1}{2}\,\Delta F_{TH}, \left(\frac{A_f}{N_s}\right)^{\frac{1}{3}}, \frac{1}{2}\Delta F_{TH}\right] \qquad \Delta F_n \text{ ksi} = 5 \text{ ksi}$$

Fatigue stress in bottom flange

$$\sigma_{bffatigue} := \frac{\Sigma MFn_{max}}{S_{bbeamD}} \qquad \sigma_{bffatigue} = 1.116 \text{ ksi}$$

$\text{Check\_bf} := \text{if}\left(\sigma_{bffatigue} \leq \Delta F_n \text{ ksi}, \text{"OK"}, \text{"NG"}\right)$ $\qquad \text{Check\_bf} = \text{"OK"}$

Fatigue Resistance of Shear Connectors

Fatigue resistance of individual shear connectors, Z_r

$$Z_r = \alpha\, d_{sc}^{\,2} \geq \frac{5.5\, d_{sc}^{\,2}}{2} \qquad \alpha := 34.5 - 4.28 \log(N_s) \qquad \text{(AASHTO 6.10.10.2-1)}$$

$\alpha = -0.248$

Where,

d_{sh} = diameter of the stud

$$Z_r := \text{if}\left(\alpha\, d_{sc}^{\,2} \geq \frac{5.5\, d_{sc}^{\,2}}{2}, \alpha\, d_{sc}^{\,2}, \frac{5.5\, d_{sc}^{\,2}}{2}\right) \qquad Z_r \text{ ksi} = 1.547 \text{ kip}$$

Appendix A (Continued)

Maximum horizontal shear per unit length

$$V_{sr} := \frac{V_{nf}\ Q_{BslabD}}{I_{stD}} \qquad V_{sr} = 6.059\,klf \qquad \text{(AASHTO 6.10.10.1.2-2)}$$

Therefore, horizontal shear is 0.505 kip/inch.

Pitch of shear connectors for strength limit state

$$P_{sc} := \frac{n_{sh}\ Z_r\ ksi}{V_{sr}} \qquad P_{sc} = 21.447\,in$$

In any case pitch of shear conenectors shall not exceed 24 inches as per AASHTO LRFD Bridge Design Specifications, 2004.

Thus provide shear connectors at longitudinal pitch of 18 inch center to center throughout the negative moment region for connecting bottom slab to bottom flange of the entire bridge.

Thus provide total of 1940 shear connectors in the negative region of bottom flange to connect bottom slab.

Appendix A (Continued)

A.13 Buckling of Bottom Steel Plate

The buckling stress of bottom flange is determined using classical theory on stability of plates

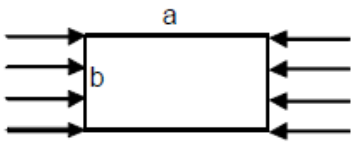

$a := 20\ in \qquad b := 96\ in$

$\frac{a}{b} = 0.208 \qquad \nu := 0.3$

$$ab := \begin{pmatrix} 0.2 \\ 0.3 \\ 0.4 \\ 0.6 \\ 0.8 \\ 1.0 \\ 1.2 \\ 1.4 \\ 1.6 \\ 1.8 \\ 2.0 \\ 2.2 \\ 2.4 \\ 2.7 \\ 3.0 \end{pmatrix} \qquad K_s := \begin{pmatrix} 22.2 \\ 10.9 \\ 6.92 \\ 4.23 \\ 3.45 \\ 3.29 \\ 3.4 \\ 3.68 \\ 3.45 \\ 3.32 \\ 3.29 \\ 3.32 \\ 3.40 \\ 3.32 \\ 3.29 \end{pmatrix}$$

$K_{s\_s} := \text{linterp}\left(ab, K_s, \frac{a}{b}\right)$

$K_{s\_s} = 21.258$

$K_{s\_sm} := \text{if}\left(K_{s\_s} > 22.2, 22.2, K_s\right)$

The stress that will cause buckling in the bottom flange can be determined using the formula given below.

$$\sigma_b := K_{s\_s} \frac{E_s}{1 - \nu^2} \left(\frac{t_{bf}}{b}\right)^2$$

The longitudinal spacing of 20 in. or less is adequate because the stress is above the yield.

Appendix A (Continued)

A.14 Temporary Bracing of Bottom Flange

Non-Composite Section Properties

Area of the bottom flange, A_{BF}

$A_{BF} := 12in\ t_{bf}$

Note: Transverse section properties are calculated on per foot basis.

$A_{BF} = 12\,in^2$

Area of bottom slab, A_{bslab}

$A_{bslab} := 12in\ t_{bs}$ $A_{bslab} = 156\,in^2$

Loads

Dead load of steel bottom flange, DL_{stl}

$DL_{stl} := 490\ pcf\ A_{BF}$

Note: 490 pcf is the unit weight of steel.

$DL_{stl} = 0.041\ klf$

Dead load of concrete bottom slab, DL_{conc}

$DL_{conc} := \gamma_{rc}\ A_{bslab}$

$DL_{conc} = 0.162\ klf$

Total factored loading used in the analysis, DL_{tot}

$DL_{tot} := 1.25\left(DL_{stl} + DL_{conc}\right)$

$DL_{tot} = 0.254\ klf$

If we consider entire flange the pressure acting on the plate is P_{DL}

$P_{DL} := \frac{DL_{tot}}{12\ in}$

$P_{DL} = 1.765 \times 10^{-3}\ ksi$

Calculate Stress Without Bracing

For the unbraced bottom flange, the bottom flange will span between webs like a simple beam under its own self-weight and weight of wet concrete.

Using the rectangular plate tables from *Design of Welded Structures* by *Blodgett*, the stress in the plate can be calculated from the loading and plate thickness.

Stress in the bottom plate, σ_1

$\sigma_1 := \frac{0.75\ P_{DL}\left(b_{bf}\right)^2}{t_{bf}^2}$ $\sigma_1 = 13.238\ ksi$

$CHECK\_16 := if\left(\sigma_1 < 20ksi, "OK", "NG"\right)$ $CHECK\_16 = "OK"$

Appendix A (Continued)

Deflection Check

$$\Delta_d := \frac{0.1422\ P_{DL}\ b_{bf}^{4}}{E_s\ t_{bf}^{3}} \qquad \Delta_d = 0.865\ in$$

$$\Delta_{allow} := \frac{b_{bf}}{360} \qquad \Delta_{allow} = 0.278\ in$$

We need to provide bracing along bottom flange to temporarily support concrete until it cures.

Calculate Deflection With Bracing

Assume bracing at every 10 feet in the form of WT's supported from two inch bottom flange extension to the exterior of box girder.

The width of the panel, w (feet) $\quad w := b_{bf}$

The length of the panel, L (feet) $\quad L_{br} := 10\ ft$

$$\frac{L_{br}}{w} = 1.2$$

The maximum deflection of plate, Δ_{braced}

$$\Delta_{braced} := \frac{0.0616\ P_{DL}\ (b_{bf})^{4}}{E_s\ t_{bf}^{3}}$$

$$\Delta_{braced} = 0.375\ in$$

The deflecion is within the limits required by AASHTO, however the deflection is not. The bracing would have to be moved even closer to limit the deflection of the bottom plate to L/360

Deflection for bracing at 5 feet, Δ_{5ft}

$$\Delta_{5ft} := \frac{0.0964\ P_{DL}\ (60in)^{4}}{E_s\ t_{bf}^{3}}$$

$$\Delta_{5ft} = 0.076\ in$$

Deflection for bracing at 2 feet, Δ_{2ft}

$$\Delta_{2ft} := \frac{0.1422\ P_{DL}\ (24in)^{4}}{E_s\ t_{bf}^{3}}$$

$$\Delta_{2ft} = 0.003\ in$$

Appendix A (Continued)

Once the braces are removed the bracing force is applied back to the composite section.

Conservatively, if the entire load is then reapplied to the section and that deflection is added to the non-composite deflection, we will have the upper bound of the solution.

Composite deflection after removal of braces, Δ_{abrace}

$$\Delta_{abrace} := \frac{0.1422\ P_{DL}\ (b_{bf})^4}{E_s \left(t_{bf} + \frac{t_{bs}}{3n}\right)^3}$$

$$\Delta_{abrace} = 0.201\ in$$

Calculate Deflection for Selected Bracing Member

Try a bottom flange brace of a WT8 x 13

Inertia of WT8 x 13, I_{brace}

$$I_{brace} := 23.5 in^4$$

Deflection of WT8 x 13, Δ_{wbrace}

$$\Delta_{wbrace} := \frac{5\ (P_{DL}\ 2ft + 13\ plf)\ (b_{bf})^4}{384\ E_s\ I_{brace}}$$

$$\Delta_{wbrace} = 0.083\ in$$

Conservatively, the maximum deflection after removal of braces, D_{tot_max}

$$\Delta_{tot\_max} := \Delta_{2ft} + \Delta_{abrace} + \Delta_{wbrace}$$

$$\Delta_{tot\_max} = 0.286\ in$$

The above estimate is conservative, in reality, the maximum deflection should be less than 0.28 inch.